
This is an electronic reprint of the original article.
This reprint may differ from the original in pagination and typographic detail.

Papadioti, I.; Aravas, N.; Lian, J.; Münstermann, S.

A strain-gradient isotropic elastoplastic damage model with J_3 dependence

Published in:
International Journal of Solids and Structures

DOI:
[10.1016/j.ijsolstr.2019.05.027](https://doi.org/10.1016/j.ijsolstr.2019.05.027)

Published: 10/11/2019

Document Version
Peer-reviewed accepted author manuscript, also known as Final accepted manuscript or Post-print

Published under the following license:
CC BY-NC-ND

Please cite the original version:
Papadioti, I., Aravas, N., Lian, J., & Münstermann, S. (2019). A strain-gradient isotropic elastoplastic damage model with J_3 dependence. *International Journal of Solids and Structures*, 174-175, 98-127.
<https://doi.org/10.1016/j.ijsolstr.2019.05.027>

This material is protected by copyright and other intellectual property rights, and duplication or sale of all or part of any of the repository collections is not permitted, except that material may be duplicated by you for your research use or educational purposes in electronic or print form. You must obtain permission for any other use. Electronic or print copies may not be offered, whether for sale or otherwise to anyone who is not an authorised user.

WITH J_3 DEPENDENCE

I. Papadioti^a, N. Aravas^{a,b}, J. Lian^{c,d}, S. Münstermann^e

^aDepartment of Mechanical Engineering, University of Thessaly, Volos 38334, Greece

^bInternational Institute for Carbon Neutral Energy Research (WPI-I2CNER), Kyushu University, 744 Moto-oka, Nishi-ku, Fukuoka 819-0395, Japan

^cDepartment of Mechanical Engineering, Aalto University, Puumiehenkuja 3, 02150 Espoo, Finland

^dImpact and Crashworthiness Lab, Department of Mechanical Engineering, Massachusetts Institute of Technology, 77 Massachusetts Avenue, Cambridge, MA 02139-4307, USA

^eDepartment of Ferrous Metallurgy, RWTH Aachen University, Intzestraße 1, D-52072 Aachen, Germany



A “plastic-strain-gradient” version of an isotropic elastoplastic damage model that depends on the third invariant J_3 of the stress deviator is developed. The model is based on the “non-local” equivalent plastic strain e^p defined by Peerlings et al. (2001) and Engelen et al. (2003) and introduces a “material length” ℓ to the constitutive equations. It is shown that the non-local equivalent plastic strain e^p at a material point P can be identified with the average value of the local von Mises equivalent plastic strain $\bar{\epsilon}^p$ over a sphere centered at P and of radius approximately equal to 3ℓ . A methodology for the numerical integration of the constitutive equations is presented. The algorithm is appropriate for rate-independent as well as rate-dependent (viscoplastic) models. The model is implemented in the ABAQUS general-purpose finite element program and both quasi-static and dynamic problems are solved. Two possible ABAQUS implementations are discussed. First, “user elements” are developed, which can be used for the solution of both quasi-static and dynamic problems. Reduced 1-point Gauss integration is discussed in 8-node hexahedral elements and the “physical stabilization” method of Puso (2000) is used to remove the resulting numerical singularities (hourglass control). Second, the implementation of the model via “user material” subroutines is discussed. *Quasi-static* problems can be solved with ABAQUS/Standard using a *COUPLED TEMPERATURE-DISPLACEMENT, STEADY STATE analysis together with user subroutine UMAT, in which temperature is identified with the non-local equivalent plastic strain e^p ; the solution of *dynamic* problems requires use of ABAQUS/Explicit together with a *DYNAMIC TEMPERATURE-DISPLACEMENT analysis option and user subroutines VUMAT and DFLUX. Several example problems are solved.

Keywords: strain gradient plasticity, J_3 dependence, damage mechanics, finite elements, numerical integration of elastoplastic equations, hourglass control

1. Introduction

Analytical criteria for local ductile failure at a material point P are usually based on the assumption that the accumulated equivalent plastic strain $\bar{\epsilon}^p$ at P reaches a critical value $\bar{\epsilon}_f^p$. Ductile failure in metals subjected to tensile loads is the result of void nucleation at inclusions, followed by void growth and coalescence.

The pioneering works of McClintock (1968) and Rice and Tracey (1969) established that porosity growth depends exponentially on stress triaxiality η , defined as the ratio of mean normal stress p to the equivalent von Mises stress σ_e . These results led to the development of several local criteria for ductile failure, which define the critical equivalent plastic strain $\bar{\epsilon}_f^p$ as a function of stress triaxiality η ; the works of Hancock and Mackenzie (1976) and Johnson and Cook (1985) are typical examples. A discussion of several fracture criteria available in the literature has been given by Bao and Wierzbicki (2004a) and Bai and Wierzbicki (2015). It is now generally accepted that for large triaxialities ($\eta > 0.4$), where void growth is the failure mechanism, and for negative triaxialities ($\eta < 0$), where shear failure occurs, the critical strain $\bar{\epsilon}_f^p$ decreases with increasing η . The situation is not as clear for intermediate values of the triaxiality in the range $0 < \eta < 0.4$: experimental results of Bao and Wierzbicki (2004a,b) on 2024-T351 aluminum

alloy indicate that $\bar{\varepsilon}_f^p$ increases with η in that intermediate triaxiality range, whereas the experiments of Halton et al. (2013) on Al-6061-T6, of Mohr and Henn (2007) on Al-7Si-Mg gravity die casting alloy, and of Luo et al. (2012) on Al-6260-T6 show the opposite.

Wierzbicki and co-workers (Bai and Wierzbicki (2008, 2010); Xue (2007); Xue and Wierzbicki (2008)) carried out carefully controlled experiments and showed that the critical strain $\bar{\varepsilon}_f^p$ depends on both the hydrostatic stress and the third principal invariant J_3 of the stress deviator. Based on these data, Bai and Wierzbicki (2008) proposed a failure criterion in which the critical strain $\bar{\varepsilon}_f^p$ is function of triaxiality η and the “normalized Lode angle parameter” $\bar{\theta}$, which depends on J_3 (BW model). Realizing the importance of damage and its effects on strain localization and ductile fracture, Lian et al. (2012) introduced the concept of damage initiation and its evolution induced softening effect on the strength to the BW fracture model, turning it into a hybrid (coupled or uncoupled) approach. The modified Bai–Wierzbicki (MBW) damage model was applied successfully to the formability prediction of steel sheets (Lian et al. (2014)) and heavy plates (Lian et al. (2015)), as well as the ductile fracture behaviour under impact loading (Novokshanov et al. (2015)). To further improve the model performance especially for complex loading history, Wu et al. (2017b) enhanced the model formulation and successfully applied it to the chip breakage prediction in cutting (Wu et al. (2017a)). However, the challenge still exists when the model is intended to be used for large-scale structure, while all the damage/fracture materials parameters are calibrated from lab scale due to its local formulation.

In the present paper we present a non-local (“plastic-strain-gradient”) version of the MBW model. The yield function is defined in terms of all three principal invariants of the stress tensor: the hydrostatic stress $p = \sigma_{kk}/3$, the von Mises equivalent stress $\sigma_e = \sqrt{3 s_{ij} s_{ij}/2}$, and $J_3 = s_{ij} s_{jk} s_{ki}/3$, where σ is the (true) stress tensor, \mathbf{s} the stress deviator, and the summation convention is used on repeated indices. The flow stress of the material depends on the equivalent plastic strain $\bar{\varepsilon}^p$ and a damage parameter D , which evolves during plastic flow. A “non-local” equivalent plastic strain e^p (Peerlings et al. (2001); Engelen et al. (2003)) is introduced and used to define the evolution of the damage parameter D . The non-local equivalent plastic strain e^p at a material point P can be interpreted as the average value of the local variable $\bar{\varepsilon}^p$ over a material sphere centered at P with radius $R \simeq 3 \ell$, where ℓ is a material length introduced in the definition of e^p .

The calibration of the local version of the model is discussed in detail by Novokshanov et al. (2015), Wu et al. (2017b), and the corresponding calibration of the non-local model is underway and will be reported elsewhere. The present paper focusses on important issues associated with the numerical implementation of the non-local model in a finite element code. These include the finite element formulation of the non-local boundary value problem and the numerical integration of the constitutive equations that account for J_3 -dependence.

Independent interpolations are used for the displacement field \mathbf{u} and the non-local plastic strain e^p . For plastically incompressible materials, the integration of the elastoplastic damage model reduces to the solution of a system of two non-linear algebraic equations. The algorithm covers the rate-independent as well as the rate-dependent (viscoplastic) versions of the model.

A three-dimensional 8-node hexahedral isoparametric finite element with one Gauss station for numerical integration is developed. The element is used to carry out efficiently large scale finite element calculations in implicit as well as explicit finite element codes, such as ABAQUS/Standard and ABAQUS/Explicit. The element is based on a “mixed formulation”: incremental displacements, stresses, incremental displacement gradients, non-local plastic strains, non-local plastic strain gradients, and non-local generalized stresses are treated as independent unknowns and their relations are enforced in a weighted integral sense. Several such mixed formulations are available in the literature for standard local plasticity models; e.g., we mention the works of Corradi (1983), Nyssen and Beckers (1984), Pinsky (1987), Simo et al. (1989), Comi and Perego (1995), Capsoni and Corradi (1997a,b), and Mendes and Castro (2009). Orthogonal interpolation fields are used (Simo and Hughes (1986); Simo and Rifai (1990)) and the problem is finally defined only in terms of the nodal values of the displacement field \mathbf{u} and the non-local equivalent plastic strain e^p . Also, to overcome the numerical singularities introduced by the reduced one-point integration, the “enhanced strain method” developed by Simo and co-workers is used (Simo and Rifai (1990); Simo and Armero (1992); Simo et al. (1993); Freischläger and Schweizerhof (1996); Kasper and Taylor (2000a,b); Areias et al. (2003)). The enriched interpolations used for the incremental displacement gradient and the non-local equivalent plastic strain gradient provide the required “hourglass control”, known as “physical stabilization, that removes the aforementioned numerical singularities (Belytschko and Bindeman (1991)). The scheme proposed by Puso (2000) is used to derive approximate but very accurate analytical expressions for the stabilisation terms, thus obviating Gauss quadrature and leading to a computationally efficient finite element formulation.

We also discuss how such non-local elastoplastic damage models can be used together with the ABAQUS general-purpose finite element code. The obvious choice is to develop a “user element” (UEL subroutine) in ABAQUS, which can then be used for the solution of both quasi-static and dynamic problems. For ~~the~~, a simpler alternative is possible, if a “user material subroutine” UMAT is used together with a coupled temperature-displacement analysis, in which temperature is identified with the non-local equivalent plastic strain e^p and the plastic work-rate $r^{pl} = \boldsymbol{\sigma} : \mathbf{D}^p$ is properly defined and used as a heat source, where \mathbf{D}^p is the plastic part of the deformation rate tensor; this minimizes the programming effort and allows for the use of all elements available in the library of ABAQUS/Standard as discussed in section 6. This approach cannot be used with ABAQUS/Standard in *dynamic* problems. *Dynamic* problems including inertia terms can be solved by using ABAQUS/Explicit together with user material subroutine VUMAT and a dynamic temperature-displacement analysis option as described in section 7. When the explicit code is used for the solution of *quasi-static* problems, care must be taken to eliminate the influence of the inertial terms in the equations of motion and of the transient terms in the energy equation; these issues are discussed in detail in section 7 and in example problems 8.2 and 8.3.

Standard notation is used throughout. Boldface symbols denote tensors the orders of which are indicated by the context. All tensor components are written with respect to a fixed Cartesian coordinate system with base vectors \mathbf{e}_i ($i = 1, 2, 3$), and the summation convention is used for repeated Latin indices. The prefix “det” indicates the determinant, a superscript T the transpose, a superposed dot the material time derivative, and the subscripts s and a the symmetric and anti-symmetric parts of a second order tensor. Let (\mathbf{a}, \mathbf{b}) be vectors, (\mathbf{A}, \mathbf{B}) second-order tensors, and $(\mathcal{C}, \mathcal{D})$ fourth-order tensors; the following products are used in the text $\mathbf{a} \cdot \mathbf{b} = a_i b_i$, $(\mathbf{a} \mathbf{b})_{ij} = a_i b_j$, $(\mathbf{A} \cdot \mathbf{a})_i = A_{ik} a_k$, $(\mathbf{a} \cdot \mathbf{A})_i = a_k A_{ki}$, $\mathbf{A} : \mathbf{B} = A_{ij} B_{ij}$, $(\mathbf{A} \mathbf{B})_{ijkl} = A_{ij} B_{kl}$, $(\mathcal{C} : \mathbf{A})_{ij} = C_{ijkl} A_{kl}$, and $(\mathcal{C} : \mathcal{D})_{ijkl} = C_{ijpq} D_{pqkl}$. The inverse \mathcal{C}^{-1} of a fourth-order tensor \mathcal{C} that has the “minor” symmetries $C_{ijkl} = C_{jikl} = C_{ijlk}$ is defined so that $\mathcal{C} : \mathcal{C}^{-1} = \mathcal{C}^{-1} : \mathcal{C} = \mathcal{I}$, where \mathcal{I} is the symmetric fourth-order identity tensor with Cartesian components $\mathcal{I}_{ijkl} = \frac{1}{2}(\delta_{ik} \delta_{jl} + \delta_{il} \delta_{jk})$, δ_{ij} being the Kronecker delta.

2. Description of constitutive model

An Eulerian formulation is used; the equations of motion and the constitutive equations are all written in the current deformed configuration of the elastoplastic body.

The elastic and plastic response of the material are treated independently, and combined later to obtain the full elastic-plastic response. The rate-of-deformation tensor \mathbf{D} at every point in the continuum is written as

$$\mathbf{D} = \mathbf{D}^e + \mathbf{D}^p, \quad (1)$$

where \mathbf{D}^e and \mathbf{D}^p are the elastic and plastic parts.

2.1. Elasticity

An isotropic linear hypoelastic form is assumed for the elastic part of the rate-of-deformation tensor:

$$\mathbf{D}^e = \mathcal{M}^e : \overset{\nabla}{\boldsymbol{\sigma}} \quad \text{or} \quad \overset{\nabla}{\boldsymbol{\sigma}} = \mathcal{L}^e : \mathbf{D}^e, \quad (2)$$

where $\overset{\nabla}{\boldsymbol{\sigma}}$ is the Jaumann or co-rotational rate of the stress tensor,

$$\mathcal{M}^e = \frac{1}{2G} \mathcal{K} + \frac{1}{3\kappa} \mathcal{J}, \quad \mathcal{L}^e = (\mathcal{M}^e)^{-1} = 2G \mathcal{K} + 3\kappa \mathcal{J}, \quad \mathcal{J} = \frac{1}{3} \boldsymbol{\delta} \boldsymbol{\delta}, \quad \mathcal{K} = \mathcal{I} - \mathcal{J}, \quad (3)$$

(G, κ) denote the elastic shear and bulk moduli respectively, $\boldsymbol{\delta}$ and \mathcal{I} the second- and fourth-order identity tensors with Cartesian components δ_{ij} (the Kronecker delta) and $\mathcal{I}_{ijkl} = \frac{1}{2}(\delta_{ik} \delta_{jl} + \delta_{il} \delta_{jk})$. The *hypoelastic* form (2) is consistent, to leading order, with *hyperelastic* behavior, because the elastic strains are small relative to the total strains (Needleman (1985); Aravas (1992)).

2.2. Rate-independent plasticity

The isotropic yield condition is described by a *smooth* function of the form

$$\Phi(p, \sigma_e, \theta, \bar{\varepsilon}^p, D) = 0, \quad (4)$$

where $\boldsymbol{\sigma}$ is the true (Cauchy) stress tensor, $p = \frac{1}{3} \sigma_{kk}$ the hydrostatic stress, $\mathbf{s} = \boldsymbol{\sigma} - p \boldsymbol{\delta}$ the stress deviator, $\sigma_e = \sqrt{\frac{3}{2} \mathbf{s} : \mathbf{s}}$ the von Mises equivalent stress, $J_3 = \frac{1}{3} \text{tr}(\mathbf{s}^3) = \text{dets}$, θ the ‘‘Lode angle’’ defined by

$$3\theta = \arcsin\left(-\frac{27 J_3}{2 \sigma_e^3}\right), \quad -\frac{\pi}{2} \leq 3\theta \leq \frac{\pi}{2}, \quad (5)$$

D is a ‘‘damage parameter’’, and $\bar{\varepsilon}^p$ the von Mises equivalent plastic strain, the rate of which is defined as

$$\dot{\bar{\varepsilon}}^p = \sqrt{\frac{2}{3} \mathbf{D}^p : \mathbf{D}^p}. \quad (6)$$

The damage parameter D in (4) takes values in the range $0 \leq D \leq 1$ and is defined in terms of the ‘‘non-local’’ equivalent plastic strain as described in sections 3.1 and 3.1.1.

The value $\theta = 0$ corresponds to pure shear, $\theta = -\frac{\pi}{6}$ to uniaxial tension, and $\theta = \frac{\pi}{6}$ to uniaxial compression. We also define the ‘‘stress triaxiality’’ η and the ‘‘normalized Lode angle’’ $\bar{\theta}$:

$$\eta = \frac{p}{\sigma_e}, \quad \bar{\theta} = -\frac{\theta}{\pi/6}. \quad (7)$$

The parameter $\bar{\theta}$ takes the values of 1 in uniaxial tension, -1 in uniaxial compression, and 0 in pure shear.

The flow rule that defines the plastic part of the deformation rate \mathbf{D}^p is defined by a ‘‘normality rule’’:

$$\mathbf{D}^p = \dot{\lambda} \mathbf{P}, \quad \mathbf{P} = \frac{\partial \Phi}{\partial \boldsymbol{\sigma}}, \quad (8)$$

where $\dot{\lambda}$ is a non-negative plastic flow parameter. Therefore, in view of (6), we can write

$$\dot{\bar{\varepsilon}}^p = \dot{\lambda} \bar{P}, \quad \bar{P} = \sqrt{\frac{2}{3} \mathbf{P} : \mathbf{P}}. \quad (9)$$

The normal \mathbf{P} to the smooth yield surface can be written in the form

$$\mathbf{P} \equiv \frac{\partial \Phi}{\partial \boldsymbol{\sigma}} = \frac{\partial \Phi}{\partial p} \frac{\partial p}{\partial \boldsymbol{\sigma}} + \frac{\partial \Phi}{\partial \sigma_e} \frac{\partial \sigma_e}{\partial \boldsymbol{\sigma}} + \frac{\partial \Phi}{\partial \theta} \frac{\partial \theta}{\partial \boldsymbol{\sigma}} = \frac{1}{3} \frac{\partial \Phi}{\partial p} \boldsymbol{\delta} + \frac{\partial \Phi}{\partial \sigma_e} \mathbf{N} + \frac{1}{\sigma_e} \frac{\partial \Phi}{\partial \theta} \mathbf{M}, \quad (10)$$

where

$$\mathbf{N} = \frac{\partial \sigma_e}{\partial \boldsymbol{\sigma}} = \frac{3}{2 \sigma_e} \mathbf{s}, \quad \mathbf{M} = \sigma_e \frac{\partial \theta}{\partial \boldsymbol{\sigma}} = \frac{1}{\cos 3\theta} (\boldsymbol{\delta} - \sin 3\theta \mathbf{N} - 2 \mathbf{N}^2). \quad (11)$$

Remarks

- Equations (8), (10), and (11) show that the principal directions of $\boldsymbol{\sigma}$, \mathbf{s} , \mathbf{N} , \mathbf{M} , \mathbf{P} , and \mathbf{D}^p coincide i.e., they are all ‘‘co-axial’’.
- The normal \mathbf{P} to the yield surface in (10) is defined in terms of the dimensionless ‘‘direction tensors’’ $\boldsymbol{\delta}$, \mathbf{N} , and \mathbf{M} , which have constant magnitude and are orthogonal:

$$\boldsymbol{\delta} : \boldsymbol{\delta} = 3, \quad \mathbf{N} : \mathbf{N} = \mathbf{M} : \mathbf{M} = \frac{3}{2}, \quad \mathbf{N} : \boldsymbol{\delta} = \mathbf{M} : \boldsymbol{\delta} = \mathbf{N} : \mathbf{M} = 0. \quad (12)$$

Also, both \mathbf{N} and \mathbf{M} are deviatoric, i.e., $N_{kk} = M_{kk} = 0$.

Tensors $(\boldsymbol{\delta}, \mathbf{N}, \mathbf{M})$ are shown as vectors $(\boldsymbol{\delta}^v, \mathbf{N}^v, \mathbf{M}^v)$ in the space of principal stresses $(\sigma_1, \sigma_2, \sigma_3)$ in Fig. 1. The so-called ‘‘deviatoric Π -plane’’ is defined by the equation $\sigma_1 + \sigma_2 + \sigma_3 = 0$ on the $(\sigma_1, \sigma_2, \sigma_3)$ space. Vectors \mathbf{N}^v and \mathbf{M}^v lie on the Π -plane, are perpendicular to each other, and $\boldsymbol{\delta}^v$ is normal to the Π -plane.

- The definition of \mathbf{M} in (11b) needs special treatment as $\theta \rightarrow \pm \frac{\pi}{6}$, since in that case $\cos 3\theta \rightarrow 0$. In the following section 2.2.1 we show that, on smooth yield surfaces, \mathbf{M} approaches unique finite values as $\theta \rightarrow \pm \frac{\pi}{6}$. \square

2.2.1. Principal stress directions

Let $(\mathbf{n}^{(1)}, \mathbf{n}^{(2)}, \mathbf{n}^{(3)} = \mathbf{n}^{(1)} \times \mathbf{n}^{(2)})$ be the common unit eigenvectors of $\boldsymbol{\sigma}$, \mathbf{s} , \mathbf{N} , \mathbf{M} , \mathbf{P} , and \mathbf{D}^p . The triad $(\mathbf{n}^{(1)}, \mathbf{n}^{(2)}, \mathbf{n}^{(3)})$ forms a right-handed orthonormal basis and we can write

$$\boldsymbol{\sigma} = \sum_{i=1}^3 \sigma_i \mathbf{n}^{(i)} \mathbf{n}^{(i)}, \quad \mathbf{s} = \sum_{i=1}^3 s_i \mathbf{n}^{(i)} \mathbf{n}^{(i)}, \quad \mathbf{N} = \sum_{i=1}^3 N_i \mathbf{n}^{(i)} \mathbf{n}^{(i)}, \quad (13)$$

$$\mathbf{M} = \sum_{i=1}^3 M_i \mathbf{n}^{(i)} \mathbf{n}^{(i)}, \quad \mathbf{P} = \sum_{i=1}^3 P_i \mathbf{n}^{(i)} \mathbf{n}^{(i)}, \quad (14)$$

where

$$s_i = \sigma_i - p = \frac{2}{3} \sigma_e N_i, \quad P_i = \frac{1}{3} \frac{\partial \Phi}{\partial p} + \frac{\partial \Phi}{\partial \sigma_e} N_i + \frac{1}{\sigma_e} \frac{\partial \Phi}{\partial \theta} M_i. \quad (15)$$

The principal stresses can be written in the form (e.g., Kachanov (1971); Nayak and Zienkiewicz (1972); Jiang and Pietruszczak (1988))

$$\sigma_i = \frac{2}{3} \sigma_e \cos \theta_i + p, \quad \text{with} \quad \theta_i = \theta + (5 - 4i) \frac{\pi}{6}, \quad -\frac{\pi}{6} \leq \theta \leq \frac{\pi}{6}, \quad (16)$$

where the numbering $i = 1, 2, 3$ in the definition of θ_i is such that $\sigma_1 \geq \sigma_2 \geq \sigma_3$. Using equations (11) we conclude that the principal components of \mathbf{N} , \mathbf{M} , and \mathbf{P} can be written in the form

$$N_i = \cos \theta_i, \quad M_i = -\sin \theta_i = \frac{dN_i}{d\theta}, \quad P_i = \frac{1}{3} \frac{\partial \Phi}{\partial p} + \frac{\partial \Phi}{\partial \sigma_e} \cos \theta_i - \frac{1}{\sigma_e} \frac{\partial \Phi}{\partial \theta} \sin \theta_i. \quad (17)$$

A schematic representation of tensors $\boldsymbol{\sigma}$, \mathbf{s} , \mathbf{N} , \mathbf{M} , and $\boldsymbol{\delta}$ in the principal coordinate system is shown in Fig. 1, where the following vectors are defined:

$$\mathbf{N}^v = N_i \mathbf{n}^{(i)}, \quad \mathbf{M}^v = M_i \mathbf{n}^{(i)}, \quad \boldsymbol{\delta}^v = \sum_{i=1}^3 \mathbf{n}^{(i)}, \quad (18)$$

and

$$\boldsymbol{\sigma}^v = \sigma_i \mathbf{n}^{(i)} = \overrightarrow{OB}, \quad \mathbf{s}^v = s_i \mathbf{n}^{(i)} = \overrightarrow{AB}. \quad (19)$$

\mathbf{N} is defined uniquely at all points of a smooth yield surface, and the unit vectors $(\sqrt{\frac{2}{3}} \mathbf{N}^v, \sqrt{\frac{2}{3}} \mathbf{M}^v, \sqrt{\frac{1}{3}} \boldsymbol{\delta}^v)$ form a right-handed orthonormal basis. Therefore $\mathbf{M}^v = \frac{1}{\sqrt{3}} \boldsymbol{\delta} \times \mathbf{N}^v$ and the components M_i are related to N_i as follows

$$M_1 = \frac{N_3 - N_2}{\sqrt{3}}, \quad M_2 = \frac{N_1 - N_3}{\sqrt{3}}, \quad M_3 = \frac{N_2 - N_1}{\sqrt{3}}. \quad (20)$$

Figure 2 shows the projection of the principal axes on the deviatoric Π -plane and the Lode angle θ .

Equations (14a), (16b), and (17b) yield

$$\lim_{\theta \rightarrow \frac{\pi}{6}} \mathbf{M} = \frac{\sqrt{3}}{2} (\mathbf{n}^{(2)} \mathbf{n}^{(2)} - \mathbf{n}^{(1)} \mathbf{n}^{(1)}), \quad \lim_{\theta \rightarrow -\frac{\pi}{6}} \mathbf{M} = \frac{\sqrt{3}}{2} (\mathbf{n}^{(2)} \mathbf{n}^{(2)} - \mathbf{n}^{(3)} \mathbf{n}^{(3)}), \quad (21)$$

i.e., the direction tensor \mathbf{M} defined in (11b) takes finite values as $\theta \rightarrow \pm \frac{\pi}{6}$ (compare to (11b)). It is also known that isotropic yield surfaces are symmetric with respect to the lines $\theta = \pm \frac{\pi}{6}$ on Fig. 2 (e.g., Hill (1950), p. 18). Therefore, when an isotropic yield surface is *smooth*

$$\lim_{\theta \rightarrow \pm \frac{\pi}{6}} \frac{\partial \Phi}{\partial \theta} = 0, \quad \text{so that (10) yields} \quad \lim_{\theta \rightarrow \pm \frac{\pi}{6}} \mathbf{P} = \left(\frac{1}{3} \frac{\partial \Phi}{\partial p} \boldsymbol{\delta} + \frac{\partial \Phi}{\partial \sigma_e} \mathbf{N} \right)_{\theta = \pm \frac{\pi}{6}}, \quad (22)$$

i.e., the normal \mathbf{P} to the *smooth* isotropic yield surface has no component in the \mathbf{M} -direction at $\theta = \pm \frac{\pi}{6}$.

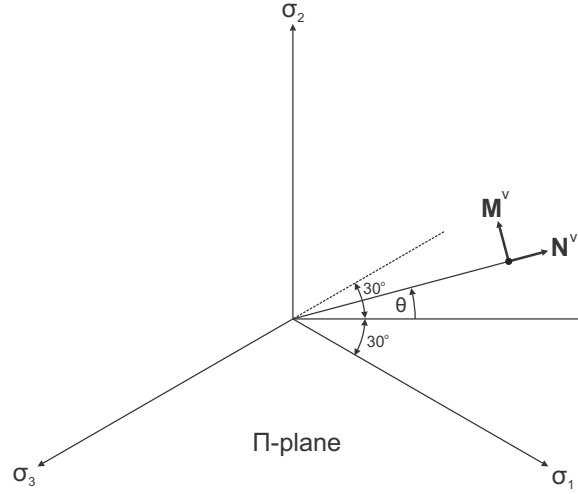


Figure 2: Lode angle θ on the deviatoric Π -plane.

2.4. Damage modeling

2.4.1. Damage model of Bai and Wierzbicki (2008, 2010) (BW)

A detailed discussion of various commonly used local ductile failure criteria for metals has been presented by Bao and Wierzbicki (2004a). These criteria postulate that fracture occurs at a point in a body when the integral

$$\int_0^{\bar{\epsilon}^p} \frac{d\bar{\epsilon}^p}{f(\eta, \theta)} \quad (27)$$

reaches a critical value at that point, where $f(\eta, \theta)$ is a dimensionless stress-dependent weighting function. Bai and Wierzbicki (2008, 2010) suggest to normalize $f(\eta, \theta)$ so that this critical value equals unity (BW model). Then, the failure criterion can be written in the form

$$D(\bar{\epsilon}_f^p) = 1, \quad \text{with} \quad D(\bar{\epsilon}^p) = \int_0^{\bar{\epsilon}^p} \frac{d\bar{\epsilon}^p}{f(\eta, \theta)}, \quad (28)$$

where $\bar{\epsilon}_f^p$ is the value of $\bar{\epsilon}^p$ when fracture occurs. The parameter D defined in (28b) can be thought of as a “damage indicator”.

If parameters (η, θ) remain constant in a loading program (“proportional loading”), equations (28) leads to

$$\bar{\epsilon}_f^p = f(\eta, \theta), \quad (29)$$

i.e., the function $f(\eta, \theta)$ defines essentially the fracture locus on the (η, θ) space.

In the case of non-proportional loading, Bai and Wierzbicki (2008) suggest to define the fracture locus (29) in terms of average quantities:

$$\bar{\epsilon}_f^p = f(\eta_{\text{av}}, \theta_{\text{av}}), \quad \text{where} \quad \eta_{\text{av}} = \frac{1}{\bar{\epsilon}_f^p} \int_0^{\bar{\epsilon}_f^p} \eta d\bar{\epsilon}^p, \quad \theta_{\text{av}} = \frac{1}{\bar{\epsilon}_f^p} \int_0^{\bar{\epsilon}_f^p} \theta d\bar{\epsilon}^p. \quad (30)$$

2.4.2. The modified damage model of Bai and Wierzbicki (MBW) (Lian et al. (2012); Wu et al. (2017b))

Physically, damage initiation at a material point is identified with the creation of a micro-defect (e.g., a microcrack) at that point. According to the definition of damage D in equation (28b), damage starts accumulating when the material

deforms plastically, i.e., when $\bar{\varepsilon}^p$ takes non-zero values. Based on experimental data, the ‘‘Aachen group’’ (Lian et al. (2012); Wu et al. (2017b)) suggested that damage initiation does not occur at $\bar{\varepsilon}^p = 0$. Instead, Lian et al. (2012) and Wu et al. (2017b) introduce a ‘‘damage initiation indicator’’ I defined as

$$I = \int_0^{\bar{\varepsilon}^p} \frac{d\bar{\varepsilon}^p}{\bar{\varepsilon}_i^p(\eta_{av}, \bar{\theta}_{av})}, \quad \eta_{av} = \frac{1}{\bar{\varepsilon}^p} \int_0^{\bar{\varepsilon}^p} \eta d\bar{\varepsilon}^p, \quad \bar{\theta}_{av} = \frac{1}{\bar{\varepsilon}^p} \int_0^{\bar{\varepsilon}^p} \bar{\theta} d\bar{\varepsilon}^p, \quad (31)$$

where $\bar{\theta}$ is the normalized Lode angle defined in (7),

$$\bar{\varepsilon}_i^p(\eta_{av}, \bar{\theta}_{av}) = (c_1 e^{-c_2 \eta_{av}} - c_3 e^{-c_4 \eta_{av}}) \bar{\theta}_{av}^2 + c_3 e^{-c_4 \eta_{av}}, \quad (32)$$

and (c_1, c_2, c_3, c_4) are dimensionless positive material constants. Damage is assumed to initiate when indicator I reaches the value of 1. If parameters (η, θ) remain constant in a loading program (‘‘proportional loading’’), then equation (31a) implies that damage initiation occurs when $\bar{\varepsilon}^p = \bar{\varepsilon}_i^p(\eta, \theta)$.

Returning to the case of general non-proportional loading, we let σ_{yi} denote the value of the material flow stress σ_y (see equations (161) and (163b) below) at damage initiation, i.e., when the condition $I = 1$ is satisfied. Once the value of $I = 1$ is reached, the dimensionless damage parameter D starts to evolve according to the relation

$$\dot{D} = \begin{cases} \frac{\sigma_{yi}}{G_f} \dot{\bar{\varepsilon}}^p & \text{if } I = 1 \text{ and } \eta > \eta_{cr}, \\ 0 & \text{otherwise,} \end{cases} \quad (33)$$

where G_f is a material parameter with dimensions of energy per unit volume, η_{cr} is a critical value of stress triaxiality below which local material failure never occurs ($\eta_{cr} \simeq -1/3$, Bao and Wierzbicki (2005)), and

$$D_{cr}(\eta_{av}, \bar{\theta}_{av}) = \min \left[(c_5 e^{-c_6 \eta_{av}} - c_7 e^{-c_8 \eta_{av}}) \bar{\theta}_{av}^2 + c_7 e^{-c_8 \eta_{av}}, D_{\max} \right], \quad (34)$$

(c_5, c_6, c_7, c_8) are dimensionless positive material constants, and D_{\max} an upper limit to the damage parameter D to make sure that D_{cr} is always ≤ 1 ($D_{\max} \lesssim 1$).

Wu et al. (2017a) introduce the ‘‘failure indicator’’ I_f , which evolves as

$$\dot{I}_f = \frac{\dot{D}}{D_{cr}(\eta_{av}, \bar{\theta}_{av})}, \quad (35)$$

and local material failure occurs when the failure indicator parameter I_f reaches the value of unity, i.e., when $I_f = 1$.

If parameters (η, θ) remain constant in a loading program (‘‘proportional loading’’), then equation (33) and (35) imply that local material failure takes place when $D = D_{cr}(\eta, \theta)$.

3. Non-local formulation

A well-known problem in the computational implementation of damage mechanics models is that finite element solutions depend on the mesh size when the material enters the softening region. The mathematical reason for this is that the governing equations lose ellipticity and the boundary value problem, as posed originally, becomes ill conditioned. In order to overcome this difficulty, it is common to ‘‘regularize’’ the problem by introducing additional terms in the constitutive equations that involve spatial gradients of strain. These additional terms restore ellipticity, increase the order of the governing equations, and in the case of plasticity they may even change the yield condition from an algebraic non-linear equation of stress to a partial differential equation of plastic strain (Benallal and Tvergaard (1995)). The additional terms in the constitutive equations involve one or more ‘‘material lengths’’ that are related to material microstructure. In all cases, the numerical solution of the problem becomes more involved and most standard finite element codes cannot be used for their numerical solution.

To overcome the aforementioned difficulties we introduce the ‘‘non-local equivalent plastic strain’’ e^p and develop a ‘‘strain-gradient’’ version of the MBW model.

3.1. Non-local equivalent plastic strain — Gradient formulation

We follow Peerlings et al. (2001) and Engelen et al. (2003) and define the “non-local” equivalent plastic strain field $e^p(\mathbf{x})$ in terms of the “local” equivalent plastic strain field $\bar{e}^p(\mathbf{x})$ from the solution of the following boundary value problem (BVP):

$$e^p - \ell^2 \nabla^2 e^p = \bar{e}^p \quad \text{in } \Omega \quad (36)$$

$$\frac{\partial e^p}{\partial n} \equiv \mathbf{n} \cdot \nabla e^p = 0 \quad \text{on } \partial\Omega, \quad (37)$$

where ℓ is a material parameter with dimensions of length, Ω is the domain occupied by the elastoplastic body in its deformed state, $\partial\Omega$ its boundary, and \mathbf{n} the unit outward normal vector to $\partial\Omega$.

The boundary condition (37) guarantees that the “total values” of e^p and \bar{e}^p in Ω coincide. In fact, integration of (36) over the domain Ω and use the divergence theorem together with (37), leads to the conclusion

$$\int_{\Omega} e^p d\Omega = \int_{\Omega} \bar{e}^p d\Omega. \quad (38)$$

The BVP (36)–(37) is solved and the non-local equivalent plastic strain e^p is determined in the **entire problem domain** Ω and not just inside the plastic zone (Peerlings et al. (2001); Engelen et al. (2003)).

The formulation of the BVP (36)–(37) and the interpretation of e^p as a weighted spatial average of the local values \bar{e}^p is discussed in detail by Peerlings et al. (2001) and Engelen et al. (2003). Here we give a slightly different interpretation of the non-local variable e^p as follows. At any given material point with current position \mathbf{x} , we calculate the average value \bar{e}_{av}^p of the local equivalent plastic strain \bar{e}^p over a material sphere V of radius R centered at \mathbf{x} :

$$\bar{e}_{\text{av}}^p(\mathbf{x}) = \frac{1}{V} \int_V \bar{e}^p(\mathbf{y}) dV(\mathbf{y}). \quad (39)$$

If we now assume that $\bar{e}^p(\mathbf{y})$ is a smooth function of position, write a Taylor series around \mathbf{x} , and introduce spherical coordinates with origin at \mathbf{x} , we find after some lengthy but straightforward calculations that

$$\bar{e}_{\text{av}}^p(\mathbf{x}) = \bar{e}^p(\mathbf{x}) + \ell^2 \nabla^2 \bar{e}^p(\mathbf{x}) + O(\ell^4 \nabla^4 \bar{e}^p), \quad (40)$$

where $\ell = \frac{R}{\sqrt{10}} = 0.32 R$. Last equation implies that

$$\ell^2 \nabla^2 \bar{e}_{\text{av}}^p(\mathbf{x}) = \ell^2 \nabla^2 \bar{e}^p(\mathbf{x}) + O(\ell^4 \nabla^4 \bar{e}^p). \quad (41)$$

Subtracting (41) from (40) we find

$$\bar{e}_{\text{av}}^p(\mathbf{x}) - \ell^2 \nabla^2 \bar{e}_{\text{av}}^p(\mathbf{x}) = \bar{e}^p(\mathbf{x}) + O(\ell^4 \nabla^4 \bar{e}^p). \quad (42)$$

Comparing last equation to (36), we conclude that we can identify the non-local equivalent plastic strain $e^p(\mathbf{x})$ in (36) with the average value $\bar{e}_{\text{av}}^p(\mathbf{x})$ of the local equivalent plastic strain \bar{e}^p over a sphere of radius $R = \sqrt{10} \ell = 3.16 \ell$ centered at \mathbf{x} , to within terms $O(\ell^4 \nabla^4 \bar{e}^p)$. Obviously, the above interpretation breaks down for material points near the boundary $\partial\Omega$, where part of the material sphere of radius R centered at the point under consideration lies outside the domain Ω occupied by the elastoplastic body.

Following a similar approach we show that, in two dimensional problems, the non-local equivalent plastic strain $e^p(\mathbf{x})$ in (36) can be identified with the average value $\bar{e}_{\text{av}}^p(\mathbf{x})$ of the local equivalent plastic strain \bar{e}^p over a *circle* of radius $R = 2 \sqrt{2} \ell = 2.83 \ell$ centered at \mathbf{x} , to within terms $O(\ell^4 \nabla^4 \bar{e}^p)$.

Finally it should be emphasized that, whereas the local equivalent plastic strain is such that $\bar{e}^p \geq 0$ by definition, the non-local e^p is defined by the solution of the BVP (36)–(37) and the possibility $\dot{e}^p < 0$ at some material points cannot be excluded. Therefore, following Peerlings et al. (2001) and Engelen et al. (2003), we define

$$\hat{e}^p(t) = \max\{e^p(\tau) \mid 0 \leq \tau \leq t\} \quad (t = \text{time}), \quad (43)$$

which ensures that $\dot{\hat{e}}^p(t) \geq 0$ always. The definition of \hat{e}^p can be written also in a Kuhn-Tucker form (Peerlings et al. (2001); Engelen et al. (2003)). The non-local parameter \hat{e}^p is used in the gradient-version of the evolution equation for damage as described in the following section.

3.1.1. The non-local version of MBW

In the present paper we use a non-local version of the MBW damage model in which the local equivalent plastic strain $\bar{\varepsilon}^p$ is replaced by the non-local equivalent plastic strain e^p in all expressions of section 2.4.2. This means that the value of damage D at a material point is not determined from the local value of the equivalent plastic strain $\bar{\varepsilon}^p$ at that point; instead, D at a point is essentially calculated by using the average value of $\bar{\varepsilon}^p$ over a material sphere of radius about 3ℓ centered at that point.

In particular, we write

$$\dot{I} = \frac{\dot{e}^p}{\bar{\varepsilon}_i^p(\eta_{av}, \bar{\theta}_{av})}, \quad \eta_{av} = \frac{1}{e^p} \int_0^{e^p} \eta d\hat{e}^p, \quad \bar{\theta}_{av} = \frac{1}{e^p} \int_0^{e^p} \bar{\theta} d\hat{e}^p, \quad (44)$$

$$\dot{D} = \alpha \frac{\sigma_{yi} \dot{e}^p}{G_f}, \quad \alpha = \begin{cases} 1 & \text{if } I = 1 \text{ and } \eta > \eta_{cr}, \\ 0 & \text{if otherwise,} \end{cases} \quad (45)$$

$$\dot{I}_f = \frac{\dot{D}}{D_{cr}(\eta_{av}, \theta_{av})}, \quad (46)$$

where $\bar{\varepsilon}_i^p(\eta_{av}, \bar{\theta}_{av})$ and $D_{cr}(\eta_{av}, \bar{\theta}_{av})$ are defined by (32) and (34). Local material failure occurs when the damage indicator I_f reaches the value $I_f = 1$.

Figure 3 shows a schematic representation of the stress-strain curve in uniaxial tension.

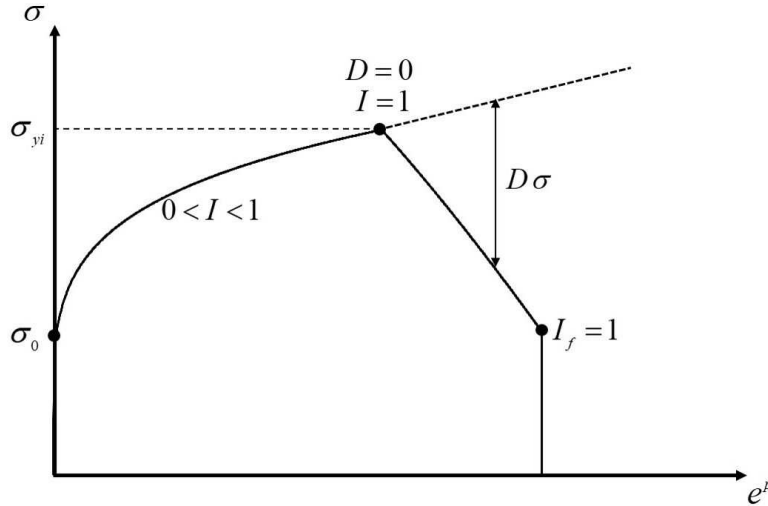


Figure 3: Schematic representation of stress-strain curve in uniaxial tension.

3.2. The plastic multiplier and the tangent modulus for rate-independent materials

The elastoplastic constitutive equations are now combined to derive an equation relating the Jaumann derivative $\overset{\nabla}{\sigma}$ to the deformation rate \mathbf{D} and the rate of the non-local equivalent plastic strain \dot{e}^p in a rate-independent material. The derivation is as follows.

Assuming plastic loading ($\dot{\lambda} > 0$), substitution of $\mathbf{D}^e = \mathbf{D} - \mathbf{D}^p = \mathbf{D} - \dot{\lambda} \mathbf{P}$ into the hypoelastic constitutive equation (2) ($\overset{\nabla}{\sigma} = \mathcal{L}^e : \mathbf{D}^e$) yields

$$\overset{\nabla}{\sigma} = \mathcal{L}^e : (\mathbf{D} - \dot{\lambda} \mathbf{P}). \quad (47)$$

Since Φ is an isotropic function, the “consistency condition” $\dot{\Phi} = 0$ can be written in the form (Dafalias (1985))

$$\dot{\Phi} = \frac{\partial \Phi}{\partial \sigma} : \overset{\nabla}{\sigma} + \frac{\partial \Phi}{\partial \bar{\varepsilon}^p} \dot{\bar{\varepsilon}}^p + \frac{\partial \Phi}{\partial D} \frac{\partial D}{\partial e^p} \dot{e}^p = 0, \quad (48)$$

or, in view of (47),

$$\mathbf{P} : \mathcal{L}^e : (\mathbf{D} - \lambda \mathbf{P}) + \frac{\partial \Phi}{\partial \bar{\varepsilon}^p} \lambda \bar{P} + \frac{\partial \Phi}{\partial D} \frac{\partial D}{\partial e^p} \dot{e}^p = 0, \quad (49)$$

which leads to

$$\lambda = \frac{1}{L} \left(\mathbf{P} : \mathcal{L}^e : \mathbf{D} + \frac{\partial \Phi}{\partial D} \frac{\partial D}{\partial e^p} \dot{e}^p \right), \quad L = \mathbf{P} : \mathcal{L}^e : \mathbf{P} + H, \quad H = -\bar{P} \frac{\partial \Phi}{\partial \bar{\varepsilon}^p}. \quad (50)$$

Substituting the value of λ from (50a) into (47) we find

$$\bar{\boldsymbol{\sigma}} = \mathcal{L} : \mathbf{D} - \mathbf{A}^{\text{nl}} \dot{e}^p, \quad (51)$$

where

$$\mathcal{L} = \mathcal{L}^e - \frac{1}{L} (\mathcal{L}^e : \mathbf{P}) (\mathcal{L}^e : \mathbf{P}), \quad \mathbf{A}^{\text{nl}} = \frac{1}{L} \frac{\partial \Phi}{\partial D} \frac{\partial D}{\partial e^p} \mathcal{L}^e : \mathbf{P}. \quad (52)$$

Also, using the value of λ from (50a) in (9) ($\dot{\bar{\varepsilon}}^p = \dot{\lambda} \bar{P}$), we find

$$\dot{\bar{\varepsilon}}^p = \frac{\bar{P}}{L} \left(\mathbf{P} : \mathcal{L}^e : \mathbf{D} + \frac{\partial \Phi}{\partial D} \frac{\partial D}{\partial e^p} \dot{e}^p \right). \quad (53)$$

The corresponding form of equation (51) for the *local* model is

$$\bar{\boldsymbol{\sigma}} = \mathcal{L}^{\text{loc}} : \mathbf{D}, \quad (54)$$

where

$$\mathcal{L}^{\text{loc}} = \mathcal{L}^e - \frac{1}{L^{\text{loc}}} (\mathcal{L}^e : \mathbf{P}) (\mathcal{L}^e : \mathbf{P}), \quad (55)$$

$$L^{\text{loc}} = \mathbf{P} : \mathcal{L}^e : \mathbf{P} + H^{\text{loc}}, \quad H^{\text{loc}} = -\bar{P} \left(\frac{\partial \Phi}{\partial \bar{\varepsilon}^p} + \alpha \frac{\partial \Phi}{\partial D} \frac{\partial D}{\partial \bar{\varepsilon}^p} \right), \quad (56)$$

and α takes on the values of either 0 or 1 according to equation (33).

4. Numerical integration of constitutive model

In this section, we develop an algorithm for the numerical integration of the constitutive equations. In a finite element environment, the solution is developed incrementally and the constitutive equations are integrated at the element Gauss integration points. As will be described in section 5, the nodal unknowns are the displacement vector \mathbf{u} and the non-local equivalent plastic strain e^p . The history dependent behavior is obtained based on the incremental displacements and non-local equivalent plastic strains ($\Delta \mathbf{u}$, Δe^p) and the state at the start of each increment.

Let \mathbf{F} denote the deformation gradient tensor, which is determined in terms of the nodal displacements within each finite element. At a given Gauss integration point, the solution (\mathbf{F}_n , $\boldsymbol{\sigma}_n$, $\bar{\varepsilon}_n^p$, D_n , e_n^p) at time t_n as well as the values (\mathbf{F}_{n+1} , e_{n+1}^p) at time $t_{n+1} = t_n + \Delta t$ are known, and the problem is to determine ($\boldsymbol{\sigma}_{n+1}$, $\bar{\varepsilon}_{n+1}^p$, D_{n+1}). In the following, quantities with a subscript n are evaluated at the start of the increment ($t = t_n$) and subscript $n + 1$ denotes values at the end of the increment ($t = t_{n+1}$).

The time variation of the deformation gradient \mathbf{F} during the time increment $[t_n, t_{n+1}]$ can be written as

$$\mathbf{F}(t) = \Delta \mathbf{F}(t) \cdot \mathbf{F}_n = \mathbf{R}(t) \cdot \mathbf{U}(t) \cdot \mathbf{F}_n, \quad t_n \leq t \leq t_{n+1}, \quad (57)$$

where $\Delta \mathbf{F}(t)$ is the deformation gradient relative to the configuration at the start of the increment, and $\mathbf{R}(t)$ and $\mathbf{U}(t)$ are the rotation and right stretch tensors associated with $\Delta \mathbf{F}(t)$. The corresponding deformation rate $\mathbf{D}(t)$ and spin $\mathbf{W}(t)$ tensors are given by

$$\mathbf{D}(t) \equiv \left[\dot{\mathbf{F}}(t) \cdot \mathbf{F}^{-1}(t) \right]_s = \left[\Delta \dot{\mathbf{F}}(t) \cdot \Delta \mathbf{F}^{-1}(t) \right]_s, \quad (58)$$

and

$$\mathbf{W}(t) \equiv \left[\dot{\mathbf{F}}(t) \cdot \mathbf{F}^{-1}(t) \right]_a = \left[\Delta \dot{\mathbf{F}}(t) \cdot \Delta \mathbf{F}^{-1}(t) \right]_a, \quad (59)$$

where the subscripts s and a denote the symmetric and anti-symmetric parts, respectively, of a tensor.

The rotation tensor $\mathbf{R}(t)$ introduced in (57) is used to define the so-called ‘‘rotation-neutralized quantities’’ $\hat{\boldsymbol{\sigma}}(t)$, $\hat{\mathbf{N}}^{(i)}(t)$, and $\hat{\mathbf{M}}(t)$ (Nagtegaal and Veldpaus (1984)):

$$\hat{\boldsymbol{\sigma}}(t) = \mathbf{R}^T(t) \cdot \boldsymbol{\sigma}(t) \cdot \mathbf{R}(t), \quad \hat{\mathbf{N}}(t) = \mathbf{R}^T(t) \cdot \mathbf{N}(t) \cdot \mathbf{R}(t), \quad \hat{\mathbf{M}}(t) = \mathbf{R}^T(t) \cdot \mathbf{M}(t) \cdot \mathbf{R}(t). \quad (60)$$

It is assumed that the Lagrangian triad associated with $\Delta \mathbf{F}(t)$ (i.e., the eigenvectors of $\mathbf{U}(t)$) remains fixed in the time interval $[t_n, t_{n+1}]$. Then it can be shown readily that

$$\mathbf{D}(t) = \mathbf{R}(t) \cdot \dot{\mathbf{E}}(t) \cdot \mathbf{R}^T(t), \quad \overset{\nabla}{\boldsymbol{\sigma}}(t) = \mathbf{R}(t) \cdot \dot{\hat{\boldsymbol{\sigma}}}(t) \cdot \mathbf{R}^T(t), \quad (61)$$

where $\mathbf{E}(t) = \ln \mathbf{U}(t)$ is the logarithmic strain relative to the configuration at t_n . It is noted that at the start of the increment ($t = t_n$)

$$\mathbf{F}_n = \mathbf{R}_n = \mathbf{U}_n = \boldsymbol{\delta}, \quad \hat{\boldsymbol{\sigma}}_n = \boldsymbol{\sigma}_n, \quad \mathbf{E}_n = \mathbf{0}, \quad (62)$$

whereas at the end of the increment ($t = t_{n+1}$)

$$\Delta \mathbf{F}_{n+1} = \mathbf{F}_{n+1} \cdot \mathbf{F}_n^{-1} = \mathbf{R}_{n+1} \cdot \mathbf{U}_{n+1} = \text{known}, \quad \text{and} \quad \mathbf{E}_{n+1} = \ln \mathbf{U}_{n+1} = \text{known}. \quad (63)$$

Taking into account that the invariants of $\hat{\boldsymbol{\sigma}}$ and $\boldsymbol{\sigma}$ are the same and that \mathbf{P} is an isotropic function of its arguments, we can write the *rate-independent* elastoplastic equations in the form

$$\dot{\mathbf{E}} = \dot{\mathbf{E}}^e + \dot{\mathbf{E}}^p, \quad (64)$$

$$\dot{\hat{\boldsymbol{\sigma}}} = \mathcal{L}^e : \dot{\mathbf{E}}^e = \mathcal{L}^e : (\dot{\mathbf{E}} - \dot{\mathbf{E}}^p), \quad (65)$$

$$\Phi(p, \sigma_e, \theta, \bar{\boldsymbol{\varepsilon}}^p, D) = 0, \quad (66)$$

$$\dot{\mathbf{E}}^p = \dot{\lambda} \mathbf{P}(\hat{\boldsymbol{\sigma}}, \bar{\boldsymbol{\varepsilon}}^p, D) = \dot{\lambda} \left(\frac{1}{3} \frac{\partial \Phi}{\partial p} \boldsymbol{\delta} + \frac{\partial \Phi}{\partial \sigma_e} \hat{\mathbf{N}} + \frac{1}{\sigma_e} \frac{\partial \Phi}{\partial \theta} \hat{\mathbf{M}} \right), \quad (67)$$

$$\dot{\bar{\boldsymbol{\varepsilon}}}^p = \sqrt{\frac{2}{3}} \dot{\mathbf{E}}^p : \dot{\mathbf{E}}^p. \quad (68)$$

The evolution equation of damage is given by (44)–(45). Equation (67) shows that $\dot{\mathbf{E}}^p$ is co-axial with $\hat{\boldsymbol{\sigma}}$.

The above elastoplastic equations are integrated numerically as follows. Recall that the non-local equivalent plastic strain e^p is a nodal variable and, therefore, its value is known at the Gauss integration points. The evolution of damage is determined first by using a forward Euler scheme in (44) and (45). As the solution develops, we monitor the evolution of damage indicator I and calculate

$$I_{n+1} = I_n + \frac{\Delta \hat{e}^p}{\bar{\boldsymbol{\varepsilon}}_i^p(\eta_{\text{av}}|_n, \theta_{\text{av}}|_n)}. \quad (69)$$

When the condition $I_{n+1} \geq 1$ is met for the first time, the corresponding value of $\sigma_{yi} = \sigma_y(\bar{\boldsymbol{\varepsilon}}_{n+1}^p)$ is stored. The evolution of damage is also calculated:

$$\Delta D = \begin{cases} \frac{\sigma_{yi}}{G_f} \Delta \hat{e}^p & \text{if } I_n \geq 1 \text{ and } \eta_n > \eta_{\text{cr}} \text{ and } D_n < D_{\text{cr}}|_n, \\ 0 & \text{otherwise,} \end{cases} \quad (70)$$

$$D_{n+1} = \min [D_n + \Delta D, D_{\text{cr}}|_n] = \text{known}, \quad (71)$$

$$I_f|_{n+1} = I_f|_n + \frac{\Delta D}{D_{\text{cr}}|_n} = \text{known}. \quad (72)$$

When the damage indicator $I_f|_{n+1}$ reaches the critical value $I_f|_{n+1} = 1$, the material loses its load carrying capacity at that Gauss point.

Equations (64) and (65) are integrated exactly:

$$\Delta \mathbf{E} = \Delta \mathbf{E}^e + \Delta \mathbf{E}^p, \quad (73)$$

$$\hat{\boldsymbol{\sigma}}_{n+1} = \hat{\boldsymbol{\sigma}}^e - \mathcal{L}^e : \Delta \mathbf{E}^p = \hat{\boldsymbol{\sigma}}^e - 2G \Delta \mathbf{E}^p - \left(\kappa - \frac{2}{3} G \right) \Delta E_{kk}^p \boldsymbol{\delta}, \quad (74)$$

where $\hat{\boldsymbol{\sigma}}^e = \boldsymbol{\sigma}_n + \mathcal{L}^e : \Delta \mathbf{E}$ is known is the ‘‘elastic predictor’’ and the notation $\Delta A = A_{n+1} - A_n$ is used.

If the elastic predictor does not violate the yield condition, i.e., $\Phi(\hat{\boldsymbol{\sigma}}^e, \bar{\boldsymbol{\varepsilon}}_n^p, D_n) \leq 0$, then

$$\boldsymbol{\sigma}_{n+1} = \mathbf{R}_{n+1} \cdot \hat{\boldsymbol{\sigma}}^e \cdot \mathbf{R}_{n+1}^T, \quad \bar{\boldsymbol{\varepsilon}}_{n+1}^p = \bar{\boldsymbol{\varepsilon}}_n^p, \quad D_{n+1} = D_n, \quad (75)$$

and the integration is completed.

If $\Phi(\hat{\boldsymbol{\sigma}}^e, \bar{\boldsymbol{\varepsilon}}_n^p, D_n) > 0$, plastic deformation takes place over the increment and a backward Euler scheme is used for the numerical integration of the flow rule (67):

$$\Delta \mathbf{E}^p = \Delta \lambda \mathbf{P}(\hat{\boldsymbol{\sigma}}_{n+1}, \bar{\boldsymbol{\varepsilon}}_{n+1}^p) = \Delta \lambda \left(\frac{1}{3} \frac{\partial \Phi}{\partial \mathbf{p}} \boldsymbol{\delta} + \frac{\partial \Phi}{\partial \sigma_e} \hat{\mathbf{N}} + \frac{1}{\sigma_e} \frac{\partial \Phi}{\partial \theta} \hat{\mathbf{M}} \right)_{n+1}. \quad (76)$$

Finally, the increment of the local equivalent plastic strain increment $\Delta \bar{\varepsilon}^p$ is determined from the expression

$$\Delta \bar{\varepsilon}^p = \sqrt{\frac{2}{3} \Delta \mathbf{E}^p : \Delta \mathbf{E}^p}. \quad (77)$$

The integration algorithm can be summarized as follows. The quantities $\Delta \lambda$ and $\Delta \mathbf{E}^p$ are treated as the primary unknowns and the yield condition (66) and the plastic flow rule (76)

$$\Phi(\hat{\boldsymbol{\sigma}}_{n+1}, \bar{\boldsymbol{\varepsilon}}_{n+1}^p) = 0, \quad (78)$$

$$\Delta \mathbf{E}^p - \Delta \lambda \mathbf{P}(\hat{\boldsymbol{\sigma}}_{n+1}, \bar{\boldsymbol{\varepsilon}}_{n+1}^p) = \mathbf{0}, \quad (79)$$

are treated as the basic equations, in which $\hat{\boldsymbol{\sigma}}_{n+1}$ and $\bar{\boldsymbol{\varepsilon}}_{n+1}^p$ are determined in terms of $\Delta \mathbf{E}^p$ as follows:

$$\hat{\boldsymbol{\sigma}}_{n+1}(\Delta \mathbf{E}^p) = \hat{\boldsymbol{\sigma}}^e - 2G \Delta \mathbf{E}^p - \left(\kappa - \frac{2}{3} G \right) \Delta E_{kk}^p \boldsymbol{\delta}, \quad (80)$$

$$\bar{\boldsymbol{\varepsilon}}_{n+1}^p(\Delta \mathbf{E}^p) = \bar{\boldsymbol{\varepsilon}}_n^p + \sqrt{\frac{2}{3} \Delta \mathbf{E}^p : \Delta \mathbf{E}^p}. \quad (81)$$

Equations (78) and (79) are solved for $\Delta \lambda$ and $\Delta \mathbf{E}^p$ by using Newton’s method. In every iteration, for the current values of $\Delta \lambda$ and $\Delta \mathbf{E}^p$, $\hat{\boldsymbol{\sigma}}_{n+1}$ and $\bar{\boldsymbol{\varepsilon}}_{n+1}^p$ are calculated by using (80) and (81). Once $\Delta \lambda$ and $\Delta \mathbf{E}^p$ are found, equations (80) and (81) define $\hat{\boldsymbol{\sigma}}_{n+1}$ and $\bar{\boldsymbol{\varepsilon}}_{n+1}^p$. Finally, $\boldsymbol{\sigma}_{n+1}$ is computed from

$$\boldsymbol{\sigma}_{n+1} = \mathbf{R}_{n+1} \cdot \hat{\boldsymbol{\sigma}}_{n+1} \cdot \mathbf{R}_{n+1}^T, \quad (82)$$

which completes the integration process.

As the solution develops, the quantities $A \equiv \int_0^{\hat{\varepsilon}^p} \eta d\hat{\varepsilon}^p$ and $B \equiv \int_0^{\hat{\varepsilon}^p} \bar{\theta} d\hat{\varepsilon}^p$ are calculated and stored. In particular, at the end of every increment η_{av} and $\bar{\theta}_{\text{av}}$ are calculate and stored:

$$\Delta A = \frac{\eta_n + \eta_{n+1}}{2} \Delta \hat{\varepsilon}^p, \quad A_{n+1} = A_n + \Delta A, \quad \eta_{\text{av}}|_{n+1} = \frac{A_{n+1}}{\hat{\varepsilon}_{n+1}^p}, \quad (83)$$

$$\Delta B = \frac{\bar{\theta}_n + \bar{\theta}_{n+1}}{2} \Delta \hat{\varepsilon}^p, \quad B_{n+1} = B_n + \Delta B, \quad \bar{\theta}_{\text{av}}|_{n+1} = \frac{B_{n+1}}{\hat{\varepsilon}_{n+1}^p}. \quad (84)$$

The computer implementation of the algorithm outlined above is simplified if principal directions are used as described in the following (see also Simo (1998); Auricchio and Taylor (1999); Borja et al. (2003)). Equation (76) shows that ΔE^p is co-axial with $\hat{\sigma}_{n+1}$. Then from (80) we conclude that $\hat{\sigma}^e$ is also co-axial with $\hat{\sigma}_{n+1}$. Therefore the eigenvectors $\hat{\mathbf{n}}^{(i)}$ of the (as yet unknown) tensors $\hat{\sigma}_{n+1}$ and ΔE^p can be determined from the eigenvectors of the (known) elastic predictor $\hat{\sigma}^e$. With known $\hat{\mathbf{n}}^{(i)}$, we write

$$\hat{\sigma}_{n+1} = \sum_{i=1}^3 \sigma_i \hat{\mathbf{n}}^{(i)} \hat{\mathbf{n}}^{(i)} \quad \text{and} \quad \Delta E^p = \sum_{i=1}^3 \Delta E_i^p \hat{\mathbf{n}}^{(i)} \hat{\mathbf{n}}^{(i)}, \quad (85)$$

and the problem reduces to the determination of the principal components ΔE_i^p and σ_i . In this case, the quantities $\Delta \lambda$ and ΔE_i^p are treated as the primary unknowns and equations (78)–(81) simplify to

$$\Phi(\sigma_1, \sigma_2, \sigma_3, \bar{\varepsilon}_{n+1}^p) = 0, \quad (86)$$

$$\Delta \varepsilon_i^p - \Delta \lambda P_i(\sigma_1, \sigma_2, \sigma_3, \bar{\varepsilon}_{n+1}^p) = 0 \quad (i = 1, 2, 3), \quad (87)$$

where

$$\sigma_i(\Delta E_1^p, \Delta E_2^p, \Delta E_3^p) = \sigma_i^e - 2G \Delta E_i^p - \left(\kappa - \frac{2}{3}G \right) (\Delta E_1^p + \Delta E_2^p + \Delta E_3^p), \quad (88)$$

$$\bar{\varepsilon}_{n+1}^p(\Delta E_1^p, \Delta E_2^p, \Delta E_3^p) = \bar{\varepsilon}_n^p + \sqrt{\frac{2}{3} \left[(\Delta E_1^p)^2 + (\Delta E_2^p)^2 + (\Delta E_3^p)^2 \right]}, \quad (89)$$

$$p = \frac{\sigma_1 + \sigma_2 + \sigma_3}{3}, \quad s_i = \sigma_i - p, \quad \sigma_e = \sqrt{\frac{3}{2} (s_1^2 + s_2^2 + s_3^2)}, \quad (90)$$

$$J_3 = s_1 s_2 s_3, \quad \theta = \frac{1}{3} \sin^{-1} \left(-\frac{27 J_3}{2 \sigma_e^3} \right), \quad \theta_i = \theta + (5 - 4i) \frac{\pi}{6}, \quad (91)$$

$$N_i = \cos \theta_i, \quad M_i = -\sin \theta_i, \quad P_i = \frac{1}{3} \frac{\partial \Phi}{\partial p} + \frac{\partial \Phi}{\partial \sigma_e} N_i + \frac{1}{\sigma_e} \frac{\partial \Phi}{\partial \theta} M_i. \quad (92)$$

The system of **four non-linear equations** (86)–(87) is solved for the four unknowns $(\Delta \lambda, \Delta E_1^p, \Delta E_2^p, \Delta E_3^p)$.

4.1. Plastic incompressibility

The problem is simplified further if the material is plastically incompressible ($\frac{\partial \Phi}{\partial p} = 0$ and $D_{kk}^p = 0$). In this case we set $\Delta E_3^p = -(\Delta E_1^p + \Delta E_2^p)$, eliminate $\Delta \lambda$ from (87), and treat $(\Delta E_1^p, \Delta E_2^p)$ as the primary unknowns to find

$$\Phi(\sigma_i, \bar{\varepsilon}_{n+1}^p) = 0, \quad (93)$$

$$\Delta E_1^p P_2(\sigma_i, \bar{\varepsilon}_{n+1}^p) - \Delta E_2^p P_1(\sigma_i, \bar{\varepsilon}_{n+1}^p) = 0, \quad (94)$$

where

$$\sigma_1(\Delta E_1^p) = \sigma_1^e - 2G \Delta E_1^p, \quad \sigma_2(\Delta E_2^p) = \sigma_2^e - 2G \Delta E_2^p, \quad (95)$$

$$\sigma_3(\Delta E_1^p, \Delta E_2^p) = \sigma_3^e + 2G(\Delta E_1^p + \Delta E_2^p), \quad (96)$$

$$\bar{\varepsilon}_{n+1}^p(\Delta E_1^p, \Delta E_2^p) = \bar{\varepsilon}_n^p + \sqrt{\frac{4}{3} \left[(\Delta E_1^p)^2 + (\Delta E_2^p)^2 + \Delta E_1^p \Delta E_2^p \right]}. \quad (97)$$

The problem reduces now to the solution of the **two non-linear equations** (93) and (94) for $(\Delta E_1^p, \Delta E_2^p)$.

4.2. Rate-dependent plasticity

If rate-dependent plasticity is used, equations (78), (86), and (93) above should be replaced by their corresponding forms of the rate-dependent yield function (23):

$$\Phi(\boldsymbol{\sigma}, \Sigma_y(\bar{\boldsymbol{\varepsilon}}^p, \dot{\bar{\boldsymbol{\varepsilon}}}^p), D) = 0, \quad (98)$$

in which the approximation $\dot{\bar{\boldsymbol{\varepsilon}}}^p \cong (\bar{\boldsymbol{\varepsilon}}_{n+1}^p - \bar{\boldsymbol{\varepsilon}}_n^p)/\Delta t$ is used. In other words, equations (78), (86), and (93) are replaced by

$$\Phi\left(\hat{\boldsymbol{\sigma}}_{n+1}, \Sigma_y\left(\bar{\boldsymbol{\varepsilon}}_{n+1}^p, \frac{\bar{\boldsymbol{\varepsilon}}_{n+1}^p - \bar{\boldsymbol{\varepsilon}}_n^p}{\Delta t}\right), D_{n+1}\right) = 0, \quad (99)$$

where $\hat{\boldsymbol{\sigma}}_{n+1}$ and $\bar{\boldsymbol{\varepsilon}}_{n+1}^p$ are defined in terms of the primary unknowns $(\Delta\lambda, \Delta E_i^p)$ by (80)–(81) or (88)–(89) or (95)–(97), and D_{n+1} is known and determined by (72b). Then, the solution follows the lines described for rate-independent materials.

Equation (99) can be thought of as a backward Euler scheme of the evolution equation for the equivalent plastic strain given in (24b).

5. Finite element formulation

Let Ω be the domain occupied by the elastoplastic body in its deformed state, $\partial\Omega$ its boundary, and \mathbf{n} the unit outward normal vector to $\partial\Omega$. The position of material particles in the deformed configuration is denoted by \mathbf{x} , t is time, ρ is the current mass density of the material, \mathbf{b} the body force per unit mass, and $(\mathbf{u}, \boldsymbol{\sigma})$ are the displacement and true (Cauchy) stress fields in the body.

Let \mathbf{u} be specified on a part $\partial_u\Omega$ as $\hat{\mathbf{u}}$ (given) and let the traction vector be specified on $\partial_\sigma\Omega$ as $\boldsymbol{\sigma} \cdot \mathbf{n} = \hat{\mathbf{t}}$ (given), where the parts $\partial_u\Omega$ and $\partial_\sigma\Omega$ are disjoint ($\partial_u\Omega \cap \partial_\sigma\Omega = \emptyset$) with $\partial_u\Omega \cup \partial_\sigma\Omega = \partial\Omega$.

In the following we discuss the finite element implementation of the elastoplastic boundary value problem. In view of the non-linearity of the problem, the calculations are carried out incrementally. Traditional finite element formulations use the displacement field $\mathbf{u}(\mathbf{x})$ as the primary unknown and the elastoplastic constitutive equations are integrated locally at the Gauss points of the elements in the mesh; the resulting values of the *local* equivalent plastic strain field $\bar{\varepsilon}^p(\mathbf{x})$ are, in general, discontinuous across element boundaries. In the present model, the BVP (36)–(37), that defines the *non-local* equivalent plastic strain field $e^p(\mathbf{x})$, puts additional continuity requirements on e^p . Therefore, we treat the displacements $\mathbf{u}(\mathbf{x})$ and the non-local equivalent plastic strain $e^p(\mathbf{x})$ as the primary unknowns and introduce finite element interpolations for both \mathbf{u} and e^p to obtain the corresponding non-linear discrete problem.

We discuss two possible methods of implementation of the non-local elastoplastic problem in the ABAQUS general-purpose finite element code. In the first method, “user elements” are developed for the solution of quasi-static and dynamic problems in ABAQUS/Standard and ABAQUS/Explicit via “user subroutines” UEL and VUEL respectively. In section 5.1 we present a traditional $(\mathbf{u} - e^p)$ formulation, in which the displacement $\mathbf{u}(\mathbf{x})$ and the non-local equivalent plastic strain fields are independently interpolated.

Failure analysis of 3D structures is often based on the finite element method with damage mechanics constitutive models. Such 3D calculations are time consuming because small time increments must be used, especially when the material enters the softening regime. One commonly used element in such calculations is the 8-node hexahedron with one Gauss integration point. The use of reduced one Gauss integration station, as opposed to eight, introduces numerical singularities to the problem and some kind of “hourglass control” is required (e.g., see Flanagan and Belytschko (1981)). In section 5.2 we discuss the development of a 3D isoparametric 8-node hexahedral element with one Gauss point that is used together with the damage model described in the present paper. We use the “enhanced strain” method of Simo and Rifai (1990) to avoid the aforementioned singularities. The element is implemented in ABAQUS/Standard and ABAQUS/Explicit and quasi-static and dynamic problems are solved.

A second possible method for the implementation of non-local constitutive models in ABAQUS is discussed in sections 6 and 7. In section 6 we show how non-local *quasi-static* problems (acceleration $\ddot{\mathbf{u}} \simeq \mathbf{0}$) can be solved by using the so-called *COUPLED TEMPERATURE-DISPLACEMENT analysis option in ABAQUS/Standard together with user subroutine UMAT. This minimizes the programming effort and allows for the use of all finite elements available in the library of ABAQUS/Standard. This approach cannot be used with ABAQUS/Standard in *dynamic* problems. Non-local *dynamic* problems can be solved by using ABAQUS/Explicit together with user subroutine VUMAT as discussed in section 7.

5.1. Traditional ($\mathbf{u} - e^p$) formulation

The displacement field $\mathbf{u}(\mathbf{x})$ and the non-local equivalent plastic strain $e^p(\mathbf{x})$ are treated as the primary unknowns. A variational formulation of the problem is:

Find $\mathbf{u}(\mathbf{x}, t)$ and $e^p(\mathbf{x}, t)$ satisfying $\mathbf{u}|_{\partial_n\Omega} = \hat{\mathbf{u}}$ such that

$$\int_{\Omega} \left[\sigma_{ij,j}(\mathbf{u}, e^p) + \rho(b_i - \ddot{u}_i) \right] u_i^* d\Omega + \int_{\partial_\sigma\Omega} \left[\hat{t}_i - \sigma_{ij}(\mathbf{u}, e^p) n_j \right] u_i^* dS = 0, \quad (100)$$

$$\int_{\Omega} \left[e^p - \ell^2 \nabla^2 e^p - \bar{\varepsilon}^p(\mathbf{u}, e^p) \right] e^{*} d\Omega + \int_{\partial\Omega} \ell^2 \frac{\partial e^p}{\partial n} e^{*} dS = 0, \quad (101)$$

for all variations \mathbf{u}^* and e^* with $\mathbf{u}^* = \mathbf{0}$ on $\partial_n\Omega$, where a comma followed by a subscript, say i , denotes partial differentiation with respect to the corresponding spatial coordinate x_i , i.e., $f_{,i} = \partial f / \partial x_i$. Integration by parts in (100) and (101) leads to the following weak form:

Find $\mathbf{u}(\mathbf{x}, t)$ and $e^p(\mathbf{x}, t)$ satisfying $\mathbf{u}|_{\partial_n\Omega} = \hat{\mathbf{u}}$ such that

$$\int_{\Omega} \rho b_i u_i^* d\Omega + \int_{\partial_\sigma\Omega} \hat{t}_i u_i^* dS - \int_{\Omega} \sigma_{ij}(\mathbf{u}, e^p) D_{ij}^*(\mathbf{u}^*) d\Omega = \int_{\Omega} \rho \ddot{u}_i u_i^* d\Omega \quad \forall \mathbf{u}^* \in \mathcal{U}, \quad (102)$$

$$\int_{\Omega} \left\{ [\bar{\varepsilon}^p(\mathbf{u}, e^p) - e^p] e^{*} - \ell^2 e_{,i}^p e_{,i}^* \right\} d\Omega = 0 \quad \forall e^* \in \mathcal{E}, \quad (103)$$

where $D_{ij}^*(\mathbf{u}^*) = (u_{i,j}^* + u_{j,i}^*)/2$, and

$$\mathcal{U} = \{ \mathbf{u}^* | \mathbf{u}^* \in H^1(\Omega), \mathbf{u}^*|_{\partial_n\Omega} = \mathbf{0} \}, \quad \mathcal{E} = \{ e^* | e^* \in H^1(\Omega) \}, \quad (104)$$

with H^k consisting of all functions that possess square-integrable spatial derivatives through order k .

Equations (102) and (103) form the basis of the finite element solutions in ABAQUS/Standard and ABAQUS/Explicit via user subroutines UEL and VUEL respectively. Four-node plane strain quadrilateral elements with 2×2 Gauss integration points and 3D 8-node hexahedral elements with $2 \times 2 \times 2$ Gauss stations are developed. The displacement $\mathbf{u}(\mathbf{x})$ and non-local equivalent plastic strain $e^p(\mathbf{x})$ fields are interpolated independently, and the nodal degrees of freedom are the components of \mathbf{u} and the values of e^p . Standard bi-linear (2D) or tri-linear (3D) isoparametric interpolations are used for both \mathbf{u} and e^p within an element. The constitutive equations are integrated numerically by using the algorithm described in section 4. Both quasi-static and dynamic problems are solved using either ABAQUS/Standard or ABAQUS/Explicit.

5.2. Enhanced strain formulation

To improve the computational efficiency in 3D problems, we use the so-called ‘‘enhanced strain method’’ of Simo and Rifai (1990) to develop a 3D 8-node hexahedral isoparametric element with one Gauss integration point. The enhanced strain method belongs to the category of ‘‘mixed finite element methods’’, which typically lead to lower-order continuity requirements on some of the fields. In such methods, static condensation of some variables at the element level is usually performed when appropriate in order to keep the total number of global degrees of freedom to a minimum. The solution is developed incrementally and the displacement field $\mathbf{u}_{n+1}(\mathbf{x})$, the spatial gradient of the displacement increment

$$\Delta \mathbf{L}_{n+1}(\mathbf{x}) \equiv \frac{\partial \Delta \mathbf{u}(\mathbf{x})}{\partial \mathbf{x}_{n+1}}, \quad (105)$$

the stress field $\boldsymbol{\sigma}_{n+1}(\mathbf{x})$, and the non-local equivalent plastic strain $e_{n+1}^p(\mathbf{x})$ are treated as independent unknowns and their relations are enforced in a weighted integral sense. In the weak form of the problem the displacement field approximation must be $H^1(\Omega)$. Approximations for e^p , $\Delta \mathbf{L}$, and $\boldsymbol{\sigma}$ need only be in $L^2(\Omega)$, where $L^2 = H^0$ is the space of all square-integrable functions. No interelement continuity is required on $(\Delta \mathbf{L}, \boldsymbol{\sigma})$ and they may be eliminated in favor of the displacement degrees of freedom by static condensation at the element level.

The variational formulation of the problem is as follows:

Given $(\mathbf{u}_n(\mathbf{x}), e_n^p(\mathbf{x}), \boldsymbol{\tau}_n(\mathbf{x}), \mathbf{g}_n(\mathbf{x}), \mathbf{q}_n(\mathbf{x}))$, find $(\Delta \mathbf{u}(\mathbf{x}), \Delta e^p(\mathbf{x}), \Delta \mathbf{L}(\mathbf{x}), \boldsymbol{\tau}(\mathbf{x}), \Delta \mathbf{g}(\mathbf{x}), \Delta \mathbf{q}(\mathbf{x}))$, satisfying $\mathbf{u}|_{\partial_t \Omega} = \hat{\mathbf{u}}$ such that

$$\int_{\Omega} \rho b_i u_i^* d\Omega + \int_{\partial_t \Omega} \hat{t}_i u_i^* dS - \int_{\Omega} \tau_{ij} u_{i,j}^* d\Omega = \int_{\Omega} \rho \ddot{u}_i u_i^* d\Omega \quad \forall \mathbf{u}^* \in \mathcal{U}, \quad (106)$$

$$\int_{\Omega} [\tau_{ij} - \sigma_{ij}(\Delta \mathbf{L}, \Delta e^p)] L_{ij}^* d\Omega = 0 \quad \forall \mathbf{L}^* \in L^2(\Omega), \quad (107)$$

$$\int_{\Omega} (\Delta L_{ij} - \Delta u_{i,j}) \sigma_{ij}^* d\Omega = 0 \quad \forall \boldsymbol{\sigma}^* \in L^2(\Omega), \quad (108)$$

$$\int_{\Omega} [e^p + q_{i,i} - \bar{\varepsilon}^p(\Delta \mathbf{L}, \Delta e^p)] e^* d\Omega - \int_{\partial \Omega} q_i n_i e^* dS = 0 \quad \forall e^* \in \mathcal{E}, \quad (109)$$

$$\int_{\Omega} (q_i + \ell^2 g_i) g_i^* d\Omega = 0 \quad \forall g_i^* \in L^2(\Omega), \quad (110)$$

$$\int_{\Omega} (\Delta g_i - \Delta e_{,i}^p) q_i^* d\Omega = 0 \quad \forall q_i^* \in L^2(\Omega), \quad (111)$$

where all quantities are evaluated at the end of the increment ($t = t_{n+1}$). In (106) and (107), $\boldsymbol{\tau}$ is the *independently* interpolated stress field, whereas $\boldsymbol{\sigma}(\Delta \mathbf{L}, e^p)$ and $\bar{\varepsilon}^p(\Delta \mathbf{L}, \Delta e^p)$ are the stress field and local equivalent plastic strain field computed from $\Delta \mathbf{L}$ and Δe^p by the constitutive equations. Also \mathbf{g} is the *independently* interpolated non-local equivalent plastic strain gradient and \mathbf{q} a generalized stress conjugate to \mathbf{g} , and the conditions $\Delta g_i = \Delta e_{,i}^p$ and $q_i = -\ell^2 e_{,i}^p$ are enforced through the weighted integral statements (110) and (111).

Next, we i) combine (106) and (107), ii) integrate by parts in (109), and iii) combine (109) and (110), to reach the alternative formulation:

Find $(\Delta \mathbf{u}, \Delta e^p, \Delta \mathbf{L}, \boldsymbol{\tau}, \Delta \mathbf{g}, \Delta \mathbf{q})$ such that

$$\begin{aligned} \int_{\Omega} \rho b_i u_i^* d\Omega + \int_{\partial_t \Omega} \hat{t}_i u_i^* dS - \int_{\Omega} \sigma_{ij}(\Delta \mathbf{L}, \Delta e^p) L_{ij}^* d\Omega + \\ + \int_{\Omega} \tau_{ij} (L_{ij}^* - u_{i,j}^*) d\Omega = \int_{\Omega} \rho \ddot{u}_i u_i^* d\Omega \quad \forall \mathbf{u}^* \in \mathcal{U}, \mathbf{L}^* \in L^2(\Omega), \end{aligned} \quad (112)$$

$$\int_{\Omega} (\Delta L_{ij} - \Delta u_{i,j}) \tau_{ij}^* d\Omega = 0 \quad \forall \boldsymbol{\tau}^* \in L^2(\Omega), \quad (113)$$

$$\int_{\Omega} \left\{ [\bar{\varepsilon}^p(\Delta \mathbf{L}, \Delta e^p) - e^p] e^* - \ell^2 g_i g_i^* \right\} d\Omega + \int_{\Omega} q_i (e_{,i}^* - g_i^*) d\Omega = 0 \quad \forall e^* \in \mathcal{E}, g_i^* \in L^2(\Omega), \quad (114)$$

$$\int_{\Omega} (\Delta e_{,i}^p - \Delta g_i) q_i^* d\Omega = 0 \quad \forall q_i^* \in L^2(\Omega). \quad (115)$$

Following Simo and Hughes (1986) and Simo and Rifai (1990), we chose the independent stress fields $\boldsymbol{\tau}(\mathbf{x})$ to be orthogonal to the difference between the interpolant $\Delta \mathbf{L}(\mathbf{x})$ and the spatial gradient of the displacement increment $\partial \Delta \mathbf{u}(\mathbf{x}) / \partial \mathbf{x}$, so that (113) is satisfied automatically and the last integral on the left hand side of (112) vanishes. Similarly, we chose $\mathbf{q}(\mathbf{x})$ to be orthogonal to the difference $\Delta \mathbf{g}(\mathbf{x}) - \nabla(\Delta e^p(\mathbf{x}))$, so that (115) is satisfied automatically and the last integral on the left hand side of (114) vanishes (see (139) and (140) below).

In particular, independent interpolations are used for $(\Delta \mathbf{u}, \Delta \mathbf{L}, \boldsymbol{\tau}, \Delta e^p, \Delta \mathbf{g}, \Delta \mathbf{q})$ within each element:

$$\{\Delta \mathbf{u}(\mathbf{x})\} = \begin{bmatrix} \mathbf{N}(\mathbf{x}) \\ \mathbf{B}_L(\mathbf{x}) \end{bmatrix} \{\Delta \mathbf{d}^e\}, \quad (116)$$

$$\{\Delta \mathbf{L}(\mathbf{x})\} = \left(\overline{\mathbf{B}_L} + \mathbf{B}_{\text{stab}}(\mathbf{x}) \right) \{\Delta \mathbf{d}^e\} + \mathbf{G}(\mathbf{x}) \{\Delta \mathbf{a}^e\}, \quad (117)$$

$$\{\boldsymbol{\tau}(\mathbf{x})\} = \{\boldsymbol{\tau}_0\} = \text{const.}, \quad (118)$$

and

$$\Delta e^p(\mathbf{x}) = \mathbf{N}_\varepsilon(\mathbf{x}) \{\Delta \mathbf{d}^e\}, \quad (119)$$

$$\{\Delta \mathbf{g}(\mathbf{x})\} = \left(\overline{\mathbf{B}_\varepsilon} + \mathbf{B}_\varepsilon^{\text{stab}}(\mathbf{x}) \right) \{\Delta \mathbf{d}^e\}, \quad (120)$$

$$\{\mathbf{q}(\mathbf{x})\} = \{\mathbf{q}_0\} = \text{const.}, \quad (121)$$

where $\{\Delta \mathbf{d}^e\}$ is the vector of the 32 nodal degrees of freedom corresponding to $\Delta \mathbf{u}$ and Δe^p in the 3D 8-node element and $\{\Delta \mathbf{a}^e\}$ is a vector of six local parameters for each individual element and provide the required additional degrees of freedom to eliminate locking in incompressible or nearly incompressible materials (Puso (2000)). The local element internal parameters $\{\Delta \mathbf{a}^e\}$ are eventually eliminated by ‘‘static condensation’’, i.e., determined in terms of $\{\Delta \mathbf{d}^e\}$ as described in the following.

The constant matrices $\overline{\mathbf{B}_L}$ and $\overline{\mathbf{B}_\varepsilon}$ are defined as (Flanagan and Belytschko (1981))

$$\overline{\mathbf{B}_L} = \frac{1}{V_e} \int_{\Omega^e} \mathbf{B}_L(\mathbf{x}) d\Omega \quad \text{and} \quad \overline{\mathbf{B}_\varepsilon} = \frac{1}{V_e} \int_{\Omega^e} \mathbf{B}_\varepsilon(\mathbf{x}) d\Omega, \quad (122)$$

where Ω_e is the domain of element e , V_e the volume of element e , and $(\mathbf{B}_L, \mathbf{B}_\varepsilon)$ are the standard ‘‘ \mathbf{B} -matrices’’ defined in terms of the spatial derivatives of $[\mathbf{N}]$ and $[\mathbf{N}_\varepsilon]$ that enter the calculation of the following gradients:

$$\{\Delta u_{i,j}(\mathbf{x})\} = \mathbf{B}_L(\mathbf{x}) \{\Delta \mathbf{d}^e\} \quad \text{and} \quad \{\Delta e_{,i}^p(\mathbf{x})\} = \mathbf{B}_\varepsilon(\mathbf{x}) \{\Delta \mathbf{d}^e\}. \quad (123)$$

The form of the interpolation matrices $([\mathbf{N}], [\mathbf{B}_{\text{stab}}], [\mathbf{G}], [\mathbf{N}_\varepsilon], [\mathbf{B}_\varepsilon^{\text{stab}}])$ is discussed in detail in Appendix A. Here we mention that matrices $[\mathbf{B}_{\text{stab}}(\mathbf{x})]$, $[\mathbf{G}(\mathbf{x})]$, and $[\mathbf{B}_\varepsilon^{\text{stab}}(\mathbf{x})]$ are defined so that

$$\int_{\Omega^e} [\mathbf{B}_{\text{stab}}(\mathbf{x})] d\Omega = [\mathbf{0}], \quad \int_{\Omega^e} [\mathbf{G}(\mathbf{x})] d\Omega = [\mathbf{0}], \quad \text{and} \quad \int_{\Omega^e} [\mathbf{B}_\varepsilon^{\text{stab}}(\mathbf{x})] d\Omega = [\mathbf{0}], \quad (124)$$

which guarantee the satisfaction of the aforementioned orthogonality conditions (see equations (139) and (140) below). Also, condition (124b) is essential for the finite elements to pass the ‘‘patch test’’ (Taylor et al. (1976); Flanagan and Belytschko (1981)).

Remarks

1. Analytical expressions for the components of the constant matrices $\overline{\mathbf{B}_L}$ and $\overline{\mathbf{B}_\varepsilon}$ are given in Flanagan and Belytschko (1981).
2. The enhanced gradient fields in (117) and (120) are richer than the standard gradients in (123). The presence of the additional matrices $[\mathbf{B}_{\text{stab}}(\mathbf{x})]$, $[\mathbf{G}(\mathbf{x})]$, and $[\mathbf{B}_\varepsilon^{\text{stab}}(\mathbf{x})]$ removes the singularities when reduced one-point Gauss integration is used. This is also discussed right after equations (149)–(150) below.

3. The enhanced gradients (117) and (120) can be written in the form

$$\{\Delta \mathbf{L}(\mathbf{x})\} = \overline{\{\Delta \mathbf{L}\}} + \{\Delta \mathbf{L}_{\text{stab}}(\mathbf{x})\} + \{\Delta \mathbf{L}_{\text{lock}}(\mathbf{x})\}, \quad (125)$$

$$\{\Delta \mathbf{g}(\mathbf{x})\} = \overline{\{\Delta \mathbf{g}\}} + \{\Delta \mathbf{g}_{\text{stab}}(\mathbf{x})\}, \quad (126)$$

where we took into account (124), an overbar indicates the average value over the element, and

$$\overline{\{\Delta \mathbf{L}\}} = \overline{[\mathbf{B}_L]} \{\Delta \mathbf{d}^e\}, \quad \overline{\{\Delta \mathbf{g}\}} = \overline{[\mathbf{B}_\varepsilon]} \{\Delta \mathbf{d}^e\}, \quad (127)$$

$$\{\Delta \mathbf{L}_{\text{stab}}(\mathbf{x})\} = [\mathbf{B}_{\text{stab}}(\mathbf{x})] \{\Delta \mathbf{d}^e\}, \quad \{\Delta \mathbf{g}_{\text{stab}}(\mathbf{x})\} = [\mathbf{B}_\varepsilon^{\text{stab}}(\mathbf{x})] \{\Delta \mathbf{d}^e\}, \quad (128)$$

$$\{\Delta \mathbf{L}_{\text{lock}}(\mathbf{x})\} = [\mathbf{G}(\mathbf{x})] \{\Delta \mathbf{a}^e\}. \quad (129)$$

I.e., the enhanced gradients $\{\Delta \mathbf{L}(\mathbf{x})\}$ and $\{\Delta \mathbf{g}(\mathbf{x})\}$ include a constant part and a stabilization part that removes the spurious modes when reduced one-point Gauss integration is used; an independent field $\{\Delta \mathbf{L}_{\text{lock}}\}$ is also added to $\{\Delta \mathbf{L}\}$ to eliminate locking in incompressible or nearly incompressible materials.

4. Conditions (124) imply that

$$\overline{\{\Delta \mathbf{L}\}} = \overline{\{\Delta u_{i,j}\}} = \overline{[\mathbf{B}_L]} \{\Delta \mathbf{d}^e\}, \quad (130)$$

$$\overline{\{\Delta \mathbf{g}\}} = \overline{\{\Delta e_{,i}^p\}} = \overline{[\mathbf{B}_\varepsilon]} \{\Delta \mathbf{d}^e\}. \quad (131)$$

5. The gradients $(\Delta \mathbf{L}, \Delta \mathbf{g})$ and the “stresses” $(\boldsymbol{\tau}, \mathbf{q})$ defined in (117)–(118) and (120)–(121) are, in general, discontinuous across elements.

6. The stresses $\boldsymbol{\sigma}(\Delta \mathbf{L}, e^p)$ that balance the external forces in the “virtual work statement” (112) are determined from the enhanced incremental displacement gradient $\Delta \mathbf{L}$ (as opposed to the gradient $\Delta u_{i,j}$) and this is what makes the method successful.

7. The stresses $\boldsymbol{\sigma}(\Delta \mathbf{L}, e^p)$ are determined using the algorithm described in section 4. The required value of the deformation gradient \mathbf{F}_{n+1} is determined as

$$\mathbf{F}_{n+1} = (\exp \Delta \mathbf{L}) \cdot \mathbf{F}_n, \quad (132)$$

which results from integration of the equation $\dot{\mathbf{F}} = \mathbf{L} \cdot \mathbf{F}$, under the assumption that the velocity gradient $\mathbf{L} = \mathbf{D} + \mathbf{W}$ is constant over the increment with $\Delta \mathbf{L} = \mathbf{L} \Delta t$.

8. In Appendix A we introduce the standard isoparametric transformation that relates the physical coordinates \mathbf{x} to the element “natural coordinates” $\boldsymbol{\xi}$ and define matrices $[\mathbf{B}_{\text{stab}}(\mathbf{x})]$, $[\mathbf{G}(\mathbf{x})]$, and $[\mathbf{B}_\varepsilon^{\text{stab}}(\mathbf{x})]$ so that they all vanish at the element local origin $\boldsymbol{\xi} = \mathbf{0}$, i.e.,

$$[\mathbf{B}_{\text{stab}}]_{\boldsymbol{\xi}=\mathbf{0}} = [\mathbf{0}], \quad [\mathbf{G}]_{\boldsymbol{\xi}=\mathbf{0}} = [\mathbf{0}], \quad [\mathbf{B}_\varepsilon^{\text{stab}}]_{\boldsymbol{\xi}=\mathbf{0}} = [\mathbf{0}]. \quad (133)$$

Using (133) in (117) and (120), and taking into account (124), we conclude that

$$\{\Delta \mathbf{L}\}_{\boldsymbol{\xi}=\mathbf{0}} = \overline{\{\Delta \mathbf{L}\}} = \overline{\{\Delta u_{i,j}\}} = \overline{[\mathbf{B}_L]} \{\Delta \mathbf{d}^e\}, \quad (134)$$

$$\{\Delta \mathbf{g}\}_{\boldsymbol{\xi}=\mathbf{0}} = \overline{\{\Delta \mathbf{g}\}} = \overline{\{\Delta e_{,i}^p\}} = \overline{[\mathbf{B}_\varepsilon]} \{\Delta \mathbf{d}^e\}. \quad \square \quad (135)$$

The interpolations for the “virtual fields” $(\mathbf{u}^*, \mathbf{L}^*, \boldsymbol{\tau}^*, e^*, \mathbf{g}^*, \mathbf{q}^*)$ are:

$$\begin{matrix} \{\mathbf{u}^*\} \\ 3 \times 1 \end{matrix} = \begin{matrix} [\mathbf{N}] \\ 3 \times 32 \end{matrix} \begin{matrix} \{\mathbf{d}^*\} \\ 32 \times 1 \end{matrix}, \quad e^* = \begin{matrix} [\mathbf{N}_\varepsilon] \\ 1 \times 32 \end{matrix} \begin{matrix} \{\mathbf{d}^{*e}\} \\ 32 \times 1 \end{matrix}, \quad (136)$$

$$\begin{matrix} \{\mathbf{L}^*\} \\ 9 \times 1 \end{matrix} = \left(\overline{[\mathbf{B}_L]} + [\mathbf{B}_{\text{stab}}] \right) \begin{matrix} \{\mathbf{d}^*\} \\ 32 \times 1 \end{matrix} + [\mathbf{G}] \begin{matrix} \{\mathbf{a}^*\} \\ 32 \times 1 \end{matrix}, \quad \begin{matrix} \{\mathbf{g}^*\} \\ 3 \times 1 \end{matrix} = \left(\overline{[\mathbf{B}_\varepsilon]} + [\mathbf{B}_\varepsilon^{\text{stab}}] \right) \begin{matrix} \{\mathbf{d}^{*e}\} \\ 32 \times 1 \end{matrix}, \quad (137)$$

$$\begin{matrix} \{\boldsymbol{\tau}^*\} \\ 9 \times 1 \end{matrix} = \begin{matrix} \{\boldsymbol{\tau}_0^*\} \\ 9 \times 1 \end{matrix} = \text{const.} \quad \begin{matrix} \{\mathbf{q}^*\} \\ 3 \times 1 \end{matrix} = \begin{matrix} \{\mathbf{q}_0^*\} \\ 3 \times 1 \end{matrix} = \text{const.} \quad (138)$$

Using the definitions (122), the interpolations (116)–(121) and (136)–(138), and the conditions (124), we can readily show that the last integrals on the left hand side of (112) and (114) vanish, and (113) and (115) are satisfied automatically, i.e.,

$$\int_{\Omega} \tau_{ij} (L_{ij}^* - u_{i,j}^*) d\Omega = 0, \quad \int_{\Omega} (\Delta L_{ij} - \Delta u_{i,j}) \tau_{ij}^* d\Omega = 0, \quad (139)$$

and

$$\int_{\Omega} q_i (e_{,i}^* - g_i^*) d\Omega = 0, \quad \int_{\Omega} (\Delta e_{,i}^p - \Delta g_i) q_i^* d\Omega = 0. \quad (140)$$

Then, the variational formulation of the problem simplifies to:

Find $(\Delta \mathbf{u}, \Delta \mathbf{L}, \Delta e^p)$ satisfying $\mathbf{u}|_{\partial_u \Omega} = \hat{\mathbf{u}}$ such that

$$\int_{\Omega} \rho b_i u_i^* d\Omega + \int_{\partial_{\sigma} \Omega} \hat{t}_i u_i^* dS - \int_{\Omega} \sigma_{ij} (\Delta \mathbf{L}, \Delta e^p) L_{ij}^* d\Omega = \int_{\Omega} \rho \ddot{u}_i u_i^* d\Omega \quad \forall \mathbf{u}^* \in \mathcal{V}, \mathbf{L}^* \in L^2(\Omega), \quad (141)$$

$$\int_{\Omega} \left\{ [\bar{\varepsilon}^p(\Delta \mathbf{L}, \Delta e^p) - e^p] e^* - \ell^2 e_{,i}^p e_{,i}^* \right\} d\Omega = 0 \quad \forall e^* \in \mathcal{G}. \quad (142)$$

It is noted that the independently interpolated fields $\boldsymbol{\tau}$ and \mathbf{q} do not enter now the variational formulation (141)–(142); this is due to conditions (124), which make the independently interpolated piecewise-constant fields $\boldsymbol{\tau}(\mathbf{x})$ and $\mathbf{q}(\mathbf{x})$, defined in (118) and (121), orthogonal to the interpolated differences $\Delta \mathbf{L} - \nabla(\Delta \mathbf{u})$ and $\nabla(\Delta e^p) - \Delta \mathbf{g}$ respectively (Simo and Hughes (1986); Simo and Rifai (1990)). The stress field $\boldsymbol{\sigma}(\Delta \mathbf{L}, \Delta e^p)$ in (141) is determined in terms of $\Delta \mathbf{L}$ and Δe^p by integrating the constitutive equations.

When the interpolations (116)–(117), (119) and (136)–(137) for $(\Delta \mathbf{u}, \Delta \mathbf{L}, \Delta e^p)$ and $(\mathbf{u}^*, \mathbf{L}^*, e^*)$ are used in the variational statement, we arrive at the following discretized problem, which is a set of non-linear equations for the global vector of nodal unknowns $\{\Delta \mathbf{d}\}_{N \times 1}$ and the local parameters $\{\Delta \mathbf{a}^e\}_{6 \times 1}$ on every element:

$$\{\mathbf{R}_u\}_{N \times 1} \equiv \{\mathbf{F}^{\text{ext}}\}_{N \times 1} - \left(\overset{\text{NELEM}}{\mathbf{A}} \{\mathbf{r}_u^e\}_{32 \times 1} \right) - [\mathbf{M}]_{N \times N} \{\ddot{\mathbf{d}}\}_{N \times 1} = \{\mathbf{0}\}, \quad (143)$$

$$\{\mathbf{r}_L^e\}_{6 \times 1} \equiv \int_{\Omega^e} [\mathbf{G}]_{6 \times 9}^T \{\boldsymbol{\sigma}\}_{9 \times 1} d\Omega = \{\mathbf{0}\}, \quad e = 1, 2, \dots, \text{NELEM}, \quad (144)$$

$$\{\mathbf{R}_\varepsilon\}_{N \times 1} \equiv \overset{\text{NELEM}}{\mathbf{A}} \{\mathbf{r}_\varepsilon^e\}_{32 \times 1} = \{\mathbf{0}\}, \quad (145)$$

where N is the total number of nodal degrees of freedom in the problem, NELEM the total number of elements, \mathbf{A} the “assembly operator”, $(\{\mathbf{F}^{\text{ext}}\}, [\mathbf{M}])$ the standard global “external load vector” and “mass matrix” of the problem respectively, $\{\ddot{\mathbf{d}}\}$ the global nodal acceleration vector, and

$$\{\mathbf{r}_u^e\}_{32 \times 1} = \int_{\Omega^e} \left(\overline{[\mathbf{B}_L]}^T + \underline{[\mathbf{B}_{\text{stab}}(\mathbf{x})]}^T \right) \{\boldsymbol{\sigma}\}_{9 \times 1} d\Omega, \quad (146)$$

$$\{\mathbf{r}_\varepsilon^e\}_{32 \times 1} = \int_{\Omega^e} (\Delta \bar{\varepsilon}^p - \Delta e^p) \{\mathbf{N}_\varepsilon(\mathbf{x})\}_{32 \times 1} d\Omega - \left(\ell^2 V_e \overline{[\mathbf{B}_\varepsilon]}^T \overline{[\mathbf{B}_\varepsilon]} + \underline{[\mathbf{k}_\varepsilon^{\text{stab}}]} \right) \{\mathbf{d}^e\}_{32 \times 1}, \quad (147)$$

$$\underline{[\mathbf{k}_\varepsilon^{\text{stab}}]}_{32 \times 32} = \ell^2 \int_{\Omega^e} \left[\underline{[\mathbf{B}_\varepsilon^{\text{stab}}(\mathbf{x})]} \right]^T \underline{[\mathbf{B}_\varepsilon^{\text{stab}}(\mathbf{x})]} d\Omega, \quad (148)$$

where $\{\boldsymbol{\sigma}\} = \{\boldsymbol{\sigma}(\Delta\mathbf{L}, \Delta e^p)\}$ and $e^p = e^p(\Delta\mathbf{L}, \Delta e^p)$ are determined from the integration of the constitutive equations.

Equations (144) are written for every element in the mesh and provide a set of six non-linear equations per element that define the local element parameters $\{\Delta\mathbf{a}^e\}$ in terms of the element nodal degrees of freedom $\{\Delta\mathbf{d}^e\}$. In Appendix B, we describe a methodology for the solution of (144) at every element.

The global vector of nodal unknowns $\{\Delta\mathbf{d}\}$ is determined from the solution of the global non-linear system of equations (143) and (145). The underlined terms in (146) and (147) are due to matrices $[\mathbf{B}_{\text{stab}}(\mathbf{x})]$ and $[\mathbf{B}_{\varepsilon}^{\text{stab}}(\mathbf{x})]$ in the interpolation of the gradients (117) and (120). The rest (non-underlined) terms in (146) and (147) appear (alone) when the traditional formulation (102)–(103) is used.

Using reduced one-point Gauss integration for the numerical evaluation of the integrals of the terms that are *not* underlined in (146) and (147), we find

$$\{\mathbf{f}_u^e\} = \{\mathbf{f}_{u0}^e\} + \{\mathbf{f}_u^{\text{stab}}\}, \quad (149)$$

$$\{\mathbf{r}_{\varepsilon}^e\} = \{\mathbf{r}_{\varepsilon0}^e\} + \{\mathbf{r}_{\varepsilon}^{\text{stab}}\}, \quad (150)$$

where

$$\{\mathbf{f}_{u0}^e\} = V_e \overline{[\mathbf{B}_L]}^T \{\boldsymbol{\sigma}_0\}, \quad \{\mathbf{f}_u^{\text{stab}}\} = \int_{\Omega^e} [\mathbf{B}_{\text{stab}}]^T \{\boldsymbol{\sigma}\} d\Omega, \quad (151)$$

$$\{\mathbf{r}_{\varepsilon0}^e\} = 8 J_0 (\Delta \bar{\varepsilon}_0^p - \Delta e_0^p) \{\mathbf{N}_{\varepsilon0}\} - \ell^2 V_e \overline{[\mathbf{B}_{\varepsilon}]}^T \overline{[\mathbf{B}_{\varepsilon}]}, \quad \{\mathbf{r}_{\varepsilon}^{\text{stab}}\} = -[\mathbf{k}_{\varepsilon}^{\text{stab}}] \{\mathbf{d}^e\}, \quad (152)$$

$[\mathbf{k}_{\varepsilon}^{\text{stab}}]$ is defined in (148), a zero subscript indicates that the corresponding quantity is evaluated at the “element local origin”, i.e., the point where the natural coordinate $\boldsymbol{\xi} = \mathbf{0}$ (see Appendix A), and $\{\boldsymbol{\sigma}_0\}$ is calculated using $\overline{[\Delta\mathbf{L}]}$ and \mathbf{F}_{n+1} in (127a) and (132) together with the integration algorithm discussed in section 4.

$\{\mathbf{f}_{u0}^e\}$ and $\{\mathbf{r}_{\varepsilon0}^e\}$ in (151a) and (152a) would result if the “uniform strain formulation”¹ of Flanagan and Belytschko (1981) were used in the traditional formulation (102)–(103) and lead to spurious singular modes if used alone. The additional underlined terms in (146) and (147) correspond to $\{\mathbf{f}_u^{\text{stab}}\}$ and $\{\mathbf{r}_{\varepsilon}^{\text{stab}}\}$ in (149)–(152), remove the spurious modes, and stabilize the calculations; these terms are due to the “enhanced interpolations” used for the gradients in (117) and (120) and provide a “physical stabilization” to the problem (Belytschko and Bindeman (1991); Puso (2000)).

In Appendix C, we develop approximate, but very accurate, analytical expressions for $\{\mathbf{f}_u^{\text{stab}}\}$ and $[\mathbf{k}_{\varepsilon}^{\text{stab}}]$, thus obviating Gauss quadrature in (151a) and (148). This leads to a computationally efficient strategy that requires the evaluation of stress $\{\boldsymbol{\sigma}_0\}$ only once per element when the non-linear global problem (143) and (145) is solved for the nodal unknowns $\{\Delta\mathbf{d}\}$. In particular, $\{\mathbf{f}_{u0}^e\}$ and $\{\mathbf{r}_{\varepsilon0}^e\}$ are calculated using (149)–(152), and $\{\mathbf{f}_u^{\text{stab}}\}$ and $[\mathbf{k}_{\varepsilon}^{\text{stab}}]$ are determined using the analytical expressions (274)–(262) and (276)–(279) in Appendix C.

6. Non-local *quasi-static* problems in ABAQUS/Standard via “UMAT”

In the special case of *quasi-static* problems, the solution can be also obtained using user material subroutine UMAT in ABAQUS/Standard together with a *COUPLED TEMPERATURE-DISPLACEMENT, STEADY STATE analysis option as described in the following. The methodology is similar to that used recently for quasi-static problems by Seupel et al. (2018), who makes use of the ABAQUS user subroutines UMAT and HETVAL to define the problem.

One version of the steady-state heat transfer problem in an isotropic material, as solved in ABAQUS, is

$$k \nabla^2 T + r(\Delta\boldsymbol{\varepsilon}, T) = 0 \quad \text{in } \Omega \quad (153)$$

$$k \mathbf{n} \cdot \nabla T = \hat{q} \quad \text{on } \partial\Omega, \quad (154)$$

¹ The “uniform strain formulation” introduced by Flanagan and Belytschko (1981) is based on the (analytically calculated) average strain over the element volume and is an alternative to using one-point Gauss integration, in which strains are evaluated at the element local origin $\boldsymbol{\xi} = \mathbf{0}$ and V_e is replaced by $8 J_0$ in (151a) and (152a). The uniform strain method ensures that the element passes the “patch test” and attains the accuracy of the numerical solution when elements are skewed (Belytschko et al. (1984)).

where T is temperature, k the thermal conductivity, r the heat supply per unit volume, \hat{q} the prescribed boundary heat flux vector, and $\Delta\boldsymbol{\varepsilon}$ a strain increment properly defined in terms of nodal displacements (see ABAQUS manuals and Hughes and Winget (1980)).

Comparing the BVP (153)–(154) with (36)–(37), we conclude that the non-local equivalent plastic strain can be identified with the temperature field in the coupled temperature-displacement ABAQUS analysis, provided the following correspondence is used:

$$T \leftrightarrow e^p, \quad k \leftrightarrow \ell^2, \quad r(\Delta\boldsymbol{\varepsilon}(\mathbf{u}), T) \leftrightarrow \bar{\varepsilon}^p(\mathbf{u}, e^p) - e^p, \quad \hat{q} \rightarrow 0. \quad (155)$$

The constitutive equations are integrated numerically in user subroutine UMAT. In UMAT, the value of e^p is provided as “temperature”, $\bar{\varepsilon}^p$ is determined from the numerical integration of the constitutive equations using the algorithm described in section 4, and r (variable RPL in UMAT) is identified with the difference $\bar{\varepsilon}^p - e^p$. The derivatives $\partial\Delta\boldsymbol{\sigma}/\partial\Delta\boldsymbol{\varepsilon}$ (DDSDDE), $\partial\boldsymbol{\sigma}/\partial T$ (DDSDDT), $\partial r/\partial\Delta\boldsymbol{\varepsilon}$ (DRPLDE), and $\partial r/\partial T$ (DRPLDT) are also evaluated in UMAT. In view of (51) and (53), i.e.,

$$\overset{\nabla}{\boldsymbol{\sigma}} = \mathcal{L} : \mathbf{D} - \mathbf{A}^{\text{nl}} \dot{e}^p \quad \text{and} \quad \dot{\bar{\varepsilon}}^p = \frac{\bar{P}}{L} \mathbf{P} : \mathcal{L}^e : \mathbf{D} + \frac{\bar{P}}{L} \frac{\partial\Phi}{\partial e^p} \dot{e}^p, \quad (156)$$

$\partial\boldsymbol{\sigma}/\partial\Delta\boldsymbol{\varepsilon}$, $\partial\boldsymbol{\sigma}/\partial T$, $\partial r/\partial\Delta\boldsymbol{\varepsilon}$ and $\partial r/\partial T$ are approximated as follows²:

$$\frac{\partial\Delta\boldsymbol{\sigma}}{\partial\Delta\boldsymbol{\varepsilon}} \simeq \mathcal{L}, \quad \frac{\partial\boldsymbol{\sigma}}{\partial T} = \frac{\partial\boldsymbol{\sigma}}{\partial e^p} \simeq -\mathbf{A}^{\text{nl}}, \quad (157)$$

and

$$\frac{\partial r}{\partial\Delta\boldsymbol{\varepsilon}} = \frac{\partial\bar{\varepsilon}^p}{\partial\Delta\boldsymbol{\varepsilon}} \simeq \frac{\bar{P}}{L} \mathbf{P} : \mathcal{L}^e, \quad \frac{\partial r}{\partial T} = \frac{\partial\bar{\varepsilon}^p}{\partial e^p} - 1 \simeq \frac{\bar{P}}{L} \frac{\partial\Phi}{\partial e^p} - 1. \quad (158)$$

Such an approximation of the Jacobian is first-order accurate as the size of the increment $\Delta t \rightarrow 0$; it should be emphasized, however, that the aforementioned approximation influences only the rate of convergence of the Newton loop and not the accuracy of the numerical solution. In the calculations, in order to integrate accurately the constitutive equations we restrict the increment size so that the magnitude of the strain increment $\Delta\mathbf{E}$ does not exceed the value of $5\sigma_y/E$. With such a restriction on the size of the increment, the aforementioned approximation of the Jacobian does not affect the quadratic rate of asymptotic convergence of the iterative Newton method.

It should be also noted that the coupled temperature-displacement in ABAQUS/Standard can be used for the solution of *quasi-static* implicit strain-gradient plasticity problems, but it cannot be used for *dynamic* problems, in which inertia effects become important.

7. Non-local *dynamic* problems in ABAQUS/Explicit via “VUMAT”

In *dynamic* problems including inertia terms, solutions can be obtained using user material subroutine VUMAT in ABAQUS/Explicit together with a *DYNAMIC TEMPERATURE-DISPLACEMENT analysis option as described in the following.

The corresponding transient heat transfer equation in an isotropic material is

$$k \nabla^2 T + r(\Delta\boldsymbol{\varepsilon}, T) = \rho c \dot{T}, \quad (159)$$

where c is the specific heat. Again, the identifications given in (155) are used in the calculations and c is given a small value, so that the transient term on the right hand side of (159) becomes negligible.

The constitutive equations are integrated numerically in VUMAT, where the non-local equivalent plastic strain e^p is again identified with temperature in the explicit coupled temperature-displacement calculations. However, r cannot be defined in VUMAT. Therefore, to define r , we use and the following “loading card” in ABAQUS/Explicit:

*DFLUX

² In rate-dependent models, in view of (99), the value of H in (50c) is replaced by $H = -\bar{P} \left(\frac{\partial\Phi}{\partial e^p} + \frac{1}{\Delta t} \frac{\partial\Phi}{\partial \dot{e}^p} \right) = -\bar{P} \frac{\partial\Phi}{\partial \Sigma_y} \left(\frac{\partial\Sigma_y}{\partial e^p} + \frac{1}{\Delta t} \frac{\partial\Sigma_y}{\partial \dot{e}^p} \right)$.

ALLEL, BFNU

where ALLEL is the set of all finite elements in the mesh, and BFNU signifies a user-defined heat supply per unit volume r (BFNU = **B**ody **F**lux **N**on **U**niform). The value of $r = \bar{\varepsilon}^p - e^p$ is defined in user subroutine VDFLUX, in which the value of e^p is provided as “temperature” and the value of $\bar{\varepsilon}^p$ is supplied by VUMAT via a user-introduced COMMON block.

The value of c should be “small” so that the contribution of the transient term on the right hand side of (159) is negligible. It should be noted though that the numerical stability limit on the time increment of the solution is proportional to c . To avoid the requirement of using an extremely large number of increments, a judicious choice for the value of c is essential. An estimate for the appropriate value of c can be obtained by considering the case of a uniform solution in which $\nabla^2 T = \nabla^2 e^p = 0$ and (159) reduces to $\bar{\varepsilon}^p - e^p = \rho c \dot{e}^p$. The exact solution in this case is $\bar{\varepsilon}^p = e^p$ and the error $\bar{\varepsilon}^p - e^p$ in the numerical solution is controlled by the magnitude of the dimensionless quantity $\rho c \dot{e}^p$. Let $\dot{\varepsilon}$ be a representative strain rate in the problem; e.g., $\dot{\varepsilon}$ can be defined as $\dot{\varepsilon} = \sqrt{2 \dot{\mathbf{e}} : \dot{\mathbf{e}}/3}$, where $\dot{\mathbf{e}}$ is the deviatoric strain rate. Since the elastic strain rates are small compared to the plastic strain rates, \dot{e}^p is of order $\dot{\varepsilon}$. Therefore, the value of c to be used in the calculations should be such that

$$\rho c \dot{\varepsilon} < \text{TOL}, \quad (160)$$

at all integration points in the finite element mesh, where $\text{TOL} = 10^{-4}$ is a reasonable value.

The explicit dynamics procedure in ABAQUS/Explicit performs a large number of small time increments efficiently. An explicit central-difference time integration rule is used together with the use of diagonal (“lumped”) element mass matrices and each increment is relatively inexpensive (compared to ABAQUS/Standard) because there is no solution of simultaneous equations. The explicit central-difference operator satisfies the dynamic equilibrium equations at the start of the increment ($t = t_n$); the accelerations calculated at $t = t_n$ are used to advance the velocity solution to time $t = t_n + \Delta t/2$ and the displacement solution to time $t_{n+1} = t_n + \Delta t$. No derivatives (Jacobians) such as $\partial \Delta \sigma / \partial \Delta \varepsilon$, $\partial \Delta \sigma / \partial T$, $\partial r / \partial \Delta \varepsilon$, or $\partial r / \partial T$ are needed in the explicit calculations.

The central difference operator is conditionally stable and the stability limit depends on the element size and the dilatational wave speed of the material.

Remark

In cases where ABAQUS/Standard has convergence difficulties, e.g., in problems involving complicated contact conditions, ABAQUS/Explicit can be used also to carry out *quasi-static* solutions by minimizing the influence of the dynamic inertia terms in the solution. If there is no damping in the problem, it is not uncommon the stresses in each element to oscillate with a small amplitude about the static equilibrium stresses. When ABAQUS/Explicit is used for the solution of quasi-static problems, the user should make sure that the kinetic energy is a small fraction of the strain energy in the problem. \square

8. Applications

In the present paper we use a pressure-independent form of the yield function (4) due to Bai and Wierzbicki (2008) as modified by Lian et al. (2012):

$$\Phi(\sigma_e, \theta, \bar{\varepsilon}^p, D) = \sigma_e - (1 - D) F(\gamma(\theta)) \sigma_y(\bar{\varepsilon}^p) = 0, \quad (161)$$

where

$$F(\gamma(\theta)) = c_\theta^s + (c_\theta^{ax} - c_\theta^s) \left[\gamma(\theta) - \frac{\gamma^{m+1}(\theta)}{m+1} \right], \quad \gamma(\theta) = \frac{\sqrt{3}}{2 - \sqrt{3}} \left(\frac{1}{\cos \theta} - 1 \right), \quad (162)$$

$$c_\theta^{ax} = \begin{cases} c_\theta^t & \text{if } \bar{\theta} \geq 0, \\ c_\theta^c & \text{if } \bar{\theta} < 0, \end{cases} \quad \sigma_y(\bar{\varepsilon}^p) = \sigma_0 \left(1 + \frac{\bar{\varepsilon}^p}{\varepsilon_0} \right)^{1/n}, \quad \varepsilon_0 = \frac{\sigma_0}{E}, \quad (163)$$

($c_\theta^s, c_\theta^t, c_\theta^c, m, n$) are dimensionless material constants, and $\sigma_y(\bar{\varepsilon}^p)$ is the flow stress of the material. This yield surface has three axes of symmetry on the deviatoric Π -plane and does not have in general a tension/compression symmetry.

In the special case where $c_\theta^c = c_\theta^t$, the yield surface does have tension/compression symmetry and six axes of symmetry on the Π -plane.

The convexity of the yield surface defined in (161)–(163) is discussed in detail by Lian et al. (2012).

Remark

The yield function (161) can be also written in the form

$$F(\sigma_e, \theta, \bar{\varepsilon}^p, D) = \Sigma_e(\sigma_e, \theta, D) - \sigma_y(\bar{\varepsilon}^p) = 0, \quad (164)$$

where $\Sigma_e(\sigma_e, \theta, D)$ is an equivalent stress defined in terms of σ_e, θ , and D :

$$\Sigma_e(\sigma_e, \theta, D) = \frac{\sigma_e}{(1-D)F(\gamma(\theta))}. \quad \square \quad (165)$$

The material properties used in the calculations presented in the following are:

$$\varepsilon_0 = \frac{\sigma_0}{E} = 1.65 \times 10^{-3}, \quad \nu = 0.3, \quad c_\theta^t = 1, \quad c_\theta^c = 0.98, \quad c_\theta^s = 0.95, \quad m = 7, \quad (166)$$

where ν is Poisson's ratio. Typical values are $E = 200$ GPa and $\sigma_0 = 330$ MPa. The chosen values of c_θ^s, c_θ^t , and c_θ^c guarantee convexity of the yield surface (Lian et al. (2012)).

The calibration of the model and the values of the constants (c_1, c_2, \dots, c_8) that enter the damage equations (32) and (34) are discussed in Buchkremer et al. (2014), Novokshanov et al. (2015), and Wu et al. (2017b). Here, we use the values

$$c_1 = 0.4943, \quad c_2 = 2.2660, \quad c_3 = 0.10, \quad c_4 = 1.1310, \quad (167)$$

$$c_5 = 0.83, \quad c_6 = 0.5449, \quad c_7 = 0.85, \quad c_8 = 0.3926. \quad (168)$$

The critical value of stress triaxiality η_{cr} in (33), below which local material failure never occurs, is (Bao and Wierzbicki (2005))

$$\eta_{cr} = -\frac{1}{3}. \quad (169)$$

Also the material parameters G_f in (33) and D_{max} in (34) take the values

$$G_f = 0.515 \sigma_0 \quad \text{and} \quad D_{max} = 1. \quad (170)$$

The values of the hardening exponent n in (163b) and the material length scale ℓ are specified separately in each problem.

The stress-strain curves in uniaxial tension and plane strain tension for the model material described above with hardening exponent $n = 5$ are shown in Fig. 3. Recall that $\eta = \frac{1}{3}$ and $\bar{\theta} = 1$ in uniaxial tension, and $\eta \approx \frac{1}{\sqrt{3}} = 0.577$ and $\bar{\theta} \approx 0$ in plane strain tension. Points marked “A” on the curves in Fig. 4 indicate the load level at which $I = 1$ (or equivalently $\bar{\varepsilon}^p = \hat{\varepsilon}^p = \bar{\varepsilon}_i^p$), and damage starts developing; points marked “x” denote material failure, i.e., $D = D_{cr}$.

All calculations are carried out incrementally. In ABAQUS/Standard the discretized nonlinear equations are solved using Newton's method. The Jacobian of the global Newton scheme is approximated by the tangent stiffness matrix derived using the moduli given by (51) $\left(\overset{\nabla}{\boldsymbol{\sigma}} = \mathcal{L} : \mathbf{D} - \mathbf{A}^{nl} \dot{\varepsilon}^p \right)$ as described in section 6.

8.1. Localization in plane strain tension

We consider the quasi-static problem of plastic flow localization in a tension specimen under plane strain conditions. We consider one quarter of the specimen and doubly symmetric solutions are found. Figure 5 shows a schematic representation of one quarter of the specimen together with the geometric boundary conditions. The right side of the specimen is traction free and the upper side is subjected to a prescribed displacement δ . The height of the specimen

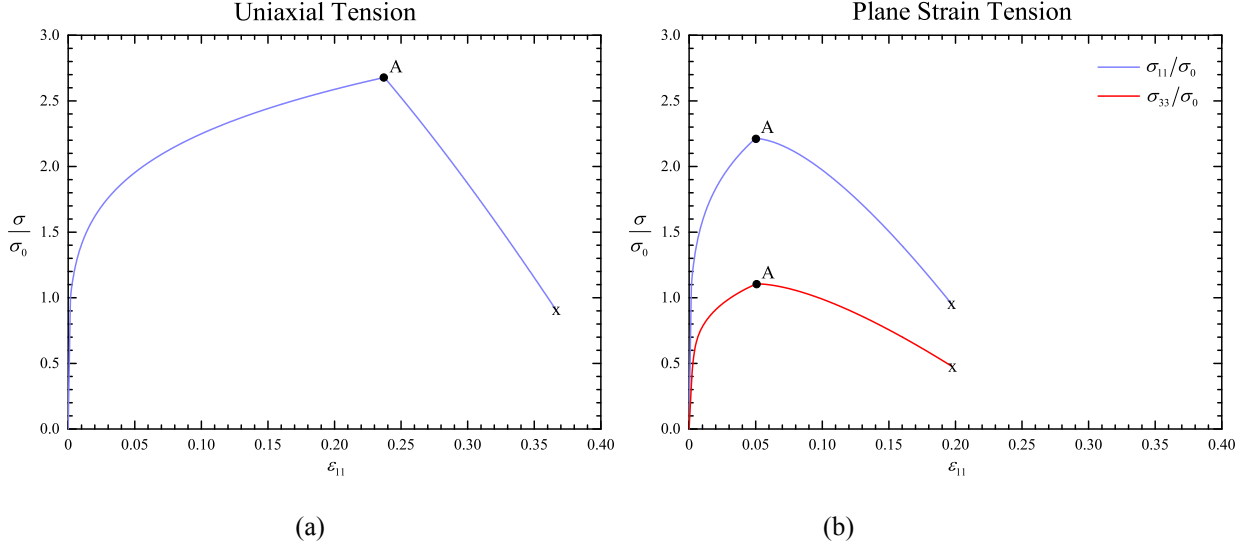


Figure 4: True stress versus axial logarithmic strain ϵ_{11} for (a) uniaxial tension and (b) plane strain tension. In plane strain, σ_{11} is the axial stress and σ_{33} the stress normal to the plane of deformation ($\sigma_{33} \approx \sigma_{11}/2$).

is $h = 1.5 w$ and the material length in the constitutive equations is $\ell = 0.08 w$, where w is the width of the specimen. The hardening exponent is $n = 5$.

We obtain first an estimate of the localization strain by using the methodology of Rice and co-workers (Rudnicki and Rice (1975); Rice (1976); Needleman and Rice (1978)). The condition for plastic flow localization in a shear band is that there exists a unit vector \mathbf{n} on the x_1 - x_2 plane in the deformed configuration such that (Needleman and Rice (1978))

$$\det \left[n_k \mathcal{L}_{kijl}^{ep} n_l + A_{ij} \right] = 0, \quad \text{where} \quad \mathbf{A} = -\frac{1}{2} \left[\boldsymbol{\sigma} - \boldsymbol{\sigma} \cdot \mathbf{n} \mathbf{n} - (\mathbf{n} \cdot \boldsymbol{\sigma} \cdot \mathbf{n}) \boldsymbol{\delta} + \mathbf{n} \mathbf{n} \cdot \boldsymbol{\sigma} \right]. \quad (171)$$

If such an \mathbf{n} exists, then the direction of the shear band is perpendicular to \mathbf{n} .

Aravas and Ponte Castañeda (2004) have shown that the localization condition (171) can be written in the form

$$B \equiv B_{11} B_{22} - B_{21} B_{12} = 0, \quad (172)$$

where³

$$B_{11} = \mathcal{L}_{1111}^{\text{loc}} n_1^2 + \left(G - \frac{\sigma_1}{2} \right) n_2^2, \quad B_{12} = \left(\mathcal{L}_{1122}^{\text{loc}} + G + \frac{\sigma_1}{2} \right) n_1 n_2, \quad (173)$$

$$B_{21} = \left(\mathcal{L}_{1122}^{\text{loc}} + G - \frac{\sigma_1}{2} \right) n_1 n_2, \quad B_{22} = \mathcal{L}_{2222}^{\text{loc}} n_2^2 + \left(G + \frac{\sigma_1}{2} \right) n_1^2, \quad (174)$$

\mathcal{L}^{loc} is the fourth-order elastoplastic tangent modulus tensor defined in (55), σ_1 is the normal stress in the direction of stretching, and index 1 corresponds to the direction of stretching, and index 2 denotes the transverse direction in the plane of deformation. The calculation of the stage at which localization of plastic flow is determined by deforming a single 4-node element in plane strain tension and using a UMAT based on the local version of the algorithm described in section 4. Within UMAT, the localization calculations are carried out as described in Aravas and Ponte Castañeda (2004). It is found that the conditions for plastic flow localization are satisfied for

$$\delta = 0.05155 h \quad \text{and} \quad \psi = 45^\circ, \quad (175)$$

³ One typo in Aravas and Ponte Castañeda (2004) is corrected in the expression for B_{11} in (173a) and two typos are corrected in the expression for B_{22} in (174b). The results reported in Aravas and Ponte Castañeda (2004) are based on the correct expressions for B_{11} and B_{22} .

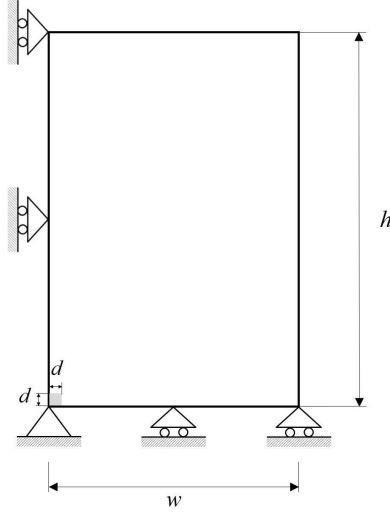


Figure 5: Schematic representation of one quarter of the plane strain tension specimen.

where $(\mathbf{e}_1, \mathbf{e}_2)$ are unit vectors along the coordinate axes on the plane of deformation.

We turn now to the numerical solution of the problem. To trigger the initiation of non-uniform deformation in the specimen, an imperfection in the material properties is introduced over a small square region of side $d = 0.05 w$ at the center of the specimen, as shown in Fig. 5. In particular, the stress σ_0 in (163b) is replaced by $0.98 \sigma_0$ in the imperfect region.

Calculations are carried out for the local ($\ell = 0$) and the non-local ($\ell \neq 0$) versions of the model. Two different finite element formulations were used for the non-local material and all gave the same results reported in the following. The particular formulations are: i) a 4-node isoparametric plane strain element via UEL in ABAQUS/Standard with 2×2 Gauss integration and a uniform volumetric part for the deformation gradient (equal to its average value over the element) and ii) a 4-node plane strain coupled temperature-displacement element (CPE4HT) in ABAQUS/Standard with 2×2 Gauss integration and a UMAT.

Three different meshes are used, namely 20×30 , 30×45 , and 40×60 initially square elements, where the first and second numbers denote the number of elements in the w and h directions respectively.

Figure 6 shows the normalized “load-extension” curves as calculated using the three different meshes. The dash lines correspond to the local solutions and the solid lines to the non-local ones. It is evident that the local solutions exhibit a strong mesh-dependence after the deformation ceases to be uniform. The corresponding non-local numerical solutions converge to the exact one as the mesh is refined at all levels of extension δ .

Figure 7 shows contour plots of the damage parameter D for the local model ($\ell = 0$) as calculated using the three different meshes at an extension level $\delta = 0.057 h$. The width of the shear band tends to zero as the mesh is refined and the strong mesh dependence of the solution is again evident. This is due to the loss of ellipticity of the governing equations, which allows for discontinuous solutions.

Figures 6 and 7 show that the local model predicts very well the onset of localization and the orientation of the shear band, but it cannot be used in the post bifurcation regime when the BVP loses ellipticity.

Figure 8 shows contour plots of the damage parameter D for the non-local model ($\ell = 0.08 w$) as calculated using the three different meshes at an extension level $\delta = 0.08 h$. The width of the shear band is now independent of the mesh size as the mesh is refined sufficiently. The equations remain elliptic at all deformation levels (Benallal and Tvergaard (1995)) and this excludes the possibility of discontinuous solutions.

8.2. Impact of a steel rod on a rigid surface

We consider the dynamic problem of a $L = 32.4$ mm long cylindrical steel rod of square cross section of $2 a \times 2 a = 6.4$ mm \times 6.4 mm, impacting a rigid wall with an initial velocity of $V_0 = 250$ m/sec. The initial mass density of the rod is $\rho_0 = 7850$ kg/m³. This is a standard benchmark problem used by many general-purpose finite element codes.

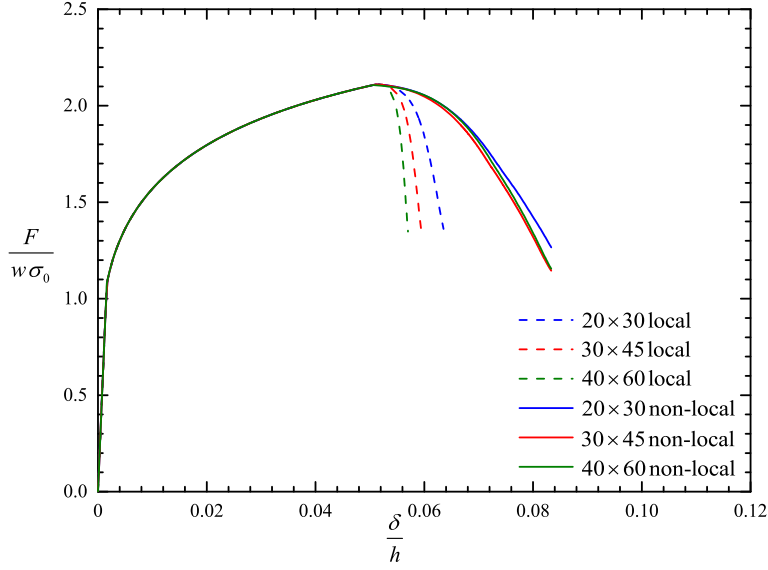


Figure 6: Normalized-load-deflection curves in plane strain tension for local and non-local model.

The high velocity impact causes large plastic deformation at the front end of the rod that is in contact with the rigid surface and is the area of interest.

Because of symmetry, one quarter of the specimen is analysed and appropriate symmetry conditions are imposed. To simulate the impact of the rod on the frictionless rigid wall, zero axial displacements are prescribed at the nodes on the front end of the rod, while all other nodes are subjected to a 250 m/sec initial velocity in the direction of the impact (perpendicular to the rigid wall). While this technique is appropriate for modeling the crushing of the front end of the rod in the absence of friction or rebound, a contact pair should be used if there are significant friction effects or if separation between the rod and the rigid wall is of interest.

A rate-dependent version of the plasticity model is used and $\sigma_y(\bar{\epsilon}^p)$ in (161) is replaced by

$$\Sigma_y(\bar{\epsilon}^p, \dot{\bar{\epsilon}}^p) = \begin{cases} \sigma_y(\bar{\epsilon}^p) & \text{if } \dot{\bar{\epsilon}}^p \leq \dot{\epsilon}_0, \\ \left(1 + d_1 \ln \frac{\dot{\bar{\epsilon}}^p}{\dot{\epsilon}_0}\right) \sigma_y(\bar{\epsilon}^p) & \text{if } \dot{\bar{\epsilon}}^p \geq \dot{\epsilon}_0, \end{cases} \quad (176)$$

where $d_1 = 0.035$ and $\dot{\epsilon}_0 = 10^{-4} \text{ s}^{-1}$. A hardening exponent $n = 10$ and a material length $\ell = 1 \text{ mm}$ are used in the calculations. This value of ℓ is chosen arbitrarily to be a fraction of a . It is emphasized though that the value of ℓ does not influence the calculations, since, as discussed in the following, the very negative triaxialities in the rod prevent damage. The main purpose of this example is to check the enhanced formulation and the associated hourglass control.

The dynamic analysis is carried out for a time period of $t = 40 \mu\text{s}$ using both ABAQUS/Standard and ABAQUS/Explicit and the results are identical. In all analyses discussed below, a $20 \times 20 \times 72$ finite element mesh of eight-node hexahedral elements is used. In ABAQUS/Standard we use a UEL with an 8-node isoparametric hexahedral element and $2 \times 2 \times 2$ Gauss integration points based on the standard ($\mathbf{u} - e^p$) formulation described in section 5.1. Another set of calculations is also carried out with ABAQUS/Standard using a UEL with an 8-node isoparametric hexahedral element and one Gauss integration point based on the enhanced strain formulation described in section 5.2. Equal time increments are used in both sets of calculations. It is found that at least 5000 time increments are required for accurate (convergent) solutions. The enhanced (reduced integration) formulation reduces the required computer time about 70%. It should be mentioned that in the early stages of the solution strain rates of the order of 10^5 s^{-1} develop at the center of the area of the rod that is in contact with the rigid wall.

In ABAQUS/Explicit the dynamic analysis is carried out using a VUMAT as described in section 7. Eight-node isoparametric hexahedral ABAQUS elements with one Gauss integration point (C3D8RT in ABAQUS library) and the ABAQUS “enhanced hourglass control” are used. A value of $c = 3 \times 10^{-13} \text{ s}/(\text{kg}/\text{m}^3)$ is used in (159) so that, for

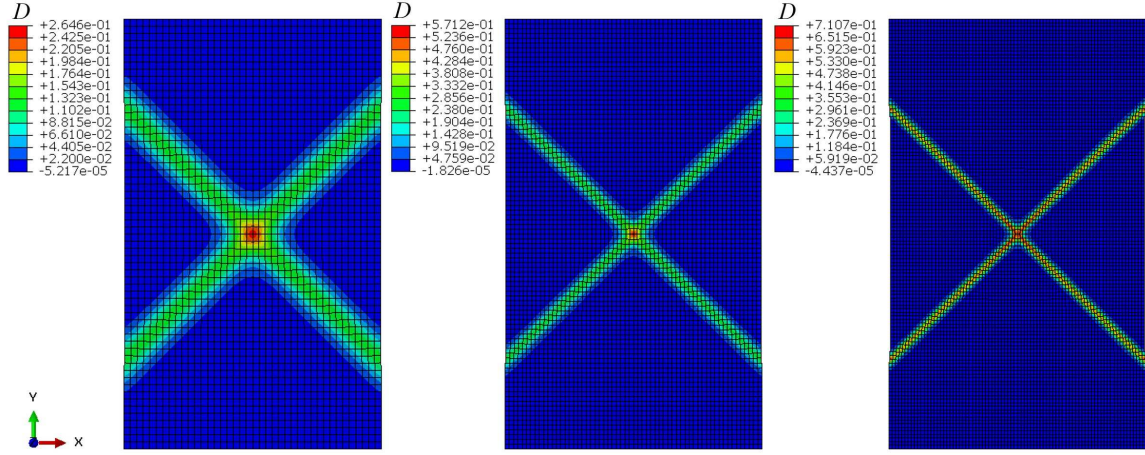


Figure 7: Contour plots of damage parameter D for the local model at $\delta = 0.057 h$. Whole specimen is shown.

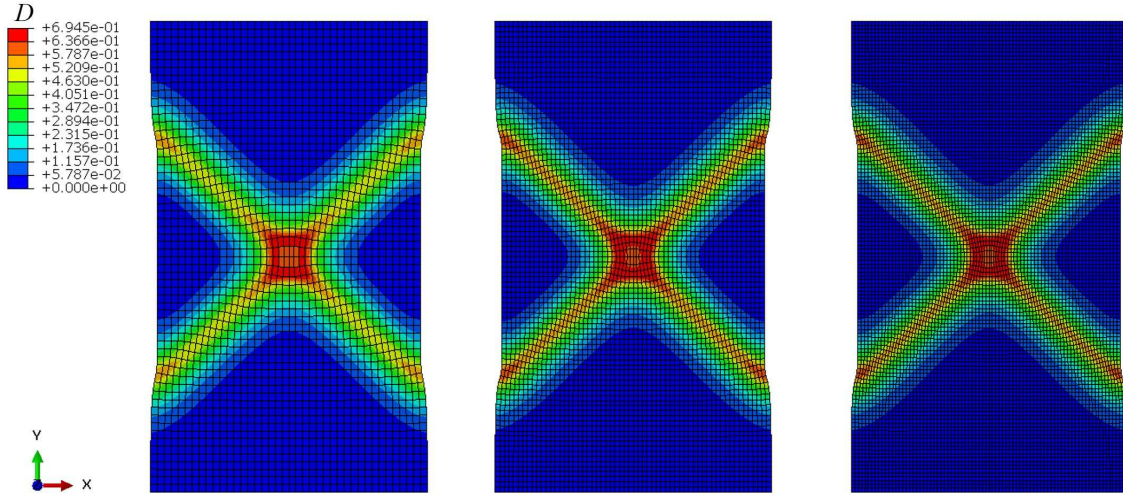


Figure 8: Contour plots of damage parameter D for the non-local model at $\delta/h = 0.08$. Whole specimen is shown.

$$\dot{\epsilon} = 10^5 \text{ s}^{-1},$$

$$\rho c \dot{\epsilon} = 2.36 \times 10^{-4}. \quad (177)$$

Numerical experiments indicate that smaller values of c do not change the results, whereas values of c one order of magnitude larger do alter the solution. At least 4 million increments are required for accurate solutions. The required computer time is more than twice (216% higher) the time required for the solution obtained by ABAQUS/Standard with UEL and one Gauss integration point. A comparison of implicit and explicit ABAQUS calculations has been given by Nagtegaal and co-workers (Nagtegaal and Taylor (1991); Rebelo et al. (1992)).

Figure 9(a) shows the variation of the normalized force F exerted by the rod on the rigid wall with time and Fig. 9(b) shows the time variation of the kinetic energy $K = \int_{\Omega} \frac{1}{2} \rho v^2 d\Omega$ and total plastic work $W^p = \int_{\Omega} \left(\int_0^t \sigma : \mathbf{D}^p dt \right) d\Omega$ in the rod normalized by the initial kinetic energy $K_0 = \frac{1}{2} \rho_0 v_0^2 a^2 L$. Dynamic effects are important at the early stages of the impact; the kinetic energy reduces with time and is dissipated in the form of plastic work in the rod, as expected. It should be noted also that the force on the rigid wall takes negative values for a short period of time, indicating that separation is actually occurring.

Contour plots of the equivalent plastic strain $\bar{\epsilon}^p$ and the non-local equivalent plastic strain e^p are shown in Fig.

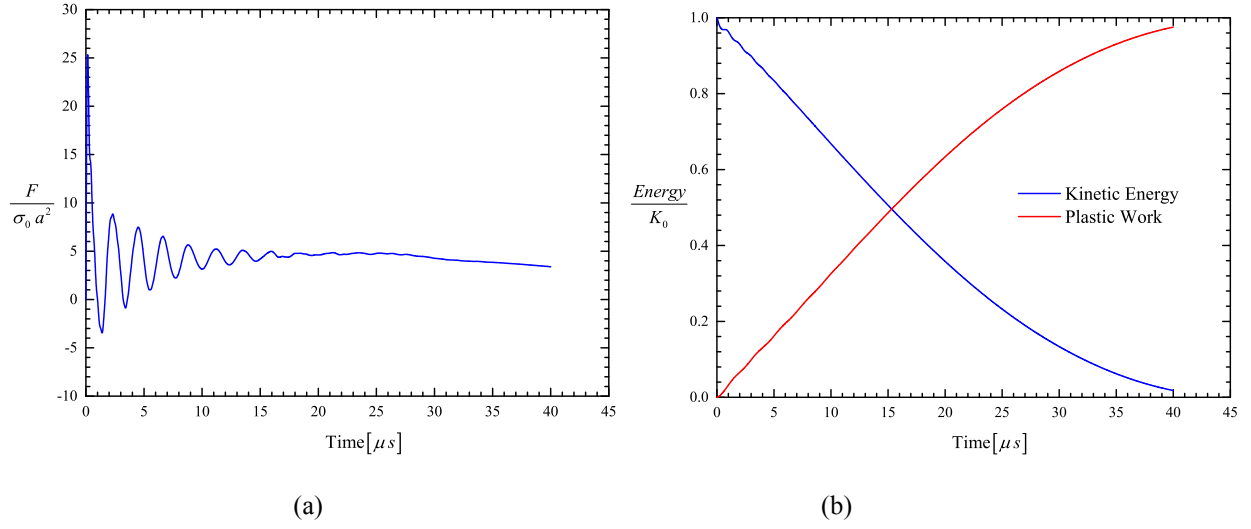


Figure 9: Time variation of normalized a) force on the plate and b) kinetic energy and plastic work (energies normalized by the initial kinetic energy $K_0 = \frac{1}{2} \rho_0 v_0^2 a^2 L$).

10 at the end of the calculations $t = 40 \mu s$. At the front end of the rod near the rigid wall the non-local values e^P are smaller than the local values $\bar{\varepsilon}^P$, since e^P represents local spatial averages of $\bar{\varepsilon}^P$ as discussed in section 3.1. It should be also noted that the non-local values e^P are calculated but they do not affect the solution in this problem since no damage is developing. The reason is that e^P takes large values in the part of the rod where very negative triaxialities develop ($\eta < \eta_{cr} = -1/3$) and this suppresses damage evolution according to (33).

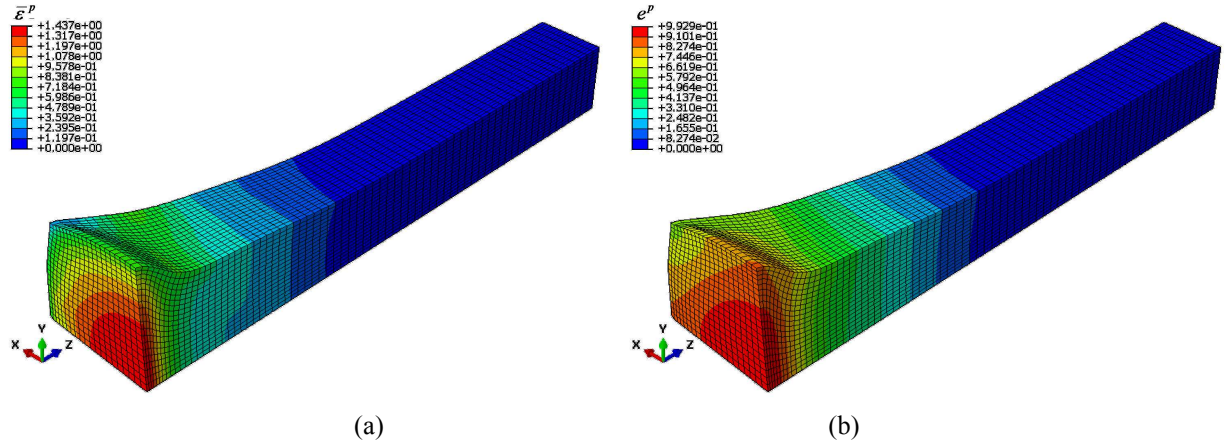


Figure 10: Contour plots at $t = 30 \mu s$ of: (a) equivalent plastic strain $\bar{\varepsilon}^P$ and (b) the non-local equivalent plastic strain e^P .

8.3. Ductile fracture

We consider the quasi-static problem of a plane strain mode-I blunt crack in a homogeneous rate-independent isotropic elastoplastic material under small scale yielding conditions. Crack-tip plasticity is accounted for in the manner of a boundary layer formulation described by Rice (1967, 1968) and used by McMeeking (1977) in his pioneering large strain crack-tip finite element calculations. Traction free boundary conditions are used on the crack face and displacement boundary conditions remote from the tip are applied incrementally to impose an asymptotic dependence on the mode-I plane strain elastic solution, i.e., the following displacement field is applied on a circular

arc at a distance $r = R$ from the crack tip:

$$\begin{Bmatrix} u_1 \\ u_2 \end{Bmatrix} = \frac{K_I}{2G} \sqrt{\frac{r}{2\pi}} (3 - 4\nu - \cos\theta) \begin{Bmatrix} \cos\frac{\theta}{2} \\ \sin\frac{\theta}{2} \end{Bmatrix}, \quad (178)$$

where (u_1, u_2) are Cartesian displacement components, x_1 and x_2 are crack-tip Cartesian coordinates, x_1 being the axis of symmetry and x_2 the direction of mode-I loading, K_I is the mode-I stress intensity factor, and (r, θ) are crack-tip polar coordinates.

Let b_0 be the initial radius of the semicircular notch at the tip of the blunt crack. The outermost radius of the finite element mesh, where the elastic asymptotic displacement field (178) is imposed, is $R \cong 1200 b_0$. Because of symmetry, only half of the region $0 \leq \theta \leq \pi$ is analyzed. The finite element mesh in the region near the crack tip is shown in Fig. 11. A total of 1658 4-node plane strain coupled temperature-displacement elements with one Gauss integration (CPE4RT in ABAQUS) and hourglass control are used in the calculations.

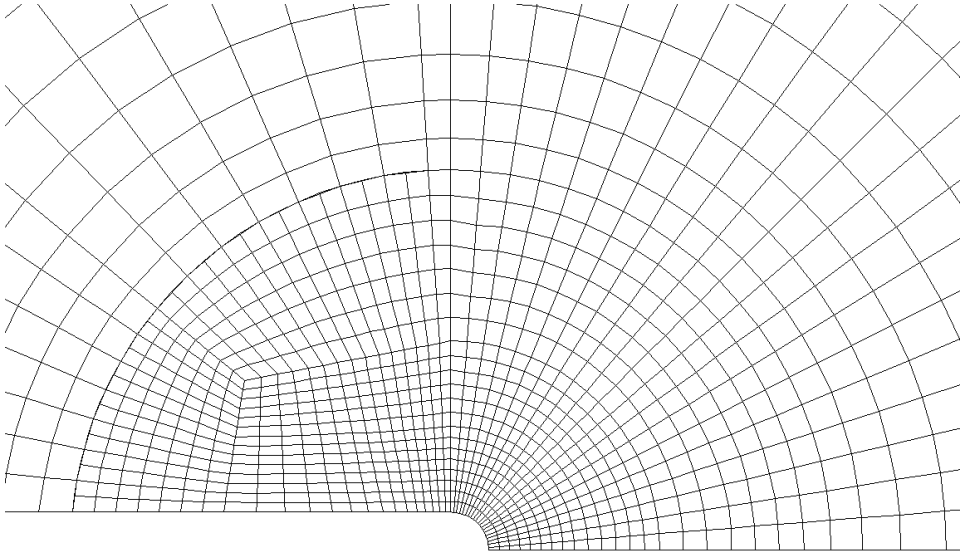


Figure 11: Finite element mesh in the region near the blunt crack tip.

A hardening exponent $n = 5$ and a material length $\ell = b_0 = 1$ mm are used in the computations.

The problem is solved using both ABAQUS/Standard with a user subroutine UMAT and ABAQUS/Explicit with a VUMAT. The material is rate-independent and time enters only as a “loading parameter” in the quasi-static problem. However, when ABAQUS/Explicit is used, the dynamic problem is solved and time enters the formulation explicitly. The values of mass density ρ and the time scale used influence the magnitude of the inertia terms and the strain rates that develop. Let $\bar{K}_I \equiv K_I/(\sigma_0 \sqrt{b_0})$ be the normalized applied load and $\dot{\epsilon} = \sqrt{2} \bar{\mathbf{e}} : \bar{\mathbf{e}}/3$ the norm of the strain rate tensor. The material parameters ρ , c , and the loading rate $\dot{\bar{K}}_I$ are chosen so that the kinetic energy is less than 1% of the total plastic work in the problem and condition (160) is satisfied, i.e., $\rho c \dot{\epsilon} = O(10^{-4})$ or less at all integration points in the finite element mesh.

A load of $\bar{K}_I = 40$ is applied. The maximum extent of the plastic zone at this load level is $r^p \simeq 0.17 R$. ABAQUS/Standard requires about 5000 increments for this first step, whereas ABAQUS/Explicit requires about 1 million increments and comparable computer time. Both codes give identical solutions up to the load $\bar{K}_I = 40$.

Figure 12 shows the variation of the local and non-local equivalent plastic strain ahead of the crack, plotted on the same scale, at various load levels; in Fig. 12 and in the following figures of this section, x is the distance of a material point in the undeformed configuration from the root of the semicircular notch. Clearly, at each material point, the

non-local value e^p is smaller than the corresponding local value $\bar{\varepsilon}^p$; this is due to the fact that e^p can be viewed as the spatial average value of $\bar{\varepsilon}^p$, as discussed in section 3.1. As $\ell \rightarrow 0$, the non-local value e^p at every material point approaches the corresponding local value $\bar{\varepsilon}^p$ at that point. The maximum values of both $\bar{\varepsilon}^p$ and e^p appear on the notch surface.

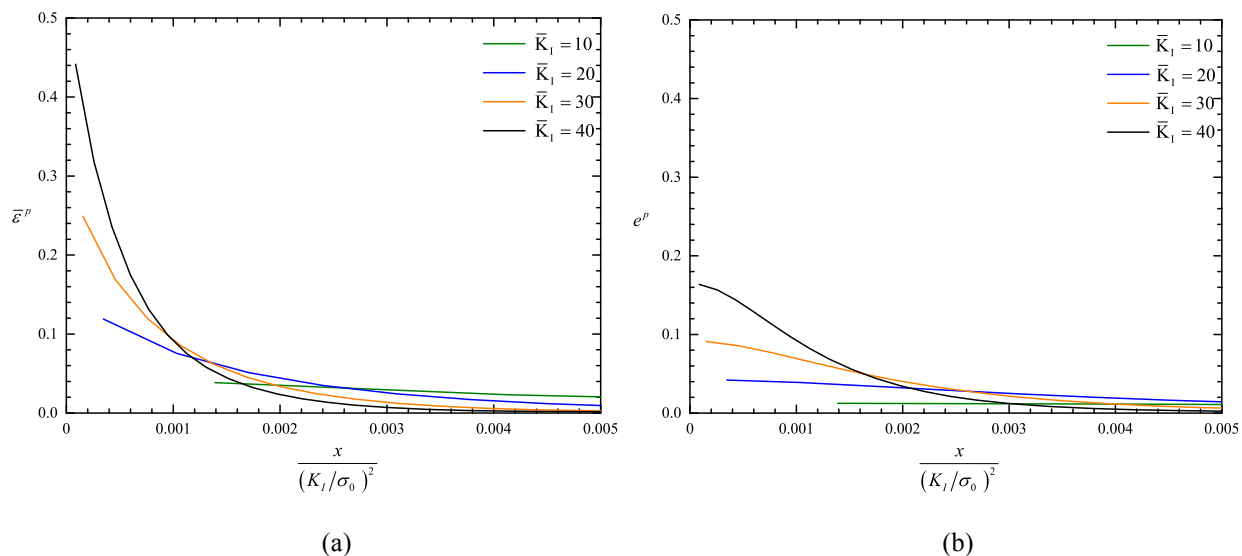


Figure 12: Distribution of the equivalent plastic strain $\bar{\varepsilon}^p$ (a) and the non-local equivalent plastic strain e^p (b) ahead of the crack tip at different load levels.

Figures 13 and 14 show the distribution of the opening stress σ_{22} , the von Mises equivalent stress σ_e , the hydrostatic stress $p = \sigma_{kk}/3$, and the triaxiality $\eta = p/\sigma_e$ ahead of the crack tip. The maximum value of the opening stress σ_{22} appears ahead of the notch whereas the maximum von Mises equivalent stress σ_e occurs on the notch surface. As shown in Fig. 14a the traction-free boundary condition reduces the value of the hydrostatic stress on the notch surface and causes the maximum of σ_{22} to occur ahead of the crack (McMeeking (1977)). At low load levels, both σ_{22} and σ_e increase with increasing \bar{K}_I ; however, as damage develops ahead of the crack, the load carrying capacity of the material decreases and leads to lower local stresses in that region.

Figure 15 shows the distribution of damage D ahead of the crack at different load levels. The evolution of damage depends on the non-local equivalent plastic strain e^p , the triaxiality η , and the Lode angle θ , as described in equations (31)–(34). Damage is initiated ahead of the crack at a load level of $\bar{K}_I = 17.8$. As shown in Fig. 15, the maximum value of D appears initially ahead of the crack and moves to the notch surface at higher loads.

ABAQUS/Standard has convergence difficulties beyond $\bar{K}_I = 40$, when material starts to fail locally; the calculations are terminated at this load level. A separate set of calculations is carried out using ABAQUS/Explicit and the solution can be continued for values of \bar{K}_I larger than 40.

The material is assumed to fail locally when the normalized damage indicator I_f reaches the value of $I_f = 1$. When the value of $I_f = 1$ is reached at the Gauss point of an element, the material is assumed to lose its load carrying capacity and the element is removed. Material failure starts on the root of the notch. Figure 16 shows contours of the damage parameter D at $\bar{K}_I = 40.1$ and $\bar{K}_I = 45$; deleted elements are shown “empty” in Fig. 16. For $\bar{K}_I = 45$, the maximum extent of the plastic zone is $r^p \approx 0.21 R$, i.e., the plastic zone is well inside the region of dominance of the applied asymptotic elastic solution.

9. Closure

In the present paper we have developed a methodology for the numerical implementation of a family of isotropic non-local elastoplastic damage models that include the effects of the third invariant J_3 of the stress deviator. The implementation in the ABAQUS general-purpose finite element code is discussed and several example problems are

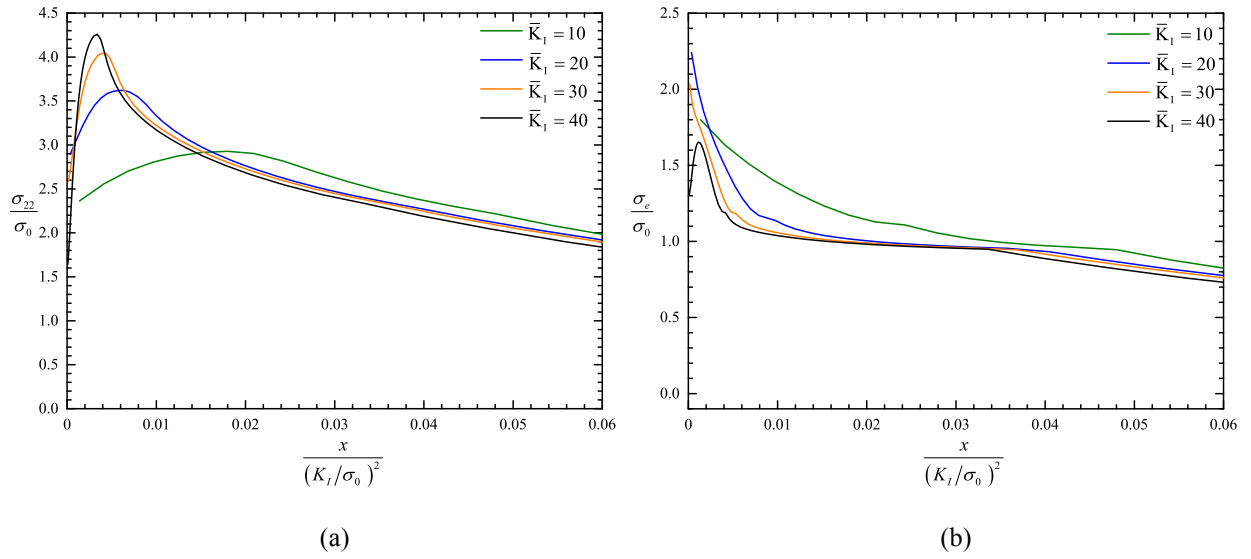


Figure 13: Distribution of (a) normalized stress σ_{22}/σ_0 and (b) normalised von Mises equivalent stress σ_e/σ_0 ahead of the crack tip at different load levels.

solved. The methodology is quite general and can be extended to anisotropic damage models for porous metals, such as those developed by Gurson (1977) and Ponte Castañeda and co-workers (Danas and Ponte Castañeda (2009a,b)). Such work is now underway.

Acknowledgments

The authors would like to thank Dr. Juan Hurtado, SIMULIA R&D Technology Director, for helpful discussions and material. The support of the European Commission through project RFCS-2015 709711 is gratefully acknowledged.

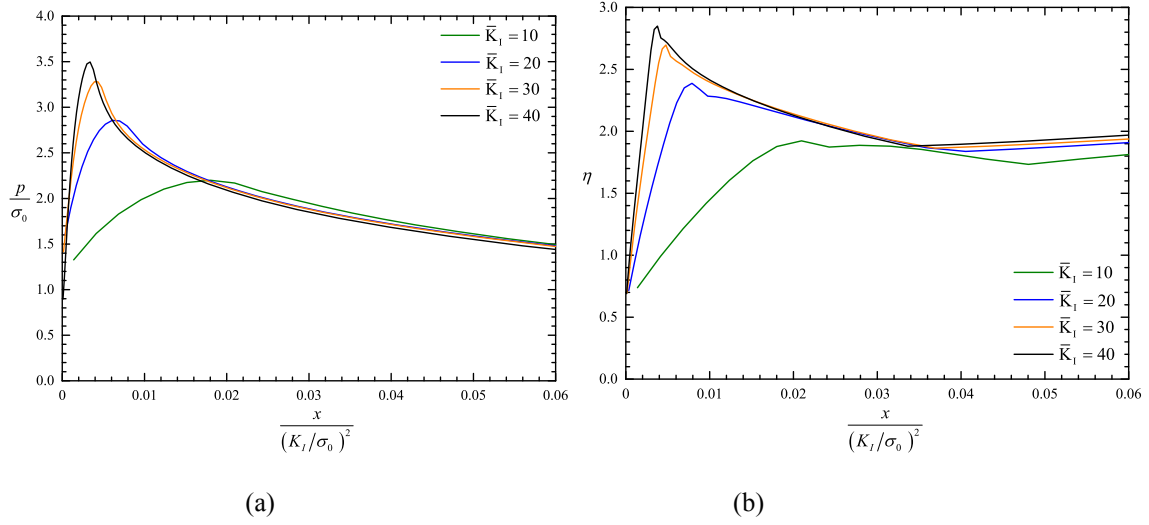


Figure 14: Distribution of (a) normalized hydrostatic stress p/σ_0 ($p = \sigma_{kk}/3$) and (b) triaxiality factor $\eta = p/\sigma_e$ ahead of the crack tip at different load levels.

Appendix A: Finite element matrices

The following convention is used in all Appendices:

- i) lower case Latin subscripts have a range of three, representing spatial coordinate directions ($i = 1, 2, 3$),
- ii) upper case Latin subscripts or superscripts have a range of eight, corresponding to element nodes ($A = 1, 2, \dots, 8$), and
- iii) lower case Greek subscripts have a range of four ($\alpha = 1, 2, 3, 4$).

In the physical domain we consider a global fixed Cartesian coordinate system with coordinates $\mathbf{x} = (x_1, x_2, x_3) = (x, y, z)$. We also introduce a bi-unit cube \square , sometimes called the “parent domain” or “master element”, with “natural coordinates” $\boldsymbol{\xi} = (\xi_1, \xi_2, \xi_3) = (\xi, \eta, \zeta)$ in the range $-1 \leq \xi_i \leq 1$ ($i = 1, 2, 3$).

Each 3D 8-node hexahedral isoparametric finite element Ω^e in the physical domain is mapped onto the master element \square with an invertible transformation of the form

$$x_i(\boldsymbol{\xi}) = \sum_{A=1}^8 N^A(\boldsymbol{\xi}) x_i^A \quad (i = 1, 2, 3), \quad (179)$$

where x_i^A is the i -th coordinate of node A in the physical domain, $N^A(\boldsymbol{\xi})$ are the element “shape functions”

$$N^A(\xi, \eta, \zeta) = \frac{1}{8}(1 + \xi^A \xi)(1 + \eta^A \eta)(1 + \zeta^A \zeta) \quad (A = 1, 2, \dots, 8), \quad (180)$$

and $(\xi^A, \eta^A, \zeta^A) = (\xi_1^A, \xi_2^A, \xi_3^A)$ are the values of the natural coordinates at the nodal points.

The components J_{ij} of the *Jacobian matrix* $[\mathbf{J}]$ and the *Jacobian* J of the transformation (179) are defined as

$$J_{ij}(\boldsymbol{\xi}) = \frac{\partial x_i(\boldsymbol{\xi})}{\partial \xi_j} \quad \text{and} \quad J(\boldsymbol{\xi}) = \det[\mathbf{J}(\boldsymbol{\xi})]. \quad (181)$$

Remark

Sometimes the point $\boldsymbol{\xi} = \mathbf{0}$ is referred to in the literature as the “centroid” of the element Ω^e . Using equation (179)

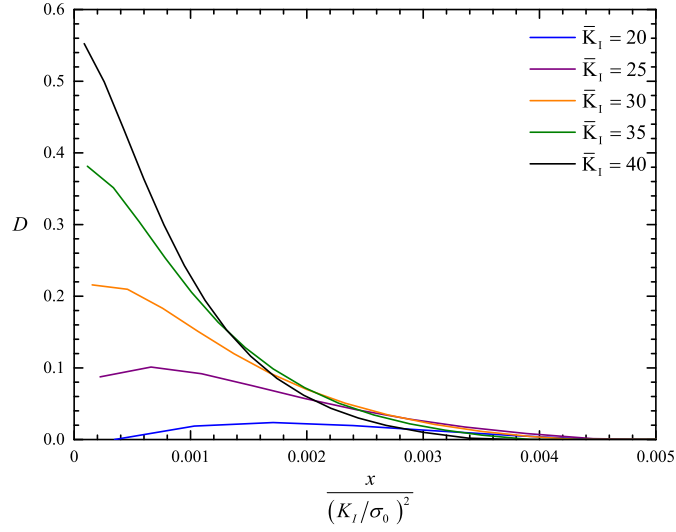


Figure 15: Distribution of the damage parameter D ahead of the crack tip at different load levels.

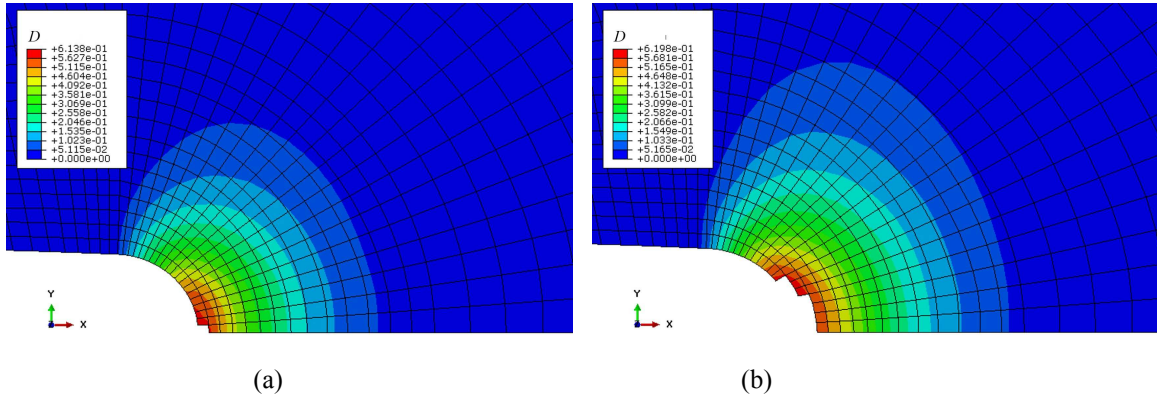


Figure 16: Contours of damage D and deleted elements at (a) $\bar{K}_I = 40.1$ and (b) $\bar{K}_I = 45$ (b). Solutions are obtained using ABAQUS/Explicit. When the value of $I_f = 1$ is reached at the Gauss point of an element, the material is assumed to lose its load carrying capacity and the element is removed. Deleted elements are shown “empty”.

we can readily show that

$$\mathbf{x}(\mathbf{0}) = \frac{1}{8} \sum_{A=1}^8 \mathbf{x}^A. \quad (182)$$

It is emphasized though that the point $\mathbf{x}(\mathbf{0})$ on the physical domain is not in general the geometric center of Ω^e , unless Ω^e is a rectangular parallelepiped. Therefore, we avoid the term “centroid” and refer to the material point at $\boldsymbol{\xi} = \mathbf{0}$ as the “*element local origin*”. \square

The “*constant Jacobian matrix*” and “*constant Jacobian*” are obtained by evaluation at the element local origin $\boldsymbol{\xi} = \mathbf{0}$:

$$[\mathbf{J}_0] = [\mathbf{J}(\mathbf{0})], \quad J_0 = J(\mathbf{0}). \quad (183)$$

We also define

$$j_{ik} = \left(\mathbf{J}_0^{-1} \right)_{ik} = \left. \frac{\partial \xi_i}{\partial x_k} \right|_{\boldsymbol{\xi}=\mathbf{0}}. \quad (184)$$

We recall that

$$\Delta L_{ij} = \frac{\partial \Delta u_i}{\partial x_j}, \quad (185)$$

and, following Simo and Rifai (1990) (see also Puso (2000)), we introduce the transformed quantities

$$\Delta \tilde{L}_{ij}(\boldsymbol{\xi}) \equiv \frac{J(\boldsymbol{\xi})}{J_0} (\mathbf{J}_0)_{mi} (\mathbf{J}_0)_{nj} \Delta L_{mn}(\boldsymbol{\xi}), \quad \text{so that} \quad \Delta L_{ij}(\boldsymbol{\xi}) \equiv \frac{J_0}{J(\boldsymbol{\xi})} j_{mi} j_{nj} \Delta \tilde{L}_{mn}(\boldsymbol{\xi}). \quad (186)$$

Equations (186) can be written in matrix form as

$$\left\{ \Delta \tilde{\mathbf{L}}(\boldsymbol{\xi}) \right\}_{9 \times 1} = \frac{J(\boldsymbol{\xi})}{J_0} [\mathcal{J}_0]_{9 \times 9} \left\{ \Delta \mathbf{L}(\boldsymbol{\xi}) \right\}_{9 \times 1} \quad \text{or} \quad \left\{ \Delta \mathbf{L}(\boldsymbol{\xi}) \right\}_{9 \times 1} = \frac{J_0}{J(\boldsymbol{\xi})} [\mathcal{K}_0]_{9 \times 9} \left\{ \Delta \tilde{\mathbf{L}}(\boldsymbol{\xi}) \right\}_{9 \times 1}, \quad (187)$$

where

$$[\Delta \mathbf{L}]_{1 \times 9} = \left[\Delta u_{1,1} \quad \Delta u_{2,2} \quad \Delta u_{3,3} \quad \Delta u_{1,2} \quad \Delta u_{2,1} \quad \Delta u_{1,3} \quad \Delta u_{3,1} \quad \Delta u_{2,3} \quad \Delta u_{3,2} \right], \quad (188)$$

$$[\mathcal{J}_0]_{9 \times 9} = [\mathcal{K}_0]_{9 \times 9}^{-1}, \quad (189)$$

$$[\mathcal{K}_0]_{9 \times 9} = \begin{bmatrix} j_{11}^2 & j_{21}^2 & j_{31}^2 & j_{11} j_{21} & j_{11} j_{21} & j_{11} j_{31} & j_{11} j_{31} & j_{21} j_{31} & j_{21} j_{31} \\ j_{12}^2 & j_{22}^2 & j_{32}^2 & j_{12} j_{22} & j_{12} j_{22} & j_{12} j_{32} & j_{12} j_{32} & j_{22} j_{32} & j_{22} j_{32} \\ j_{13}^2 & j_{23}^2 & j_{33}^2 & j_{13} j_{23} & j_{13} j_{23} & j_{13} j_{33} & j_{13} j_{33} & j_{23} j_{33} & j_{23} j_{33} \\ j_{11} j_{12} & j_{21} j_{22} & j_{31} j_{32} & j_{11} j_{22} & j_{12} j_{21} & j_{11} j_{32} & j_{12} j_{31} & j_{21} j_{32} & j_{22} j_{31} \\ j_{11} j_{12} & j_{21} j_{22} & j_{31} j_{32} & j_{12} j_{21} & j_{11} j_{22} & j_{12} j_{31} & j_{11} j_{32} & j_{22} j_{31} & j_{21} j_{32} \\ j_{11} j_{13} & j_{21} j_{23} & j_{31} j_{33} & j_{11} j_{23} & j_{13} j_{21} & j_{11} j_{33} & j_{13} j_{31} & j_{21} j_{33} & j_{23} j_{31} \\ j_{11} j_{13} & j_{21} j_{23} & j_{31} j_{33} & j_{13} j_{21} & j_{11} j_{23} & j_{13} j_{31} & j_{11} j_{33} & j_{23} j_{31} & j_{21} j_{33} \\ j_{12} j_{13} & j_{22} j_{23} & j_{32} j_{33} & j_{12} j_{23} & j_{13} j_{22} & j_{12} j_{33} & j_{13} j_{32} & j_{22} j_{33} & j_{23} j_{32} \\ j_{12} j_{13} & j_{22} j_{23} & j_{32} j_{33} & j_{13} j_{22} & j_{12} j_{23} & j_{13} j_{32} & j_{12} j_{33} & j_{23} j_{32} & j_{22} j_{33} \end{bmatrix}. \quad (190)$$

Equation (186b) shows that, given $\Delta \tilde{\mathbf{L}}$ in the natural space (ξ, η, ζ) , the enhanced gradient $\Delta \mathbf{L}$ in the physical space (x, y, z) is obtained by convecting $\Delta \tilde{\mathbf{L}}$ by the Jacobian of the isoparametric map according to (186b) or, equivalently, (187b).

If we use the approximation $\mathbf{J}(\boldsymbol{\xi}) \approx \mathbf{J}_0$ in (186a), we can show that the components $\Delta \tilde{L}_{ij}$ can be written in the form

$$\Delta \tilde{L}_{ij} \approx \frac{\partial \Delta \tilde{u}_i}{\partial \xi_j} = \sum_{A=1}^8 \frac{\partial N^A}{\partial \xi_j} \Delta \tilde{u}_i^A, \quad \Delta \tilde{u}_i \equiv (\mathbf{J}_0)_{ki} \Delta u_k, \quad (191)$$

where $\Delta \tilde{u}_i$ ($i = 1, 2, 3$) are the components of the convected incremental displacement and $\Delta \tilde{u}_i^A$ ($A = 1, 2, \dots, 8$) the corresponding nodal values. Equation (191a) shows that we can interpret $\Delta \tilde{\mathbf{L}}$ as an incremental displacement gradient in the natural space (ξ, η, ζ) , where the appropriate convected displacement increment is defined by (191b) above.

Using the transformation (191b) we can show that the transformed nodal displacements can be written in matrix form as

$$\left\{ \Delta \tilde{\mathbf{d}}^e \right\}_{1 \times 32} = [\mathcal{G}]_{32 \times 32} \left\{ \Delta \mathbf{d}^e \right\}_{1 \times 32}, \quad (192)$$

where

$$[\Delta \mathbf{d}^e]_{32 \times 1} = \left[\begin{array}{cccc} [\Delta \mathbf{d}_1]_{4 \times 1} & [\Delta \mathbf{d}_2]_{4 \times 1} & \cdots & [\Delta \mathbf{d}_8]_{4 \times 1} \end{array} \right], \quad (193)$$

$$[\Delta \mathbf{d}_A]_{4 \times 1} = \left[\Delta u_1^A \quad \Delta u_2^A \quad \Delta u_3^A \quad \Delta e_A^p \right], \quad A = 1, 2, \dots, 8, \quad (194)$$

$$[\mathbf{I}_0]_{4 \times 4}^T = \left[\begin{array}{cc} [\mathbf{J}_0]_{3 \times 3}^T & \mathbf{0}_{1 \times 1} \\ \mathbf{0}_{1 \times 1} & \mathbf{0}_{1 \times 1} \end{array} \right], \quad [\mathcal{G}]_{32 \times 32} = \left[\begin{array}{ccc} [\mathbf{I}_0]_{4 \times 4}^T & & \\ & \ddots & \\ & & [\mathbf{I}_0]_{4 \times 4}^T \end{array} \right], \quad (195)$$

with $(\Delta u_i^A, \Delta e^P)$ being the increments of the components of displacement and of the non-local equivalent plastic strain at node A .

The idea now is to define the finite element interpolation of the enhanced field transformed $\Delta \tilde{\mathbf{L}}(\xi)$ in the natural space (ξ, η, z) and then to convect it in accordance with (186a) to determine the corresponding enhanced $\Delta \mathbf{L}$ in the physical space (x, y, z) . The resulting interpolation for $\Delta \mathbf{L}$ is automatically frame invariant provided that the interpolation of $\Delta \tilde{\mathbf{L}}(\xi)$ is $\{\xi, \eta, \zeta\}$ -invariant. We recall the enhanced gradient fields (117) and (120):

$$\{\Delta \mathbf{L}(\mathbf{x})\}_{9 \times 1} = \left(\overline{[\mathbf{B}_L]}_{9 \times 32} + [\mathbf{B}_{\text{stab}}(\mathbf{x})]_{9 \times 32} \right) \{\Delta \mathbf{d}^e\}_{32 \times 1} + [\mathbf{G}(\mathbf{x})]_{9 \times 6} \{\Delta \mathbf{a}^e\}_{6 \times 1}, \quad (196)$$

$$\{\Delta \mathbf{g}(\mathbf{x})\}_{3 \times 1} = \left(\overline{[\mathbf{B}_\varepsilon]}_{3 \times 32} + [\mathbf{B}_\varepsilon^{\text{stab}}(\mathbf{x})]_{3 \times 32} \right) \{\Delta \mathbf{d}^e\}_{32 \times 1}. \quad (197)$$

The constant matrices $\overline{[\mathbf{B}_L]}$ and $\overline{[\mathbf{B}_\varepsilon]}$ in (196) and (197) are defined in (122). Following Puso (2000), we define $[\mathbf{B}_{\text{stab}}(\mathbf{x})]$, $[\mathbf{G}(\mathbf{x})]$, and $[\mathbf{B}_\varepsilon^{\text{stab}}(\mathbf{x})]$ by convecting appropriately defined matrices on the natural space (ξ, η, z) . We start by writing

$$\{\Delta \tilde{\mathbf{L}}_{\text{stab}}(\xi)\}_{9 \times 1} = [\tilde{\mathbf{B}}_{\text{stab}}(\xi)]_{9 \times 32} \{\Delta \tilde{\mathbf{d}}^e\}_{32 \times 1}, \quad (198)$$

where

$$[\tilde{\mathbf{B}}_{\text{stab}}(\xi)]_{9 \times 32} = \begin{bmatrix} [\tilde{\mathbf{B}}_1(\xi)]_{9 \times 4} & [\tilde{\mathbf{B}}_2(\xi)]_{9 \times 4} & \cdots & [\tilde{\mathbf{B}}_8(\xi)]_{9 \times 4} \end{bmatrix}, \quad (199)$$

with

$$[\tilde{\mathbf{B}}_A(\xi)]_{9 \times 4} = \begin{bmatrix} \gamma_1^A \eta + \gamma_3^A \zeta + \gamma_4^A \eta \zeta & 0 & 0 & 0 \\ 0 & \gamma_1^A \xi + \gamma_2^A \zeta + \gamma_4^A \zeta \xi & 0 & 0 \\ 0 & 0 & \gamma_2^A \eta + \gamma_3^A \xi + \gamma_4^A \xi \eta & 0 \\ \gamma_2^A \zeta & 0 & 0 & 0 \\ 0 & \gamma_3^A \zeta & 0 & 0 \\ \gamma_2^A \eta & 0 & 0 & 0 \\ 0 & 0 & \gamma_1^A \eta & 0 \\ 0 & \gamma_3^A \xi & 0 & 0 \\ 0 & 0 & \gamma_1^A \xi & 0 \end{bmatrix} \quad A = 1, 2, \dots, 8, \quad (200)$$

$$\{\gamma_\alpha\}_{8 \times 1} = \frac{1}{8} \left[\{\mathbf{h}_\alpha\}_{8 \times 1} - \sum_{i=1}^3 \left([\mathbf{h}_\alpha]_{1 \times 8} \{\mathbf{x}_i\}_{8 \times 1} \right) \overline{\{\mathbf{b}_i\}}_{8 \times 1} \right] \quad \alpha = 1, 2, 3, 4, \quad (201)$$

$$[\mathbf{h}_1]_{1 \times 8} = \begin{bmatrix} 1 & -1 & 1 & -1 & 1 & -1 & 1 & -1 \end{bmatrix}, \quad (202)$$

$$[\mathbf{h}_2]_{1 \times 8} = \begin{bmatrix} 1 & 1 & -1 & -1 & -1 & -1 & 1 & 1 \end{bmatrix}, \quad (203)$$

$$[\mathbf{h}_3]_{1 \times 8} = \begin{bmatrix} 1 & -1 & -1 & 1 & -1 & 1 & 1 & -1 \end{bmatrix}, \quad (204)$$

$$[\mathbf{h}_4]_{1 \times 8} = \begin{bmatrix} -1 & 1 & -1 & 1 & 1 & -1 & 1 & -1 \end{bmatrix}, \quad (205)$$

$$\overline{\{\mathbf{b}_i\}}_{8 \times 1} = \frac{1}{V_e} \int_{\Omega^e} \frac{\partial}{\partial x_i} \{\mathbf{N}\}_{8 \times 1} d\Omega \quad i = 1, 2, 3, \quad (206)$$

where γ_α^A is the A -th component of $\{\gamma_\alpha\}$ ($\alpha = 1, 2, 3, 4$, $A = 1, 2, \dots, 8$). Analytical expressions for the components of $\overline{\{\mathbf{b}_i\}}$ can be found in Flanagan and Belytschko (1981).

Next, we combine equation (200) with $\{\Delta \mathbf{L}_{\text{stab}}(\xi)\} = [\mathbf{B}_{\text{stab}}(\xi)] \{\Delta \mathbf{d}^e\}$ and the transformation (187b) to find the expression

$$[\mathbf{B}_{\text{stab}}(\xi)]_{9 \times 32} = \frac{J_0}{J(\xi)} [\mathcal{K}_0]_{9 \times 9} [\tilde{\mathbf{B}}_{\text{stab}}(\xi)]_{9 \times 32} [\mathcal{G}]_{32 \times 32}, \quad (207)$$

which defines the $[\mathbf{B}_{\text{stab}}]$ -matrix in the physical space (x, y, z) .

The form of $[\tilde{\mathbf{B}}_A(\xi)]$ in (200) is discussed in detail by Puso (2000). Here we mention that the last six rows of $[\tilde{\mathbf{B}}_A(\xi)]$ in (200) are chosen so that shear locking is eliminated when the element is a rectangular parallelepiped (Freischläger and Schweizerhof (1996)). We also note that the expression for $[\tilde{\mathbf{B}}_{\text{stab}}(\xi)]$ in (199) can be written in the following alternative form:

$$[\tilde{\mathbf{B}}_{\text{stab}}(\xi)]_{9 \times 32} = \sum_{\alpha=1}^4 [\hat{\mathbf{B}}_{\alpha}(\xi)]_{9 \times 4} [\mathbf{\Gamma}_{\alpha}]_{4 \times 32}^T, \quad (208)$$

where

$$[\hat{\mathbf{B}}_1(\xi)]_{9 \times 4} = \begin{bmatrix} \eta & 0 & 0 & 0 \\ 0 & \xi & 0 & 0 \\ 0 & 0 & 0 & 0 \\ 0 & 0 & 0 & 0 \\ 0 & 0 & 0 & 0 \\ 0 & 0 & 0 & 0 \\ 0 & 0 & \eta & 0 \\ 0 & 0 & 0 & 0 \\ 0 & 0 & \xi & 0 \end{bmatrix}, \quad [\hat{\mathbf{B}}_2(\xi)]_{9 \times 4} = \begin{bmatrix} 0 & 0 & 0 & 0 \\ 0 & \zeta & 0 & 0 \\ 0 & 0 & \eta & 0 \\ \zeta & 0 & 0 & 0 \\ 0 & 0 & 0 & 0 \\ \eta & 0 & 0 & 0 \\ 0 & 0 & 0 & 0 \\ 0 & 0 & 0 & 0 \\ 0 & 0 & 0 & 0 \end{bmatrix}, \quad [\hat{\mathbf{B}}_3(\xi)]_{9 \times 4} = \begin{bmatrix} \zeta & 0 & 0 & 0 \\ 0 & 0 & 0 & 0 \\ 0 & 0 & \xi & 0 \\ 0 & 0 & 0 & 0 \\ 0 & \zeta & 0 & 0 \\ 0 & 0 & 0 & 0 \\ 0 & 0 & 0 & 0 \\ 0 & 0 & 0 & 0 \\ 0 & \xi & 0 & 0 \end{bmatrix}, \quad (209)$$

$$[\hat{\mathbf{B}}_4(\xi)]_{9 \times 4} = \begin{bmatrix} \eta \zeta & 0 & 0 & 0 \\ 0 & \zeta \xi & 0 & 0 \\ 0 & 0 & \xi \eta & 0 \\ 0 & 0 & 0 & 0 \\ 0 & 0 & 0 & 0 \\ 0 & 0 & 0 & 0 \\ 0 & 0 & 0 & 0 \\ 0 & 0 & 0 & 0 \\ 0 & 0 & 0 & 0 \end{bmatrix}, \quad [\mathbf{\Gamma}_{\alpha}]_{32 \times 4} = \begin{bmatrix} \gamma_{\alpha}^1 [\boldsymbol{\delta}]_{4 \times 4} \\ \gamma_{\alpha}^2 [\boldsymbol{\delta}]_{4 \times 4} \\ \vdots \\ \gamma_{\alpha}^8 [\boldsymbol{\delta}]_{4 \times 4} \end{bmatrix}, \quad [\boldsymbol{\delta}]_{4 \times 4} = \begin{bmatrix} 1 & & & \\ & 1 & & \\ & & 1 & \\ & & & 1 \end{bmatrix}. \quad (210)$$

We also note the following identity

$$[\mathcal{G}]_{32 \times 32}^T [\mathbf{\Gamma}_{\alpha}]_{32 \times 4} = [\mathbf{\Gamma}_{\alpha}]_{32 \times 4} [\mathbf{I}_0]_{4 \times 4} \quad (211)$$

or

$$[\mathbf{M}_{\alpha}]_{4 \times 32} \equiv [\mathbf{\Gamma}_{\alpha}]_{32 \times 4}^T [\mathcal{G}]_{32 \times 32} = [\mathbf{I}_0]_{4 \times 4}^T [\mathbf{\Gamma}_{\alpha}]_{32 \times 4}^T = \left[\gamma_{\alpha}^1 [\mathbf{I}_0]_{4 \times 4}^T \quad \gamma_{\alpha}^2 [\mathbf{I}_0]_{4 \times 4}^T \quad \cdots \quad \gamma_{\alpha}^8 [\mathbf{I}_0]_{4 \times 4}^T \right]. \quad (212)$$

When we replace the left-hand-side of (211) with the right-hand-side in a computer code, we reduce significantly the number of arithmetic operations involved.

Similarly, the $[\mathbf{G}(\xi)]$ -matrix in the physical space (x, y, z) is formed by convecting an appropriately defined $[\tilde{\mathbf{G}}(\xi)]$ -

matrix in the natural plane (ξ, η, ζ) (Puso (2000)):

$$[\mathbf{G}(\xi)]_{9 \times 6} = \frac{J_0}{J(\xi)} [\mathcal{K}_0]_{9 \times 9} [\tilde{\mathbf{G}}(\xi)]_{9 \times 6}, \quad [\tilde{\mathbf{G}}(\xi)]_{9 \times 6} = \begin{bmatrix} \xi & 0 & 0 & \eta\xi & \zeta\eta & \zeta\xi \\ 0 & \eta & 0 & \eta\xi & \zeta\eta & \zeta\xi \\ 0 & 0 & \zeta & \eta\xi & \zeta\eta & \zeta\xi \\ 0 & 0 & 0 & 0 & 0 & 0 \\ 0 & 0 & 0 & 0 & 0 & 0 \\ 0 & 0 & 0 & 0 & 0 & 0 \\ 0 & 0 & 0 & 0 & 0 & 0 \\ 0 & 0 & 0 & 0 & 0 & 0 \\ 0 & 0 & 0 & 0 & 0 & 0 \end{bmatrix}. \quad (213)$$

The last three columns in $[\tilde{\mathbf{G}}(\xi)]$ provide the bilinear terms in interpolation (117) of $\Delta \mathbf{L}$ necessary to avoid incompressibility locking.

Finally, the stabilization matrix $[\mathbf{B}_\varepsilon^{\text{stab}}(\xi)]$ that enters the enhanced gradient \mathbf{g} of the non-local equivalent plastic e^p in (120) is defined as

$$[\mathbf{B}_\varepsilon^{\text{stab}}(\xi)]_{3 \times 32} = \frac{J_0}{J(\xi)} [\mathbf{J}_0]_{3 \times 3}^{-1} [\tilde{\mathbf{B}}_\varepsilon^{\text{stab}}(\xi)]_{3 \times 32}, \quad (214)$$

where

$$[\tilde{\mathbf{B}}_\varepsilon^{\text{stab}}(\xi)]_{3 \times 32} = \begin{bmatrix} [\hat{\mathbf{B}}_\varepsilon^1(\xi)]_{3 \times 4} & [\hat{\mathbf{B}}_\varepsilon^2(\xi)]_{3 \times 4} & \cdots & [\hat{\mathbf{B}}_\varepsilon^8(\xi)]_{3 \times 4} \end{bmatrix}, \quad (215)$$

$$[\hat{\mathbf{B}}_\varepsilon^A(\xi)]_{3 \times 4} = \begin{bmatrix} 0 & 0 & 0 & \gamma_1^A \eta + \gamma_3^A \zeta + \gamma_4^A \eta \zeta \\ 0 & 0 & 0 & \gamma_1^A \xi + \gamma_2^A \zeta + \gamma_4^A \zeta \xi \\ 0 & 0 & 0 & \gamma_2^A \eta + \gamma_3^A \xi + \gamma_4^A \xi \eta \end{bmatrix} \quad (A = 1, 2, \dots, 8). \quad (216)$$

An alternative expression for $[\tilde{\mathbf{B}}_\varepsilon^{\text{stab}}(\xi)]$, as defined in (215), is

$$[\tilde{\mathbf{B}}_\varepsilon^{\text{stab}}(\xi)]_{3 \times 32} = \sum_{\alpha=1}^4 [\hat{\mathbf{B}}_\varepsilon^\alpha(\xi)]_{3 \times 4} [\mathbf{\Gamma}_\alpha]_{4 \times 32}^T, \quad (217)$$

where

$$[\hat{\mathbf{B}}_\varepsilon^1(\xi)]_{3 \times 4} = \begin{bmatrix} 0 & 0 & 0 & \eta \\ 0 & 0 & 0 & \xi \\ 0 & 0 & 0 & 0 \end{bmatrix}, \quad [\hat{\mathbf{B}}_\varepsilon^2(\xi)]_{3 \times 4} = \begin{bmatrix} 0 & 0 & 0 & 0 \\ 0 & 0 & 0 & \zeta \\ 0 & 0 & 0 & \eta \end{bmatrix}, \quad (218)$$

$$[\hat{\mathbf{B}}_\varepsilon^3(\xi)]_{3 \times 4} = \begin{bmatrix} 0 & 0 & 0 & \zeta \\ 0 & 0 & 0 & 0 \\ 0 & 0 & 0 & \xi \end{bmatrix}, \quad [\hat{\mathbf{B}}_\varepsilon^4(\xi)]_{3 \times 4} = \begin{bmatrix} 0 & 0 & 0 & \eta \zeta \\ 0 & 0 & 0 & \zeta \xi \\ 0 & 0 & 0 & \xi \eta \end{bmatrix}. \quad (219)$$

Appendix B: Calculation of $\{\Delta \mathbf{a}^e\}$ in terms of $\{\Delta \mathbf{d}^e\}$

Equations (144) are written for every element in the finite element mesh and provide a set of six non-linear equations per element that define the local element parameters $\{\Delta \mathbf{a}^e\}$ in terms of the element nodal degrees of freedom $\{\Delta \mathbf{d}^e\}$. We recall that (144) has the form

$$\int_{\square} [\mathbf{G}(\boldsymbol{\xi})]_{6 \times 9}^T \{\boldsymbol{\sigma}_{n+1}(\boldsymbol{\xi})\}_{9 \times 1} J_{n+1}(\boldsymbol{\xi}) d\square = \{\mathbf{0}\}_{6 \times 1}, \quad (220)$$

for all elements, where $J(\boldsymbol{\xi})$ is the Jacobian of the transformation of the mapping from the master element to domain Ω^e in physical space (see equation (181b) in Appendix A). We also note that (144) is also satisfied at the start of the increment, i.e.,

$$\int_{\square} [\mathbf{G}(\boldsymbol{\xi})]_{6 \times 9}^T \{\boldsymbol{\sigma}_n(\boldsymbol{\xi})\}_{9 \times 1} J_n(\boldsymbol{\xi}) d\square = \{\mathbf{0}\}_{6 \times 1}. \quad (221)$$

In plastically incompressible materials, $J_{n+1} \approx J_n$ to first order, since the elastic strains are small. Then, last two equations imply that

$$\int_{\Omega^e} [\mathbf{G}(\boldsymbol{\xi})]_{6 \times 9}^T \{\Delta \boldsymbol{\sigma}(\boldsymbol{\xi})\}_{9 \times 1} d\Omega = \{\mathbf{0}\}_{6 \times 1}, \quad (222)$$

on all elements in the problem.

In the following we use the constitutive equation (51) $\overset{\nabla}{\boldsymbol{\sigma}} = \mathcal{L} : \mathbf{D} - \mathbf{A}^{\text{nl}} \dot{e}^p$, to linearize (222) and then introduce standard approximations used in physical stabilization methods to determine analytically $\{\Delta \mathbf{a}^e\}$ in terms of $\{\Delta \mathbf{d}^e\}$.

We start by writing the constitutive equation (51) $\overset{\nabla}{\boldsymbol{\sigma}} = \mathcal{L} : \mathbf{D} - \mathbf{A}^{\text{nl}} \dot{e}^p$, in the form

$$\dot{\boldsymbol{\sigma}} = \mathbf{C} : \mathbf{L} - \mathbf{A}^{\text{nl}} \dot{e}^p, \quad (223)$$

where

$$C_{ijpq} = \mathcal{L}_{ijpq} + \frac{1}{2} (\sigma_{iq} \delta_{jp} + \sigma_{jq} \delta_{ip} - \sigma_{ip} \delta_{jq} - \sigma_{jp} \delta_{iq}). \quad (224)$$

Equation (223) leads to the following approximate expression for $\Delta \boldsymbol{\sigma}$:

$$\Delta \boldsymbol{\sigma} \approx \mathbf{C} : \Delta \mathbf{L} - \mathbf{A}^{\text{nl}} \Delta e^p, \quad (225)$$

where \mathbf{C} and \mathbf{A}^{nl} are evaluated at the start of the increment at $t = t_n$. We introduce next the finite element interpolations for $\Delta \mathbf{L}$ and Δe^p from (117) and (119) to find

$$\begin{aligned} \{\Delta \boldsymbol{\sigma}(\boldsymbol{\xi})\}_{9 \times 1} \cong & \left([\mathbf{C}(\boldsymbol{\xi})]_{9 \times 9} \left(\overline{[\mathbf{B}_L]}_{9 \times 32} + [\mathbf{B}_{\text{stab}}(\boldsymbol{\xi})]_{9 \times 32} \right) - \{\mathbf{A}^{\text{nl}}(\boldsymbol{\xi})\}_{9 \times 1} [\mathbf{N}_{\varepsilon}(\boldsymbol{\xi})]_{1 \times 32} \right) \{\Delta \mathbf{d}^e\}_{32 \times 1} + \\ & + [\mathbf{C}(\boldsymbol{\xi})]_{9 \times 9} [\mathbf{G}(\boldsymbol{\xi})]_{9 \times 6} \{\Delta \mathbf{a}^e\}_{6 \times 1}, \end{aligned} \quad (226)$$

where

$$[\Delta \boldsymbol{\sigma}]_{1 \times 9} = \{\Delta \boldsymbol{\sigma}\}^T = \left[\Delta \sigma_{11} \quad \Delta \sigma_{22} \quad \Delta \sigma_{33} \quad \Delta \sigma_{12} \quad \Delta \sigma_{21} \quad \Delta \sigma_{13} \quad \Delta \sigma_{31} \quad \Delta \sigma_{23} \quad \Delta \sigma_{32} \right], \quad (227)$$

$$[\mathbf{A}^{\text{nl}}]_{1 \times 9} = \{\mathbf{A}^{\text{nl}}\}^T = \left[A_{11}^{\text{nl}} \quad A_{22}^{\text{nl}} \quad A_{33}^{\text{nl}} \quad A_{12}^{\text{nl}} \quad A_{21}^{\text{nl}} \quad A_{13}^{\text{nl}} \quad A_{31}^{\text{nl}} \quad A_{23}^{\text{nl}} \quad A_{32}^{\text{nl}} \right]. \quad (228)$$

Note that $\{\Delta \boldsymbol{\sigma}(\boldsymbol{\xi})\}$ in (226) is linear in $\{\Delta \mathbf{d}^e\}$ and $\{\Delta \mathbf{a}^e\}$.

Evaluation of (226) at $\boldsymbol{\xi} = \mathbf{0}$ yields

$$\{\Delta \boldsymbol{\sigma}_0\}_{9 \times 1} \equiv \{\Delta \boldsymbol{\sigma}(\mathbf{0})\}_{9 \times 1} = \left([\mathbf{C}_0]_{9 \times 9} \overline{[\mathbf{B}_L]}_{9 \times 32} - \{\mathbf{A}_0^{\text{nl}}\}_{9 \times 1} [\mathbf{N}_{\varepsilon 0}]_{1 \times 32} \right) \{\Delta \mathbf{d}^e\}_{32 \times 1}, \quad (229)$$

where we took into account (133) and a zero subscript indicates that the corresponding quantity is evaluated at $\boldsymbol{\xi} = \mathbf{0}$.

Next, we introduce two fundamental approximations used in physical stabilization methods (Puso (2000)):

- (i) the values of the constitutive matrices $[\mathbf{C}(\boldsymbol{\xi})]$ and $[\mathbf{A}^{\text{nl}}(\boldsymbol{\xi})]$ over the whole element domain are approximated with their values at the corresponding local origin, i.e., we set $[\mathbf{C}(\boldsymbol{\xi})] \cong [\mathbf{C}_0]$ and $[\mathbf{A}^{\text{nl}}(\boldsymbol{\xi})] \cong [\mathbf{A}_0^{\text{nl}}]$,
- (ii) the value of the Jacobian $J(\boldsymbol{\xi})$ over the whole element domain is approximated with its value at the corresponding local origin, i.e., we set $J(\boldsymbol{\xi}) \cong J(\mathbf{0}) \equiv J_0$.

Then, (226) can be written in the form

$$\{\Delta\boldsymbol{\sigma}(\boldsymbol{\xi})\}_{9 \times 1} \cong \{\Delta\boldsymbol{\sigma}_0\}_{9 \times 1} + \{\Delta\boldsymbol{\sigma}_{\text{stab}}(\boldsymbol{\xi})\}_{9 \times 1}, \quad (230)$$

where $\{\Delta\boldsymbol{\sigma}_0\}$ is defined in (229) and

$$\{\Delta\boldsymbol{\sigma}_{\text{stab}}(\boldsymbol{\xi})\}_{9 \times 1} = \left([\mathbf{C}_0]_{9 \times 9} [\mathbf{B}_{\text{stab}}(\boldsymbol{\xi})]_{9 \times 32} - \{\mathbf{A}_0^{\text{nl}}\}_{9 \times 1} [\hat{\mathbf{N}}_\varepsilon(\boldsymbol{\xi})]_{1 \times 32} \right) \{\Delta\mathbf{d}^e\}_{32 \times 1} + [\mathbf{C}_0]_{9 \times 9} [\mathbf{G}(\boldsymbol{\xi})]_{9 \times 6} \{\Delta\mathbf{a}^e\}_{6 \times 1}, \quad (231)$$

with $[\hat{\mathbf{N}}_\varepsilon(\boldsymbol{\xi})] = [\mathbf{N}_\varepsilon(\boldsymbol{\xi})] - [\mathbf{N}_\varepsilon(\mathbf{0})]$.

Finally, we substitute (230)–(231) into (222) to find

$$[\mathbf{K}_{au}]_{6 \times 32} \{\Delta\mathbf{d}^e\}_{32 \times 1} + [\mathbf{K}_{aa}]_{6 \times 6} \{\Delta\mathbf{a}^e\}_{6 \times 1} \cong \{\mathbf{0}\}_{6 \times 1} \quad \text{or} \quad \{\Delta\mathbf{a}^e\}_{6 \times 1} \cong -[\mathbf{K}_{aa}]_{6 \times 6}^{-1} [\mathbf{K}_{au}]_{6 \times 32} \{\Delta\mathbf{d}^e\}_{32 \times 1}, \quad (232)$$

where

$$[\mathbf{K}_{aa}]_{6 \times 6} = \int_{\Omega^e} [\mathbf{G}]_{6 \times 9}^T [\mathbf{C}_0]_{9 \times 9} [\mathbf{G}]_{9 \times 6} d\Omega, \quad [\mathbf{K}_{au}]_{6 \times 32} = \int_{\Omega^e} [\mathbf{G}]_{6 \times 9}^T \left([\mathbf{C}_0]_{9 \times 9} [\mathbf{B}_{\text{stab}}]_{9 \times 32} - \{\mathbf{A}_0^{\text{nl}}\}_{9 \times 1} [\hat{\mathbf{N}}_\varepsilon]_{1 \times 32} \right) d\Omega. \quad (233)$$

Matrix $[\mathbf{G}(\boldsymbol{\xi})]$ is chosen in Appendix A such that $[\mathbf{K}_{aa}]$ is diagonal and the inversion required in (232b) is trivial. Also, analytical expressions can be obtained for $[\mathbf{K}_{aa}]$ and $[\mathbf{K}_{au}]$ as described in the following. Therefore, the calculation of $\{\Delta\mathbf{a}^e\}$ in (232b) is very efficient computationally.

The analytical evaluation of $[\mathbf{K}_{aa}]$ and $[\mathbf{K}_{au}]$ is as follows. We use the transformations (207) and (213a) for $[\mathbf{B}_{\text{stab}}]$ and $[\mathbf{G}]$, and introduce the transformed matrices

$$[\tilde{\mathbf{C}}_0]_{9 \times 9} = [\mathcal{K}_0]_{9 \times 9}^T [\mathbf{C}_0]_{9 \times 9} [\mathcal{K}_0]_{9 \times 9}, \quad \{\tilde{\mathbf{A}}_0^{\text{nl}}\}_{9 \times 1} = [\mathcal{K}_0]_{9 \times 9}^T \{\mathbf{A}_0^{\text{nl}}\}_{9 \times 1}, \quad (234)$$

where $[\mathcal{K}_0]$ is defined in (190), so that equations (233) can be written in the form

$$[\mathbf{K}_{aa}]_{6 \times 6} = \int_{\Omega^e} [\tilde{\mathbf{G}}]_{6 \times 9}^T [\tilde{\mathbf{C}}_0]_{9 \times 9} [\tilde{\mathbf{G}}]_{9 \times 6} d\Omega, \quad [\mathbf{K}_{au}]_{6 \times 32} = \int_{\Omega^e} [\tilde{\mathbf{G}}]_{6 \times 9}^T \left([\tilde{\mathbf{C}}_0]_{9 \times 9} [\tilde{\mathbf{B}}_{\text{stab}}]_{9 \times 32} - \{\tilde{\mathbf{A}}_0^{\text{nl}}\}_{9 \times 1} [\hat{\mathbf{N}}_\varepsilon]_{1 \times 32} \right) d\Omega. \quad (235)$$

Let \tilde{C}_{ij} and \tilde{A}_i be the elements of $[\tilde{\mathbf{C}}_0]$ and $\{\tilde{\mathbf{A}}_0^{\text{nl}}\}$ and use the approximation $d\Omega = J(\boldsymbol{\xi}) d\boldsymbol{\xi} \cong J_0 d\boldsymbol{\xi}$. Then, using (235a) and equation (213b) for $[\tilde{\mathbf{G}}]$, we find the following analytical expressions for the elements of the diagonal matrix $[\mathbf{K}_{aa}]$ (see also Puso (2000))

$$(\mathbf{K}_{aa})_{ii} = \frac{8J_0}{3} \tilde{C}_{ii} \quad i = 1, 2, 3 \quad (\text{no summation on } i), \quad (236)$$

$$\begin{aligned} (\mathbf{K}_{aa})_{44} &= (\mathbf{K}_{aa})_{55} = (\mathbf{K}_{aa})_{66} = \\ &= \frac{8J_0}{9} \left(\tilde{C}_{11} + \tilde{C}_{22} + \tilde{C}_{33} + \tilde{C}_{12} + \tilde{C}_{21} + \tilde{C}_{23} + \tilde{C}_{32} + \tilde{C}_{13} + \tilde{C}_{31} \right). \end{aligned} \quad (237)$$

Also, taking into account that

$$\{\hat{\mathbf{N}}_\varepsilon(\boldsymbol{\xi})\}_{32 \times 1} = \sum_{I=1}^8 \hat{N}_I(\boldsymbol{\xi})_{32 \times 1} \{\boldsymbol{\delta}_I\}, \quad \{\boldsymbol{\delta}_I\}_J = \begin{cases} 0 & \text{if } J \neq 4I, \\ 1 & \text{if } J = 4I, \end{cases} \quad I = 1, 2, \dots, 8, \quad J = 1, 2, \dots, 32, \quad (238)$$

and using (235b), we conclude that we can write $[\mathbf{K}_{au}]$ in the form

$$[\mathbf{K}_{au}] = [\mathbf{K}_{au1}] - [\mathbf{K}_{au2}], \quad (239)$$

where

$$[\mathbf{K}_{au1}] = \sum_{\alpha=1}^4 [\mathbf{K}_{au1}^{\alpha}] [\mathbf{M}_{\alpha}], \quad [\mathbf{K}_{au2}] = \sum_{l=1}^8 \{\mathbf{K}_{au2}^l\} \{\delta_l\}, \quad (240)$$

with

$$[\mathbf{M}_{\alpha}] = \begin{bmatrix} \gamma_{\alpha}^1 [\mathbf{I}_0]^T & \gamma_{\alpha}^2 [\mathbf{I}_0]^T & \cdots & \gamma_{\alpha}^8 [\mathbf{I}_0]^T \end{bmatrix}, \quad (241)$$

$$[\mathbf{K}_{au1}^{\alpha}] = J_0 \int_{\square} [\tilde{\mathbf{G}}(\xi)]^T [\tilde{\mathbf{C}}_0] [\hat{\mathbf{B}}_{\alpha}(\xi)] d\xi, \quad (242)$$

$$\{\mathbf{K}_{au2}^l\} = J_0 \int_{\square} [\tilde{\mathbf{G}}(\xi)]^T \{\tilde{\mathbf{A}}_0^{nl}\} \hat{N}_i(\xi) d\xi, \quad (243)$$

γ_{α}^l is defined in (201), and $[\mathbf{I}_0]$ in (195a).

The integrals in (242) and (243) can be evaluated analytically. Substituting $[\tilde{\mathbf{B}}_{\text{stab}}(\xi)] = \sum_{\alpha=1}^4 [\hat{\mathbf{B}}_{\alpha}(\xi)] [\Gamma_{\alpha}]^T$ from (208) and using (213b) for $[\tilde{\mathbf{G}}]$ together with (209)–(210) for $[\hat{\mathbf{B}}_{\alpha}(\xi)]$, we find the following analytical expressions for the elements of matrices $[\mathbf{K}_{au1}^{\alpha}]$ and $\{\mathbf{K}_{au2}^l\}$:

$$[\mathbf{K}_{au1}^1] = \frac{8J_0}{3} \begin{bmatrix} 0 & \tilde{\mathbf{C}}_{12} & \tilde{\mathbf{C}}_{19} & 0 \\ \tilde{\mathbf{C}}_{21} & 0 & \tilde{\mathbf{C}}_{27} & 0 \\ 0 & 0 & 0 & 0 \\ 0 & 0 & 0 & 0 \\ 0 & 0 & 0 & 0 \\ 0 & 0 & 0 & 0 \end{bmatrix}, \quad [\mathbf{K}_{au1}^2] = \frac{8J_0}{3} \begin{bmatrix} 0 & 0 & 0 & 0 \\ \tilde{\mathbf{C}}_{26} & 0 & \tilde{\mathbf{C}}_{23} & 0 \\ \tilde{\mathbf{C}}_{34} & \tilde{\mathbf{C}}_{32} & 0 & 0 \\ 0 & 0 & 0 & 0 \\ 0 & 0 & 0 & 0 \\ 0 & 0 & 0 & 0 \end{bmatrix}, \quad (244)$$

$$[\mathbf{K}_{au1}^3] = \frac{8J_0}{3} \begin{bmatrix} 0 & \tilde{\mathbf{C}}_{18} & \tilde{\mathbf{C}}_{13} & 0 \\ 0 & 0 & 0 & 0 \\ \tilde{\mathbf{C}}_{31} & \tilde{\mathbf{C}}_{35} & 0 & 0 \\ 0 & 0 & 0 & 0 \\ 0 & 0 & 0 & 0 \\ 0 & 0 & 0 & 0 \end{bmatrix}, \quad (245)$$

$$[\mathbf{K}_{au1}^4] = \frac{8J_0}{9} \begin{bmatrix} 0 & 0 & 0 & 0 \\ 0 & 0 & 0 & 0 \\ 0 & 0 & 0 & 0 \\ 0 & 0 & 0 & 0 \\ \tilde{\mathbf{C}}_{11} + \tilde{\mathbf{C}}_{21} + \tilde{\mathbf{C}}_{31} & 0 & \tilde{\mathbf{C}}_{13} + \tilde{\mathbf{C}}_{23} + \tilde{\mathbf{C}}_{33} & 0 \\ 0 & \tilde{\mathbf{C}}_{12} + \tilde{\mathbf{C}}_{22} + \tilde{\mathbf{C}}_{32} & 0 & 0 \end{bmatrix}, \quad (246)$$

and

$$\{\mathbf{K}_{au2}^1\} = \frac{J_0}{9} \begin{bmatrix} -3\tilde{A}_1 \\ -3\tilde{A}_2 \\ -3\tilde{A}_3 \\ \tilde{A}_1 + \tilde{A}_2 + \tilde{A}_3 \\ \tilde{A}_1 + \tilde{A}_2 + \tilde{A}_3 \\ \tilde{A}_1 + \tilde{A}_2 + \tilde{A}_3 \end{bmatrix}, \quad \{\mathbf{K}_{au2}^2\} = \frac{J_0}{9} \begin{bmatrix} 3\tilde{A}_1 \\ -3\tilde{A}_2 \\ -3\tilde{A}_3 \\ -(\tilde{A}_1 + \tilde{A}_2 + \tilde{A}_3) \\ \tilde{A}_1 + \tilde{A}_2 + \tilde{A}_3 \\ -(\tilde{A}_1 + \tilde{A}_2 + \tilde{A}_3) \end{bmatrix}, \quad (247)$$

$$\{\mathbf{K}_{au2}^3\}_{6 \times 1} = \frac{J_0}{9} \begin{Bmatrix} 3\tilde{A}_1 \\ 3\tilde{A}_2 \\ -3\tilde{A}_3 \\ \tilde{A}_1 + \tilde{A}_2 + \tilde{A}_3 \\ -(\tilde{A}_1 + \tilde{A}_2 + \tilde{A}_3) \\ -(\tilde{A}_1 + \tilde{A}_2 + \tilde{A}_3) \end{Bmatrix}, \quad \{\mathbf{K}_{au2}^4\}_{6 \times 1} = \frac{J_0}{9} \begin{Bmatrix} -3\tilde{A}_1 \\ 3\tilde{A}_2 \\ -3\tilde{A}_3 \\ -(\tilde{A}_1 + \tilde{A}_2 + \tilde{A}_3) \\ -(\tilde{A}_1 + \tilde{A}_2 + \tilde{A}_3) \\ \tilde{A}_1 + \tilde{A}_2 + \tilde{A}_3 \end{Bmatrix}, \quad (248)$$

$$\{\mathbf{K}_{au2}^5\}_{6 \times 1} = \frac{J_0}{9} \begin{Bmatrix} -3\tilde{A}_1 \\ -3\tilde{A}_2 \\ 3\tilde{A}_3 \\ \tilde{A}_1 + \tilde{A}_2 + \tilde{A}_3 \\ -(\tilde{A}_1 + \tilde{A}_2 + \tilde{A}_3) \\ -(\tilde{A}_1 + \tilde{A}_2 + \tilde{A}_3) \end{Bmatrix}, \quad \{\mathbf{K}_{au2}^6\}_{6 \times 1} = \frac{J_0}{9} \begin{Bmatrix} 3\tilde{A}_1 \\ -3\tilde{A}_2 \\ 3\tilde{A}_3 \\ -(\tilde{A}_1 + \tilde{A}_2 + \tilde{A}_3) \\ -(\tilde{A}_1 + \tilde{A}_2 + \tilde{A}_3) \\ \tilde{A}_1 + \tilde{A}_2 + \tilde{A}_3 \end{Bmatrix}, \quad (249)$$

$$\{\mathbf{K}_{au2}^7\}_{6 \times 1} = \frac{J_0}{9} \begin{Bmatrix} 3\tilde{A}_1 \\ 3\tilde{A}_2 \\ 3\tilde{A}_3 \\ \tilde{A}_1 + \tilde{A}_2 + \tilde{A}_3 \\ \tilde{A}_1 + \tilde{A}_2 + \tilde{A}_3 \\ \tilde{A}_1 + \tilde{A}_2 + \tilde{A}_3 \end{Bmatrix}, \quad \{\mathbf{K}_{au2}^8\}_{6 \times 1} = \frac{J_0}{9} \begin{Bmatrix} -3\tilde{A}_1 \\ 3\tilde{A}_2 \\ 3\tilde{A}_3 \\ -(\tilde{A}_1 + \tilde{A}_2 + \tilde{A}_3) \\ \tilde{A}_1 + \tilde{A}_2 + \tilde{A}_3 \\ -(\tilde{A}_1 + \tilde{A}_2 + \tilde{A}_3) \end{Bmatrix}. \quad (250)$$

Summarizing we note that the elements of $[\mathbf{K}_{aa}]$ are determined in (236)–(237) and $[\mathbf{K}_{au}]$ is defined by (239)–(240) and (242)–(250).

Appendix C: Analytical expressions for stabilization terms

In this Appendix we derive analytical expressions for matrices $\{\mathbf{f}_u^{\text{stab}}\}$ and $[\mathbf{k}_\varepsilon^{\text{stab}}]$ introduced in (151b) and (148).

We recall the definition of $\{\mathbf{f}_u^{\text{stab}}\}$:

$$\{\mathbf{f}_u^{\text{stab}}\} = \int_{\square} [\mathbf{B}_{\text{stab}}(\boldsymbol{\xi})]^T \{\boldsymbol{\sigma}(\boldsymbol{\xi})\} J(\boldsymbol{\xi}) d\boldsymbol{\xi}, \quad (251)$$

where all quantities are evaluated at the end of the increment.

Next, we use (230) to write $\{\boldsymbol{\sigma}(\boldsymbol{\xi})\} \simeq \{\boldsymbol{\sigma}_0\} + \{\boldsymbol{\sigma}_{\text{stab}}(\boldsymbol{\xi})\}$ and take into account (124a) to conclude that

$$\{\mathbf{f}_u^{\text{stab}}\} \simeq \int_{\square} [\mathbf{B}_{\text{stab}}(\boldsymbol{\xi})]^T \{\boldsymbol{\sigma}_{\text{stab}}(\boldsymbol{\xi})\} J(\boldsymbol{\xi}) d\boldsymbol{\xi}. \quad (252)$$

Using the definition of $[\mathbf{B}_{\text{stab}}]$ in (207), together with (208) and (212), we find

$$\{\mathbf{f}_u^{\text{stab}}\}_{32 \times 1} = \sum_{\alpha=1}^4 [\mathbf{M}_\alpha]_{32 \times 4}^T \{\mathbf{f}_\alpha\}_{4 \times 1}, \quad (253)$$

where

$$\{\mathbf{f}_\alpha\}_{4 \times 1} = J_0 \int_{\square} [\hat{\mathbf{B}}_\alpha(\boldsymbol{\xi})]_{4 \times 9}^T [\mathcal{K}_0]_{9 \times 9}^T \{\boldsymbol{\sigma}_{\text{stab}}(\boldsymbol{\xi})\}_{9 \times 1} d\boldsymbol{\xi}, \quad \alpha = 1, 2, 3, 4, \quad (254)$$

In plastically incompressible materials, $J_0 \simeq J_0|_n$ to first order. We also use the approximation $[\mathcal{K}_0] \simeq [\mathcal{K}_0]_n$, to find

$$\{\mathbf{f}_\alpha\} = \{\mathbf{f}_\alpha\}_n + \{\Delta \mathbf{f}_\alpha\}, \quad \alpha = 1, 2, 3, 4, \quad (255)$$

where

$$\{\Delta \mathbf{f}_\alpha\}_{4 \times 1} = J_0 \int_{\square} [\hat{\mathbf{B}}_\alpha(\boldsymbol{\xi})]_{4 \times 9}^T [\mathcal{K}_0]_{9 \times 9}^T \{\Delta \boldsymbol{\sigma}_{\text{stab}}(\boldsymbol{\xi})\}_{9 \times 1} d\boldsymbol{\xi}. \quad (256)$$

Using (231) for $\{\Delta \boldsymbol{\sigma}_{\text{stab}}\}$, we find

$$\{\Delta \mathbf{f}_\beta\}_{4 \times 1} \simeq [\mathbf{K}^\beta]_{4 \times 32} \{\Delta \mathbf{d}^e\}_{32 \times 1} + [\mathbf{K}_{au1}^\beta]_{4 \times 6}^T \{\Delta \mathbf{a}^e\}_{6 \times 1}, \quad \beta = 1, 2, 3, 4, \quad (257)$$

where $\{\Delta \mathbf{a}^e\}$ is found from the solution of the local problem in the element as described in Appendix B, $[\mathbf{K}_{au1}^\beta]$ as defined in (242)–(246),

$$[\mathbf{K}^\beta]_{4 \times 32} = [\mathbf{K}_1^\beta]_{4 \times 32} - [\mathbf{K}_2^\beta]_{4 \times 32}, \quad \beta = 1, 2, 3, 4, \quad (258)$$

$$[\mathbf{K}_1^\beta]_{4 \times 32} = \sum_{\gamma=1}^4 [\mathbf{K}^{\beta\gamma}]_{4 \times 4} [\mathbf{M}_\gamma]_{4 \times 32}, \quad [\mathbf{K}^{\beta\gamma}]_{4 \times 4} = J_0 \int_{\square} [\hat{\mathbf{B}}_\beta(\boldsymbol{\xi})]_{4 \times 9}^T [\tilde{\mathbf{C}}_0]_{9 \times 9} [\hat{\mathbf{B}}_\gamma(\boldsymbol{\xi})]_{9 \times 4} d\boldsymbol{\xi}, \quad (259)$$

$$[\mathbf{K}_2^\beta]_{4 \times 32} = \sum_{I=1}^8 \{\mathbf{K}_2^{\beta I}\}_{4 \times 1} [\boldsymbol{\delta}_I]_{1 \times 32}, \quad \{\mathbf{K}_2^{\beta I}\}_{4 \times 1} = J_0 \int_{\square} [\hat{\mathbf{B}}_\beta(\boldsymbol{\xi})]_{4 \times 9}^T \{\tilde{\mathbf{A}}_0^{\text{nl}}\}_{9 \times 1} \hat{N}_I(\boldsymbol{\xi}) d\boldsymbol{\xi}, \quad (260)$$

and $[\boldsymbol{\delta}_I]$ is defined in (238).

We use the expressions (209)–(210) for $[\hat{\mathbf{B}}_\beta(\boldsymbol{\xi})]$ and evaluate analytically the integrals in (259b) and (260b) to find:

$$[\mathbf{K}^{14}]_{4 \times 4} = [\mathbf{K}^{24}]_{4 \times 4} = [\mathbf{K}^{34}]_{4 \times 4} = [\mathbf{K}^{41}]_{4 \times 4} = [\mathbf{K}^{42}]_{4 \times 4} = [\mathbf{K}^{43}]_{4 \times 4} = [\mathbf{0}]_{4 \times 4}, \quad (261)$$

$$[\mathbf{K}^{11}]_{4 \times 4} = \frac{8J_0}{3} \begin{bmatrix} \tilde{C}_{11} & 0 & \tilde{C}_{17} & 0 \\ 0 & \tilde{C}_{22} & \tilde{C}_{29} & 0 \\ \tilde{C}_{71} & \tilde{C}_{92} & \tilde{C}_{77} + \tilde{C}_{99} & 0 \\ 0 & 0 & 0 & 0 \end{bmatrix}, \quad [\mathbf{K}^{12}]_{4 \times 4} = \frac{8J_0}{3} \begin{bmatrix} \tilde{C}_{16} & 0 & \tilde{C}_{13} & 0 \\ 0 & 0 & 0 & 0 \\ \tilde{C}_{76} & 0 & \tilde{C}_{73} & 0 \\ 0 & 0 & 0 & 0 \end{bmatrix}, \quad (262)$$

$$[\mathbf{K}^{13}]_{4 \times 4} = \frac{8J_0}{3} \begin{bmatrix} 0 & 0 & 0 & 0 \\ 0 & \tilde{C}_{28} & \tilde{C}_{23} & 0 \\ 0 & \tilde{C}_{98} & \tilde{C}_{93} & 0 \\ 0 & 0 & 0 & 0 \end{bmatrix}, \quad [\mathbf{K}^{21}]_{4 \times 4} = \frac{8J_0}{3} \begin{bmatrix} \tilde{C}_{61} & 0 & \tilde{C}_{67} & 0 \\ 0 & 0 & 0 & 0 \\ \tilde{C}_{31} & 0 & \tilde{C}_{37} & 0 \\ 0 & 0 & 0 & 0 \end{bmatrix}, \quad (263)$$

$$[\mathbf{K}^{22}]_{4 \times 4} = \frac{8J_0}{3} \begin{bmatrix} \tilde{C}_{44} + \tilde{C}_{66} & \tilde{C}_{42} & \tilde{C}_{63} & 0 \\ \tilde{C}_{24} & \tilde{C}_{22} & 0 & 0 \\ \tilde{C}_{36} & 0 & \tilde{C}_{33} & 0 \\ 0 & 0 & 0 & 0 \end{bmatrix}, \quad [\mathbf{K}^{23}]_{4 \times 4} = \frac{8J_0}{3} \begin{bmatrix} \tilde{C}_{41} & \tilde{C}_{45} & 0 & 0 \\ \tilde{C}_{21} & \tilde{C}_{25} & 0 & 0 \\ 0 & 0 & 0 & 0 \\ 0 & 0 & 0 & 0 \end{bmatrix}, \quad (264)$$

$$[\mathbf{K}^{31}]_{4 \times 4} = \frac{8J_0}{3} \begin{bmatrix} 0 & 0 & 0 & 0 \\ 0 & \tilde{C}_{82} & \tilde{C}_{89} & 0 \\ 0 & \tilde{C}_{32} & \tilde{C}_{39} & 0 \\ 0 & 0 & 0 & 0 \end{bmatrix}, \quad [\mathbf{K}^{32}]_{4 \times 4} = \frac{8J_0}{3} \begin{bmatrix} \tilde{C}_{14} & \tilde{C}_{12} & 0 & 0 \\ \tilde{C}_{54} & \tilde{C}_{52} & 0 & 0 \\ 0 & 0 & 0 & 0 \\ 0 & 0 & 0 & 0 \end{bmatrix}, \quad (265)$$

$$[\mathbf{K}^{33}]_{4 \times 4} = \frac{8J_0}{3} \begin{bmatrix} \tilde{C}_{11} & \tilde{C}_{15} & 0 & 0 \\ \tilde{C}_{51} & \tilde{C}_{55} + \tilde{C}_{88} & \tilde{C}_{83} & 0 \\ 0 & \tilde{C}_{38} & \tilde{C}_{33} & 0 \\ 0 & 0 & 0 & 0 \end{bmatrix}, \quad [\mathbf{K}^{44}]_{4 \times 4} = \frac{8J_0}{9} \begin{bmatrix} \tilde{C}_{11} & 0 & 0 & 0 \\ 0 & \tilde{C}_{22} & 0 & 0 \\ 0 & 0 & \tilde{C}_{33} & 0 \\ 0 & 0 & 0 & 0 \end{bmatrix}, \quad (266)$$

and

$$\{\mathbf{K}_2^{11}\}_{4 \times 1} = -\{\mathbf{K}_2^{13}\}_{4 \times 1} = \{\mathbf{K}_2^{15}\}_{4 \times 1} = -\{\mathbf{K}_2^{17}\}_{4 \times 1} = -\frac{J_0}{3} \begin{Bmatrix} \tilde{A}_1 \\ \tilde{A}_2 \\ \tilde{A}_7 + \tilde{A}_9 \\ 0 \end{Bmatrix}, \quad (267)$$

$$\{\mathbf{K}_2^{12}\}_{4 \times 1} = -\{\mathbf{K}_2^{14}\}_{4 \times 1} = \{\mathbf{K}_2^{16}\}_{4 \times 1} = -\{\mathbf{K}_2^{18}\}_{4 \times 1} = -\frac{J_0}{3} \begin{Bmatrix} \tilde{A}_1 \\ -\tilde{A}_2 \\ \tilde{A}_7 - \tilde{A}_9 \\ 0 \end{Bmatrix}, \quad (268)$$

$$\{\mathbf{K}_2^{21}\}_{4 \times 1} = \{\mathbf{K}_2^{22}\}_{4 \times 1} = -\{\mathbf{K}_2^{27}\}_{4 \times 1} = -\{\mathbf{K}_2^{28}\}_{4 \times 1} = -\frac{J_0}{3} \begin{Bmatrix} \tilde{A}_4 + \tilde{A}_6 \\ \tilde{A}_2 \\ \tilde{A}_3 \\ 0 \end{Bmatrix}, \quad (269)$$

$$\{\mathbf{K}_2^{23}\}_{4 \times 1} = \{\mathbf{K}_2^{24}\}_{4 \times 1} = -\{\mathbf{K}_2^{25}\}_{4 \times 1} = -\{\mathbf{K}_2^{26}\}_{4 \times 1} = \frac{J_0}{3} \begin{Bmatrix} -\tilde{A}_4 + \tilde{A}_6 \\ -\tilde{A}_2 \\ \tilde{A}_3 \\ 0 \end{Bmatrix}, \quad (270)$$

$$\{\mathbf{K}_2^{31}\}_{4 \times 1} = \{\mathbf{K}_2^{34}\}_{4 \times 1} = -\{\mathbf{K}_2^{36}\}_{4 \times 1} = -\{\mathbf{K}_2^{37}\}_{4 \times 1} = -\frac{J_0}{3} \begin{Bmatrix} \tilde{A}_1 \\ \tilde{A}_5 + \tilde{A}_8 \\ \tilde{A}_3 \\ 0 \end{Bmatrix}, \quad (271)$$

$$\{\mathbf{K}_2^{32}\}_{4 \times 1} = \{\mathbf{K}_2^{33}\}_{4 \times 1} = -\{\mathbf{K}_2^{35}\}_{4 \times 1} = -\{\mathbf{K}_2^{38}\}_{4 \times 1} = \frac{J_0}{3} \begin{Bmatrix} -\tilde{A}_1 \\ -\tilde{A}_5 + \tilde{A}_8 \\ \tilde{A}_3 \\ 0 \end{Bmatrix}, \quad (272)$$

$$\left\{ \mathbf{K}_2^{41} \right\}_{4 \times 1} = \left\{ \mathbf{K}_2^{47} \right\}_{4 \times 1} = \frac{J_0}{9} \begin{Bmatrix} \tilde{A}_1 \\ \tilde{A}_2 \\ \tilde{A}_3 \\ 0 \end{Bmatrix}, \quad \left\{ \mathbf{K}_2^{42} \right\}_{4 \times 1} = \left\{ \mathbf{K}_2^{48} \right\}_{4 \times 1} = \frac{J_0}{9} \begin{Bmatrix} \tilde{A}_1 \\ -\tilde{A}_2 \\ -\tilde{A}_3 \\ 0 \end{Bmatrix}, \quad (273)$$

$$\left\{ \mathbf{K}_2^{43} \right\}_{4 \times 1} = \left\{ \mathbf{K}_2^{45} \right\}_{4 \times 1} = \frac{J_0}{9} \begin{Bmatrix} -\tilde{A}_1 \\ -\tilde{A}_2 \\ \tilde{A}_3 \\ 0 \end{Bmatrix}, \quad \left\{ \mathbf{K}_2^{44} \right\}_{4 \times 1} = \left\{ \mathbf{K}_2^{46} \right\}_{4 \times 1} = \frac{J_0}{9} \begin{Bmatrix} -\tilde{A}_1 \\ \tilde{A}_2 \\ -\tilde{A}_3 \\ 0 \end{Bmatrix}. \quad (274)$$

where \tilde{C}_{ij} and \tilde{A}_i are the elements of $[\tilde{\mathbf{C}}_0]$ and $\{\tilde{\mathbf{A}}_0^{\text{nl}}\}$.

Summarizing we note that $\{\mathbf{f}_u^{\text{stab}}\}$ is determined analytically from (253), (255), (257), (242)–(246), and (258)–(274).

Next we consider the calculation of $[\mathbf{k}_\varepsilon^{\text{stab}}]$ defined in (148):

$$[\mathbf{k}_\varepsilon^{\text{stab}}]_{32 \times 32} = \ell^2 \int_{\square} [\mathbf{B}_\varepsilon^{\text{stab}}(\boldsymbol{\xi})]_{32 \times 3}^T [\mathbf{B}_\varepsilon^{\text{stab}}(\boldsymbol{\xi})]_{3 \times 32} J(\boldsymbol{\xi}) d\boldsymbol{\xi}, \quad (275)$$

where all quantities are evaluated at the end of the increment. Using the definition of $[\mathbf{B}_\varepsilon^{\text{stab}}]$ in (214), together with (217), we conclude that

$$[\mathbf{k}_{\text{stab}}^e]_{32 \times 32} = \ell^2 J_0 \sum_{\alpha=1}^4 \sum_{\beta=1}^4 [\boldsymbol{\Gamma}_\alpha]_{32 \times 4}^T [\mathbf{H}_{\alpha\beta}]_{4 \times 4} [\boldsymbol{\Gamma}_\beta]_{4 \times 32}, \quad (276)$$

where

$$[\mathbf{H}_{\alpha\beta}]_{4 \times 4} = \int_{\square} [\hat{\mathbf{B}}_\varepsilon^\alpha(\boldsymbol{\xi})]_{4 \times 3}^T [\mathbf{D}_0]_{3 \times 3} [\hat{\mathbf{B}}_\varepsilon^\beta(\boldsymbol{\xi})]_{3 \times 4} d\boldsymbol{\xi}, \quad [\mathbf{D}_0]_{3 \times 3} = [\mathbf{K}_0]_{3 \times 3}^T [\mathbf{K}_0]_{3 \times 3}, \quad \alpha, \beta = 1, 2, 3, 4. \quad (277)$$

We use the expressions (218)–(219) for $[\hat{\mathbf{B}}_\varepsilon^\alpha(\boldsymbol{\xi})]$ and evaluate analytically the integrals in (277a) to find:

$$(H_{\alpha\beta})_{\gamma\delta} = E_{\alpha\beta} \delta_{4\gamma} \delta_{4\delta}, \quad \alpha, \beta, \gamma, \delta = 1, 2, 3, 4, \quad (278)$$

$$[E_{\alpha\beta}]_{4 \times 4} = \frac{8}{3} \begin{bmatrix} D_{11} + D_{22} & D_{12} & D_{23} & 0 \\ D_{13} & D_{22} + D_{33} & D_{12} & 0 \\ D_{23} & D_{12} & D_{11} + D_{33} & 0 \\ 0 & 0 & 0 & \frac{1}{3}(D_{11} + D_{22} + D_{33}) \end{bmatrix}, \quad (279)$$

where D_{ij} are the elements of $[\mathbf{D}_0]$.

Summarizing we note that $[\mathbf{k}_{\text{stab}}^e]$ is determined analytically from (276), (278), and (279).

References

- Aravas, N., 1992. Finite elastoplastic transformations of transversely isotropic metals. *Int. J. Solids Struct.* 29, 2137–2157.
- Aravas, N., Ponte Castañeda, 2004. Numerical methods for porous metals with deformation-induced anisotropy. *Comp. Methods Appl. Mech. Engrg.* 193, 3767–3805.
- Areias, P.M.A., César de Sá, J.M.A., Conceição António, C.A., Fernandes, A.A., 2003. Analysis of 3D problems using a new enhanced strain hexahedral element. *Int. J. Num. Meth. Engrg.* 58, 1637–1682.
- Auricchio, F., Taylor, R.L., 1999. A return-map algorithm for general associative isotropic elasto-plastic materials in large deformation regimes. *Int. J. Plast.* 15, 1359–1378.
- Bai, Y.L., Wierzbicki, T., 2008. A new model of metal plasticity and fracture with pressure and Lode dependence. *Int. J. Plast.* 24, 1071–1096.
- Bai, Y.L., Wierzbicki, T., 2010. Application of extended Mohr-Coulomb criterion to ductile fracture. *Int. J. Fract.* 161, 1–20.
- Bai, Y.L., Wierzbicki, T., 2015. A comparative study of three groups of ductile fracture loci in the 3D space. *Eng. Fract. Mech.* 135, 147–167.
- Bao, Y., Wierzbicki, T., 2004a. A comparative study on various ductile crack formation criteria. *J. Eng. Mat. Techn.* 126, 314–324.
- Bao, Y., Wierzbicki, T., 2004b. On fracture locus in the equivalent strain and stress triaxiality space. *Int. J. Mech. Sci.* 46, 81–98.

- Bao, Y., Wierzbicki, T., 2005. On the cut-off value of negative triaxiality for fracture. *Eng. Fract. Mech.* 72, 1049–1069.
- Belytschko, T., Bindeman, L.P., 1991. Assumed strain stabilization of the 4-node quadrilateral with 1-point quadrature for nonlinear problems. *Comp. Methods Appl. Mech. Engrg.* 88, 311–340.
- Belytschko, T., Ong, J.S.-J., Liu, W.K., Kennedy, J.M., 1984. Hourglass control in linear and nonlinear problems. *Comp. Methods Appl. Mech. Engrg.* 43, 251–276.
- Benallal, A., Tvergaard, V., 1995. Nonlocal continuum effects on bifurcation in the plane strain tension-compression test. *J. Mech. Phys. Solids.* 43, 741–770.
- Borja, R.A., Sama, K.M., Sanz, P.F., 2003. On the numerical integration of three-invariant elastoplastic constitutive models. *Comp. Methods Appl. Mech. Engrg.* 192, 1227–1258.
- Buchkremer, S., Wu, B., Lung, D., Münstermann, S., Klocke, F., Bleck, W., 2014. FE-simulation of machining processes with a new material model. *J. Mater. Process. Technol.* 214, 599–611.
- Capsoni, A., Corradi, L., 1997a. A mixed finite element model for plane strain elastic-plastic analysis Part I. Formulation and assesment of overall behavior. *Comp. Methods Appl. Mech. Engrg.* 141, 67–79.
- Capsoni, A., Corradi, L., 1997b. A mixed finite element model for plane strain elastic-plastic analysis Part II. Application to the 4-node bilinear element. *Comp. Methods Appl. Mech. Engrg.* 141, 81–93.
- Comi, C., Perego, U., 1995. A unified approach for variationally consistent finite elements in elastoplasticity. *Comp. Methods Appl. Mech. Engrg.* 121, 323–344.
- Corradi, L., 1983. A displacement formulation of the finite element problem. *Meccanica* 18, 77–91.
- Dafalias, Y.F., 1985. The plastic spin. *J. Appl. Mech.* 52, 249–256.
- Danas, K., Ponte Castañeda, P., 2009a. A finite strain model for anisotropic viscoplastic porous media: I – Theory. *Eur. J. Mech. A: Solids* 28, 387–401.
- Danas, K., Ponte Castañeda, P., 2009b. A finite strain model for anisotropic viscoplastic porous media: II – Applications. *Eur. J. Mech. A: Solids* 28, 402–416.
- Engelen, R.A.B., Geers, M.G.D., Baaijens, F.P.T., 2003. Nonlocal implicit gradient-enhanced elasto-plasticity for the modelling of softening behaviour. *Int. J. Plast.* 19, 403–433.
- Flanagan, D.P., Belytschko, T., 1981. A uniform strain hexahedron and quadrilateral with orthogonal hourglass control. *Int. J. Num. Meth. Engrg.* 17, 679–706.
- Freischläger, C., Schweizerhof, K., 1996. On the systematic development of trilinear three-dimensional solid elements based on Simo's enhanced strain formulation. *Int. J. Solids Struct.* 33, 2993–3017.
- Gurson, A.L., 1977. Continuum theory of ductile rupture by void nucleation and growth: part I — Yield criteria and flow rules for porous ductile media. *J. Engng. Mater. Tech.* 99, 2–15.
- Halton, S.S., Kyriakides, S., Ravi-Chandar, K., 2013. Ductile failure under combined shear and tension. *Int. J. Solids Struct.* 50, 1507–1522.
- Hancock, J.W., Mackenzie, A.C., 1976. On the mechanism of ductile failure in high-strength steels subjected to multi-axial stress-states. *J. Mech. Phys. Solids* 24, 147–175.
- Hibbitt, H.D., 1984. ABAQUS/EPGEN — A general purpose finite element code with emphasis in nonlinear applications. *Nucl. Engng. Des.* 77, 271–297.
- Hill, R., 1950. *The Mathematical Theory of Plasticity*, Oxford University Press, Oxford.
- Hughes T.J.R., Winget, J., 1980. Finite rotation effects in numerical integration of rate constitutive equations arising in large-deformation analysis. *Int. J. Num. Meth. Engrg.* 15, 1862–1867.
- Jiang J., Pietruszczak, S., 1988. Convexity of yield loci for pressure sensitive materials. *Comput. Geotechn.* 5, 51–63.
- Johnson, G.R., Cook, W.H., 1985. Fracture characteristics of three metals subjected to various strains, strain rates, temperatures and pressures. *Eng. Fract. Mech.* 21, 31–48.
- Kachanov, L.M., 1971. *Foundations of the Theory of Plasticity*, North-Holland Publishing Co., Amsterdam.
- Kasper E.P., Taylor, R.L., 2000a. A mixed-enhanced strain method Part I: Geometrically linear problems. *Comput. Stuct.* 75, 237–250.
- Kasper E.P., Taylor, R.L., 2000b. A mixed-enhanced strain method Part II: Geometrically nonlinear problems. *Comput. Stuct.* 75, 51–260.
- Lian, J., Sharaf, M., Archie, F., Münstermann, S., 2012. A hybrid approach for modelling of plasticity and failure behaviour of advanced high-strength steel sheets. *Int. J. Damage Mech.* 22, 188–218.
- Lian, J., Jia, X.X., Münstermann, S., Bleck, W., 2014. A generalized damage model accounting for instability and ductile fracture for sheet metals. *Key Eng. Mater.* 106–110.
- Lian, J., Wu, J., Münstermann, S., 2015. Evaluation of the cold formability of high-strength low-alloy steel plates with the modified Bai-Wierzbicki damage model. *Int. J. Damage Mech.* 24, 383–417.
- Luo, M., Dunand, M., Mohr, D., 2012. Experiments and modeling of anisotropic aluminum extrusions under multi-axial loading – Part II: Ductile fracture. *Int. J. Plast.* 32-33, 36–58.
- McClintock, F.A., 1968. A criterion for ductile fracture by the growth of holes. *J. Appl. Mech.* 35, 363–371.
- McMeeking, R.M., 1977. Finite deformation analysis of crack tip opening in elastic-plastic materials and implications for fracture. *J. Mech. Phys. Solids* 25, 357–381.
- Mendes, L.A.M., Castro, L.M.S.S., 2009. Hybrid-mixed stress finite element models in elastoplastic analysis. *Finite Elem. Anal. Des.* 45, 863–875.
- Mohr, D., Henn, S., 2007. Calibration of stress triaxiality dependent crack formation criteria: a new hybrid experimental-numerical method. *Exp. Mech.* 47, 805–820.
- Nagtegaal, J.C., Veldpaus, F.E., 1984. On the implementation of finite strain plasticity equations in a numerical model. In: Pittman, J.F.T., Zienkiewicz, O.C., Wood, R.D., Alexander, J.M. (Eds.), *Numerical Analysis of Forming Processes*, papers presented at the international conference held at Swansea, UK, 12–16 July 1982. John Wiley & Sons Ltd., Chichester, pp. 351–371.
- Nagtegaal, J.C., Taylor, L.M., 1991. Comparison of implicit and explicit finite element methods for analysis of sheet forming problems. *Conference on Finite Element Simulation of 3-D Sheet Metal Forming Processes in Automotive Industry*, 14–16 May 1991, Zürich, VDI Berichte NR. 894, 705–725.

- Nayak, G.C., Zienkiewicz, O.C., 1972. Convenient form of stress invariants for plasticity. *Proc. ASCE J. Struct. Div.* 98, 949–954.
- Needleman, A., 1985. On finite element formulations for large elastic-plastic deformations. *Comput. Struct.* 20, 247–257.
- Needleman, A., Rice, J.R., 1978. Limits to ductility set by plastic flow localization. In (Eds): Koistinen, D.P., Wang, N-M., *Mechanics of Sheet Metal Forming*. Plenum Press, New York-London, pp. 237–267.
- Needleman, A., Tvergaard, V., 1987. An analysis of ductile rupture modes at a crack tip. *J. Mech. Phys. Solids* 35, 151–183.
- Novoksharov, D., Dobereiner, B., Sharaf, M., Münstermann, S., Lian, J., 2015. A new model for upper shelf impact toughness assessment with a computationally efficient parameter identification algorithm. *Eng. Fract. Mech.* 148, 281–303.
- Nyssen, C., Beekers, P., 1984. A unified approach for displacements, equilibrium and hybrid finite element models in elasto-plasticity. *Comp. Methods Appl. Mech. Engrg.* 44, 131–151.
- Peerlings, R.H.J., Geers, M.G.D., Borst, de, R., Brekelmans, W.A.M., 2001. A critical comparison of nonlocal and gradient-enhanced softening continua. *Int. J. Solids Struct.* 38, 7723–7746.
- Pinsky, P.M., 1987. A finite element formulation for elastoplasticity based on a three-field variational equation. *Comp. Methods Appl. Mech. Engrg.* 61, 41–60.
- Puso, M.A., 2000. A highly efficient enhanced assumed strain physically stabilized hexahedral element. *Int. J. Num. Meth. Engrg.* 49, 1029–1064.
- Rebello, N., Nagtegaal, J.C., Taylor, L.M., 1992. Comparison of implicit and explicit finite element methods in the simulation of metal forming processes. In: Chenot, J.L., Wood, R.D., Zienkiewicz, O.C. (Eds.), *Proceedings of 4th International Conference on Numerical Methods in Industrial Forming Processes, NUMIFORM 92*, 14-18 September 1992, Valbonne, France, CRC Press, pp. 99–108.
- Rice, J.R., 1967. Mechanics of crack tip deformation and extension by fatigue. In: *Fatigue Crack Propagation*, ASTM STP 415, Am. Soc. Testing Mats., pp. 247–311.
- Rice, J.R., 1968. A path independent integral and the approximate analysis of strain concentration by notches and cracks. *J. Appl. Mech.* 35, 379–386.
- Rice, J.R., 1976. The localization of plastic deformation. In (Ed.): Koiter, W.T., *Proceedings of the 14th International Congress on Theoretical and Applied Mechanics*. North-Holland Publishing Corporation, pp. 207–220.
- Rice, J.R., Tracey, D.M., 1969. On the ductile enlargement of voids in triaxial stress fields. *J. Mech. Phys. Solids* 17, 201–217.
- Rudnicki, J.W., Rice, J.R., 1975. Conditions for the localization of deformation in pressure-sensitive dilatant materials. *J. Mech. Phys. Solids* 23, 371–394.
- Seupel, A., Hütter, G., Kuna, M., 2018. An efficient FE-implementation of implicit gradient-enhanced damage models to simulate ductile fracture. *Eng. Fract. Mech.* 199, 41–60.
- Simo, J.C., 1998. Numerical analysis and simulation of plasticity. In: Ciarlet, P.G., Lions, J.L. (Eds.), *Handbook of Numerical Analysis*, Vol. VI, Elsevier Science B.V., pp. 183–499.
- Simo, J.C., Armero, F., 1992. Geometrically non-linear enhanced strain mixed methods and the method of incompatible modes. *Int. J. Num. Meth. Engrg.* 33, 1413–1449.
- Simo, J.C., Armero, F., Taylor, R.L., 1993. Improved versions of assumed strain tri-linear elements for 3D finite deformation problems. *Comp. Methods Appl. Mech. Engrg.* 110, 359–386.
- Simo, J.C., Hughes, T.J.R., 1986. On the variational foundations of the assumed strain methods. *J. Appl. Mech.* 53, 51–54.
- Simo, J.C., Hughes, T.J.R., 1998. *Computational Inelasticity*, Springer-Verlag, New York Inc.
- Simo, J.C., Kennedy, J.G., Taylor, R.L., 1989. Complementary mixed finite element formulations for elastoplasticity. *Comp. Methods Appl. Mech. Engrg.* 74, 177–206.
- Simo, J.C., Rifai, M.S., 1990. A class of mixed assumed strain methods and the method of incompatible modes. *Int. J. Num. Meth. Engrg.* 29, 1595–1638.
- Taylor, R.L., Beresford, P.J., Wilson, E.L., 1976. A non-conforming element for stress analysis. *Int. J. Num. Meth. Engrg.* 10, 1211–1219.
- Tvergaard V., Needleman, A., 1986. Effect of material rate sensitivity on failure modes in the Charpy V-notch test. *J. Mech. Phys. Solids* 34, 213–241.
- Wu, B., Buchkremer, S., Münstermann, S., Lian, J., Veselovac, D., Bleck, W., Klocke, F., 2017a. Modeling of Chip Breakage in Machining of AISI 1045 Steel by Using an Improved Damage Mechanics Model. *Steel Res. Int.* 88, 1600338-n/a.
- Wu, B., Li, X., Di, Y., Brinell, V., Lian, J., Münstermann, S., 2017b. Extension of the modified Bai-Wierzbicki model for predicting ductile fracture under complex loading conditions. *Fatigue Fract. Eng. Mater. Struct.* 40, 2152–2168.
- Xue, L., 2007. Damage accumulation and fracture initiation in uncracked ductile solids subject to triaxial loading. *Int. J. Solids Struct.* 44, 5163–5181.
- Xue, L., Wierzbicki, T., 2008. Ductile fracture initiation and propagation modeling using damage plasticity theory. *Eng. Fract. Mech.* 75, 3276–3293.